

**Development and Characterization of an *in vitro* Culture System as a  
Physiological Model for Chronic Hepatitis B Infection**

by

**Alexandria V. Sams**

Bachelor of Science (magna cum laude), Biomedical Engineering  
Yale University, 2000

Submitted to the Department of Biological Engineering in Partial Fulfillment  
of the Requirements for the Degree of  
**Doctor of Philosophy in Biological Engineering**

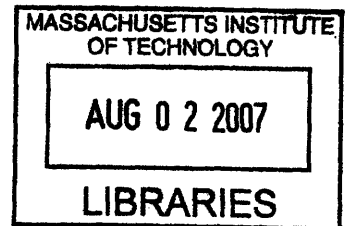
at the

**Massachusetts Institute of Technology**

**June 2007**

© 2007 Massachusetts Institute of Technology

All rights reserved



ARCHIVES

Signature of Author \_\_\_\_\_  
Department of Biological Engineering  
June 2007

Certified by \_\_\_\_\_  
Dr. Linda G. Griffith  
Professor, Biological Engineering & Mechanical Engineering  
Thesis Supervisor


Accepted by \_\_\_\_\_  
Dr. Alan J. Grodzinsky  
Professor, Electrical, Mechanical, & Biological Engineering  
Chair, Biological Engineering Graduate Program Committee



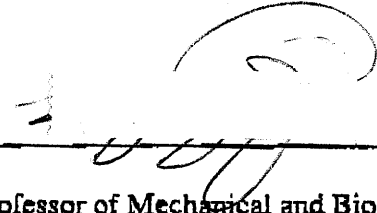


This doctoral thesis has been examined by a committee of the Biological Engineering Department as follows:

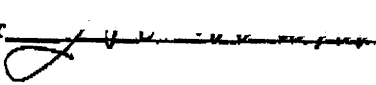
Chairperson, Graduate Thesis Committee

  
K. Dane Wittrup  
Mares Professor of Chemical Engineering and Bioengineering  
MIT

Thesis Advisor, Committee Member

  
Linda G. Griffith  
Professor of Mechanical and Biological Engineering  
MIT

Thesis Committee Member

  
5/23/07  
Jack R. Wands  
Jeffrey and Kimberly Greenberg - Artemis and Martha Joulowsky Professor in  
Gastroenterology and Professor of Medical Science  
Brown University



# **Development and Characterization of an *in vitro* Culture System as a Physiological Model for Chronic Hepatitis B Infection**

by  
**Alexandria V. Sams**

Submitted to the Biological Engineering Department in Partial Fulfillment of the Requirements for the Degree of Doctor of Philosophy in Biological Engineering

## **Abstract**

Human Hepatitis B virus (HBV) is the prototype member of the family Hepadnaviridae that consists of enveloped, partially double stranded DNA viruses that specifically target hepatocytes for viral replication. Although a vaccine has been available for more than 20 years chronic HBV infection afflicts 350-400 million worldwide. It is estimated that 0.5-1.2 million people die each year from HBV-attributable cases of chronic hepatitis, cirrhosis, and hepatocellular carcinoma.

Significant disadvantages exist among currently available therapeutics (e.g. IFN $\alpha$ , lamivudine, adefovir, etc.) that include limited efficacy and the promotion of drug-resistant viral strains. These therapeutics are the research products of the HBV molecular biology that can be manipulated in the laboratory setting. Future antiviral drug therapy is dependent upon the development of better cell culture systems that will allow the study of the complete viral life cycle.

The use of primary human and primate hepatocytes is restricted by multiple experimental limitations including a rapid loss of susceptibility to infection in culture, lot-to-lot variability inherent in primary cell culture, and the necessity of treatment with chemical agents such as DMSO for reproducible infection. Permissive cell lines are capable of supporting viral replication upon transfection with the HBV genome. These cell lines have helped to elucidate the later events in the viral life cycle. However, there is less understanding of the early stages that include virus attachment, internalization, uncoating, nuclear transport, and genome repair.

Our group has developed an *in vitro* system that recreates many of the features of a perfused capillary bed structure. Various metrics (e.g. biochemical production, tissue morphology, liver-enriched mRNA expression, and drug metabolism) confirm that this system maintains a well-differentiated liver phenotype. Using DHBV as a surrogate model, this study has attempted to demonstrate that hepatocytes maintained in a more sophisticated culture system retain susceptibility to infection. This study has endeavored to establish the perfused three-dimensional culture system as potential tool to study early events of the viral life cycle. This research lays the foundation for the future development of a human HBV infection model in which early stages of the viral life cycle can be studied and therapeutic targets identified.

Thesis Supervisor: Linda G. Griffith

Title: Professor of Mechanical and Biological Engineering

## **Acknowledgements**

I would like to acknowledge my advisor, Dr. Linda Griffith, for her guidance and support. Her commitment to scientific enlightenment and her determined spirit have truly inspired me. I would also like to express my gratitude to my committee whose counsel and insight were essential to this research. I would like to extend a special thanks to Dr. Jack Wands for allocating time and resources in his lab at Brown University in order for me to develop the necessary training and skills to accomplish this research. I am indebted to Dr. Jisu Li, Rolf Carlson, and Donna Pratt in the Wands laboratory for their assistance during my time at Brown.

I would like to express my deepest gratitude to my fellow lab mates. Artemis Kalezi, Sharon Karackattu, Laura Vineyard, Karel Domansky, Walker Inman, Nate Tedford, and Ben Cosgrove provided me with fundamental tools to facilitate my research. Thanks to Ricardo, Corey, Ajit, Anand, Joe M., Ta, Brian, Albert, Joe S., Emily, Megan, and Romie for the thoughtful discussions and beneficial advice.

I would also like to thank my family and loved ones whose support has sustained me throughout my tenure at MIT.

# Table of Contents

<b>Abstract</b>	<b>5</b>
<b>Acknowledgements</b>	<b>6</b>
<b>List of Figures</b>	<b>10</b>
<b>List of Tables</b>	<b>12</b>
<b>Chapter 1</b>	
<b>Introduction, Background and Motivation</b>	<b>13</b>
1.1 Global Impact	13
1.2 Currently Available Therapeutics	14
1.3 General Anatomy	17
1.4 Liver Microenvironment: Sinusoid & Intrahepatic Bile Duct System	21
1.4.1 Hepatocytes	22
1.4.2 Liver Sinusoidal Endothelial Cells	23
1.4.3 Kupffer Cells	25
1.4.4 Hepatic Stellate Cells	25
1.4.5 Pit Cells	26
1.4.6 Cholangiocytes	27
1.5 Interactions within the Sinusoidal Microenvironment	28
1.5.1 Cell-Matrix Interactions	28
1.5.2 Soluble Ligands	29
1.5.3 Cell-Cell Interactions	30
1.6 Hepatitis B Virus	31
1.6.1 Genome Organization	31
1.6.2 Envelope Proteins	32
1.6.3 Core Protein	33
1.6.4 Viral Polymerase	34
1.6.5 HBx Protein	34
1.7 Animal Models	35
1.7.1 Host Receptors	38
1.7.1.1 Duck Carboxypeptidase D	39
1.7.2 Liver Specificity	43
1.8 Objectives & Specific Aims	45
<b>Chapter 2</b>	
<b>Development of 3D Perfused Liver Microenvironment</b>	<b>49</b>
2.1 Key aspects of the liver microenvironment	49
2.2 Fostering tissue morphogenesis in vitro	50
2.3 Microscopic design parameters	51
2.4 Isolation of primary rat hepatocytes	53
2.4.1 Formation of spheroidal aggregates	54
2.5 Assembly & seeding of the 3D perfused microreactor	54
2.6 Evaluation of the hepatic in the 3D perfused microreactor	56
2.6.1 Analysis of albumin and urea secretion	56
2.6.2 Tissue morphological analysis	57

2.6.3	Liver-enriched mRNA and protein expression	60
2.7	Scaling up the microreactor	61
2.7.1	Development of the giant microreactor	61
2.7.2	Characterization of the giant microreactor	63
2.7.3	Development of the multiwell microreactor	65
2.7.4	Characterization of the multiwell microreactor	67
<b>Chapter 3</b>		
<b>A Novel Method to Render Primary Rat Hepatocytes Susceptible to Duck Hepatitis B Virus</b>		
		<b>69</b>
3.1	Introduction	69
3.2	Materials & Methods	72
3.2.1	Primary rat hepatocyte isolation and culture	72
3.2.2	Multiwell microreactor culture	72
3.2.3	Generation of recombinant adenovirus vectors	74
3.2.4	DHBV-positive serum isolation	74
3.2.5	DHBV infection	75
3.2.6	Western blot analysis	75
3.2.7	Isolation & detection of DHBV DNA in primary rat hepatocytes	76
3.2.8	Fluorescence Activated Cell Sorting (FACS) analysis	77
3.2.9	Fluorescence & Immunofluorescence analysis	77
3.2.10	Statistical analysis	78
3.3	Results	79
3.3.1	DCPD expression in primary rat hepatocytes in standard tissue culture	79
3.3.2	DCPD protects against Ad-mediated cytotoxicity	86
3.3.3	Evidence of DHBV internalization and replication in DCPD-transfected rat hepatocytes	95
3.3.4	DCPD expression in rat hepatocytes maintained in multi-well Microreactor	102
3.3	Discussion	104
<b>Chapter 4</b>		
<b>Prolonged Susceptibility to DHBV infection in Primary Rat Hepatocytes Maintained in a 3D Perfused Culture System</b>		
		<b>109</b>
4.1	Introduction	109
4.2	Materials & Methods	112
4.2.1	Primary rat hepatocyte isolation and culture	112
4.2.2	Preparation of spheroidal cell aggregates in spinner flasks	113
4.2.3	Giant microreactor culture	113
4.2.4	Multi-well microreactor culture	114
4.2.5	Generation of recombinant adenovirus vectors	115
4.2.6	DHBV-positive serum isolation	116
4.2.7	DHBV Infection	117
4.2.7.1	Standard 2D culture	117
4.2.7.2	Multi-well microreactor	117

4.2.8	Sodium dodecyl sulfate-polyacrylamide gel electrophoresis (SDS-PAGE) and western blot analysis	118
4.2.9	Isolation & detection of DHBV DNA in primary rat hepatocytes	118
4.2.10	Immunofluorescence analysis	120
4.2.11	Statistical Analysis	120
4.3	Results	121
4.3.1	Maintenance of factors necessary for DHBV replication	121
4.3.2	Early and late DCPD transfection in monolayer culture	124
4.3.3	Early and late DCPD transfection in microreactor culture	128
4.3.4	Development of real-time PCR assay to quantify total DHBV DNA and cccDNA	132
4.3.5	DCPD protects against Ad-mediated cytotoxicity in microreactor culture	136
4.3.6	DHBV DNA evidence in DCPD-transfected PRHs	138
4.4	Discussion	143
<b>Chapter 5</b>		
<b>Conclusions and Recommendations</b>		<b>148</b>
<b>References</b>		<b>152</b>
<b>Appendices</b>		
<b>Appendix 1-MilliF Microreactor Assembly Protocol</b>		<b>165</b>
<b>Appendix 2-MilliF Microreactor Seeding &amp; Maintenance Protocol</b>		<b>171</b>
<b>Appendix 3-Giant Microreactor Assembly, Seeding, &amp; Maintenance Protocol</b>		<b>174</b>
<b>Appendix 4-Multi-well Microreactor Assembly, Seeding, &amp; Maintenance Protocol</b>		<b>180</b>

## List of Figures

<b>Figure 1-1.</b> Worldwide Geographic Distribution of Chronic Hepatitis B Virus Infection as of 2005	13
<b>Figure 1-2.</b> Classic Hepatic Lobule and Rappaport's Acinus	19
<b>Figure 1-3.</b> Zonation of Rappaport's Acinus	20
<b>Figure 1-4.</b> Sinusoidal Microenvironment & Cell Type Breakdown	22
<b>Figure 1-5.</b> Liver Sinusoid	24
<b>Figure 1-6.</b> HBV genome organization	31
<b>Figure 1-7.</b> Scanning electron micrographs (SEMs) & diagram of different HBV particles	32
<b>Figure 2-1.</b> Diagram of scaffold, microporous filter, and support scaffold	52
<b>Figure 2-2.</b> Schematic of microreactor and the fluidic system	53
<b>Figure 2-3.</b> Schematic of isolation procedure for hepatocyte-enriched fraction	53
<b>Figure 2-4.</b> Images of microreactor components and assembly	55
<b>Figure 2-5.</b> Transmission electron micrographs (TEMs) of tissue in microreactor	57
<b>Figure 2-6.</b> Scanning electron micrographs (SEMs) of tissue in microreactor	58
<b>Figure 2-7.</b> Cell viability stain of tissue in microreactor	59
<b>Figure 2-8.</b> Image of giant microreactor	62
<b>Figure 2-9.</b> Phase-contrast image of tissue structures in giant microreactor	63
<b>Figure 2-10.</b> Relative gene expression across culture systems	64
<b>Figure 2-11.</b> Schematic of multi-well microreactor	65
<b>Figure 2-12.</b> Relative gene expression in multi-well microreactor	67
<b>Figure 2-13.</b> Cell viability stain of tissue in multi-well microreactor	68
<b>Figure 2-14.</b> Relative gene expression in single cell vs. spheroid seeded multi-well	68
<b>Figure 3-1.</b> Schematic of multi-well microreactor	73
<b>Figure 3-2.</b> DCPD transfection of PRHs in monolayer culture	82
<b>Figure 3-3.</b> FACS analysis of DCPD-transfected PRHs	84
<b>Figure 3-4.</b> DCPD protects against adenovirus-mediated cytotoxicity	88
<b>Figure 3-5.</b> Difference in total viral particles per Ad vector	94
<b>Figure 3-6.</b> DHBV preS envelope protein demonstrates evidence of viral replication in DCPD-transfected PRHs	98
<b>Figure 3-7.</b> DHBV DNA evidence in DCPD-transfected PRHs	101
<b>Figure 3-8.</b> Confocal images of DCPD-transfected microreactor at multiple timepoints following Ad exposure	103
<b>Figure 4-1.</b> Diagram of multi-well microreactor	114
<b>Figure 4-2.</b> Glycine decarboxylase expression over 21 days in culture	122
<b>Figure 4-3.</b> Liver-enriched mRNA and protein expression in culture	123
<b>Figure 4-4.</b> Early and late DCPD transfection in monolayer culture	126
<b>Figure 4-5.</b> DCPD transfection of spheroidal cell aggregates	129
<b>Figure 4-6.</b> Early and late DCPD transfection in single cell seeded microreactors	130
<b>Figure 4-7.</b> Development of real-time PCR analysis of real-time PCR analysis for DHBV DNA quantification	134



<b>Figure 4-8.</b>	Real-time PCR primers/probes specific for total DHBV DNA and cccDNA	135
<b>Figure 4-9.</b>	Measurement of total cell number in DCPD-transfected monolayer & microreactor cultures	137
<b>Figure 4-10.</b>	DHBV DNA quantification in DCPD-transfected monolayer culture (Ad MOI=10)	141
<b>Figure 4-11.</b>	DHBV DNA quantification in DCPD-transfected (Ad MOI=10) microreactor	142

## List of Tables

<b>Table 1-1.</b> Different proposals for the functional unit of the liver	21
<b>Table 3-1.</b> FACS analysis of DCPD-transfected PRHs 72h following Ad exposure	85
<b>Table 3-2.</b> FACS analysis of DCPD-transfected PRHs 48h following DHBV exposure	96
<b>Table 4-1.</b> Primer/probes designed to amplify different DHBV DNA forms	120
<b>Table 4-2.</b> Experimental timecourse for early and late DCPD transfection in both monolayer and microreactor cultures	140

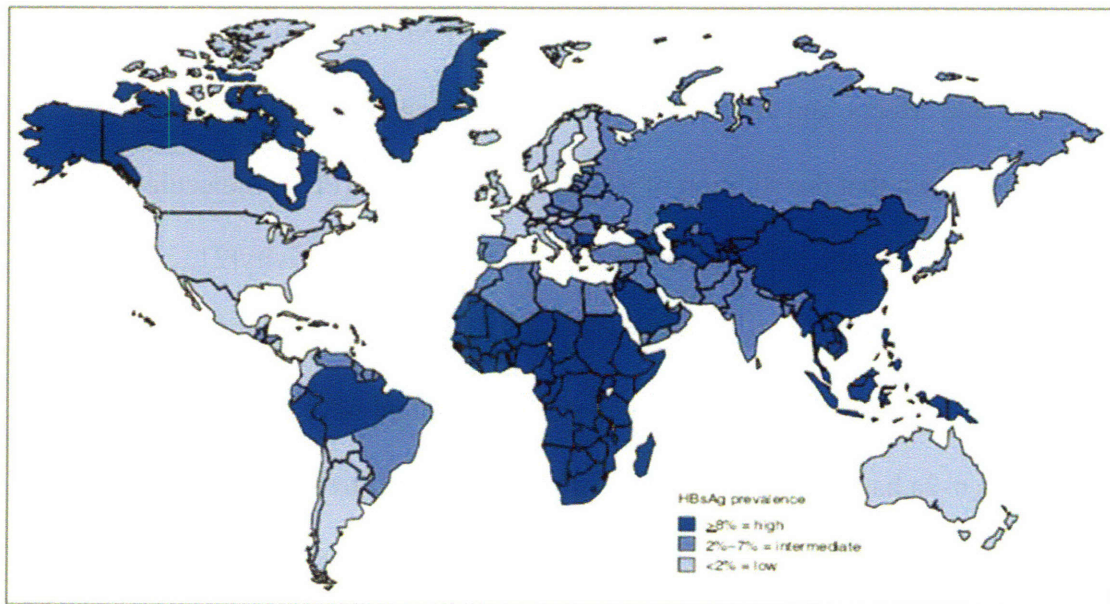
# Chapter 1

## Introduction, Background and Motivation

### 1.1 Global Impact

Human Hepatitis B Virus (HBV) is the prototype member of the family *Hepadnaviridae* that consists of enveloped, partially double-stranded DNA viruses that specifically target cells in the liver for viral replication. Although a vaccine has been available for more than 20 years chronic hepatitis B afflicts ~5% of the world's population (350 – 400 million) [11]. It is estimated that 500,000 to 1.2 million people die each year from HBV-attributable cases of chronic hepatitis, cirrhosis, and hepatocellular carcinoma [12, 13].

In terms of geographic distribution of the chronic HBV infection more than 75% of the world's carriers are located in the Western Pacific and Southeast Asia region which include over 40 countries (Fig. 1-1) [14, 15]. In the U.S. there are ~1.25 million



**Figure 1-1.** Worldwide geographic distribution of chronic hepatitis B virus infection as of 2005. HBsAg is a viral antigen used as a serologic marker to indicate active HBV infection. HBsAg prevalence may vary within countries by subpopulation and locality. Figure taken from [8].

chronically infected individuals and ~one-third will develop clinical complications due to chronic HBV infection [13]. In an effort to assess the economic burden one study estimated that over a 2-year period chronically infected HBV patients spent ~\$40,512 for healthcare services and drugs [16]. Considering the high morbidity and mortality of HBV-related diseases the accumulated costs are substantial. In countries where HBV is endemic the costs are even more significant. A South Korean study estimated that in 1997 \$623.3 million (USD) were spent on HBV disease-related medical costs (~3% of the South Korean national healthcare expenditure for 1997) [17].

## **1.2 Current anti-HBV Therapeutics**

Interferon alpha (IFN $\alpha$ ) is the only agent known to induce long-term remission, characterized by the reduction of viral DNA and hepatitis B e antigen (HBeAg) to undetectable levels in the patient's serum, in ~one-third of patients treated over a course of 4-6 months [18-20]. This naturally occurring cytokine has a dual mode of action; first it inhibits viral replication; and second it enhances the immunological response of the host against the virus. The disadvantages associated with IFN $\alpha$  include a limited efficacy rate, undesirable side effects, and an inconvenient dosing regimen (3 injections per week). Studies have shown that the addition of a polyethylene glycol (PEG) molecule to IFN $\alpha$  significantly increases the half-life and leads to more sustained activity[21, 22]. This prolonged half-life results in the need for only one injection per week. Among the two pegylated IFNs (peginterferon  $\alpha$ -2a, peginterferon  $\alpha$ -2b) that have been studied, peginterferon  $\alpha$ -2a has been approved for chronic hepatitis B treatment in the US.

In addition nucleoside analogues such as lamivudine have been approved for treatment of chronic HBV infection. Nucleoside analogues are synthetic molecules that,

following conversion into nucleoside triphosphate equivalents, compete with natural nucleoside triphosphates for incorporation into viral DNA by the viral DNA polymerase. Since these analogues lack a bond site necessary to link it to an adjacent nucleoside their incorporation effectively terminates the elongation of nascent viral DNA chains and therefore inhibits viral replication. Lamivudine which is administered orally has minimal side effects. However, it does display a modest efficacy rate of 20-30% following a 12 month dosing regimen [23]. Following therapy termination most patients experience a relapse evidenced by the detection of viral DNA and HBeAg in the serum [24]. Continuous lamivudine treatment is necessary for a sustained therapeutic effect. This is a major drawback when combined with the observation that lamivudine-resistant HBV species emerge during long-term treatment [23, 24]. These species have mutations in the YMDD amino acid motif in the HBV DNA polymerase gene. Within 30 months YMDD mutants can make up to 70% of the HBV population [23]. This emergence of YMDD mutants is also associated with relapses [23].

Clinical trials with adefovir dipivoxil, another nucleoside analogue, demonstrated a significant reduction in viral markers in the serum of patients who had developed lamivudine-resistant HBV strains[25, 26]. Entecavir, the latest nucleoside analogue to be approved in the US, has also shown to be efficacious in patients demonstrating lamivudine resistance [27]. The optimal treatment duration, long-term safety, and durability of the response is still being investigated.

Today, combination therapies of the drugs mentioned above are being evaluated as potential treatment strategies [28-30]. However, due to the persistence of HBV in infected patients long-term antiviral therapy is normally required. As mentioned above a patient

undergoing this long-term therapy risks selecting drug-resistant mutant HBV strains and developing progressive liver disease. In-depth analysis of such mutant strains, including their infectivity and replication fitness, has been hampered by the lack of user-friendly cell culture systems and animal models which will be discussed in detail later in the chapter. Understanding the process of selection of drug-resistant mutants is critical to developing a combination therapy that will prevent such drug resistance.

Neither IFN $\alpha$  nor the various nucleoside analogues available represent the final solution for treatment of chronic HBV infection. IFN $\alpha$  has limited efficacy and considerable side effects while nucleoside analogues must be continuously taken and lead to the development of drug resistant mutants. Current therapeutics are the result of research based on the present understanding of certain aspects of the viral life cycle which are manipulable in the laboratory setting. Future antiviral drug therapy is dependent on the development of better cell culture systems. To date, no successful in vitro system has been developed for chronic HBV infection wherein the entire viral life cycle can be studied. More is known about the later events in the viral life cycle (i.e. transcription, encapsidation reverse transcription, virion assembly, export) due to studies in which the viral genome is transfected into established hepatoma cell lines (e.g. HepG2, Huh7). However, there is less understanding of the early stages that include virus attachment, internalization, uncoating, genome repair, and nuclear transport. These cell lines do not mimic natural infection which limits their usefulness. An in vitro system that will allow researchers to target other aspects of the viral life cycle is needed.

Such an in vitro system would incorporate the understanding that the liver's function is connected to the liver's structure. Standard cell culture systems do not

successfully mimic liver structure and fail to maintain liver function. This thesis will detail the development of a user-friendly in vitro system in which the entire HBV life cycle can be studied. A brief review of liver organization will better inform the later discussion of the liver's role in HBV infection. In the rest of this chapter the unique architecture of the human liver, the host organ for HBV will be reviewed. The genomic organization and the protein components of the virus will be summarized. Currently available in vitro models will be surveyed, focusing specifically on Duck HBV (DHBV) which was used exclusively in this thesis research. Finally, the cellular determinants of both the host restriction and tissue restriction of DHBV will be reviewed.

In the subsequent chapters the key features of the three-dimensional microscale bioreactor will be reported. This will be followed by a detailed description of the methods used to cross the species barrier and study DHBV in rat liver cells. Next, efforts to demonstrate that cells maintained in our system remain susceptible to DHBV infection after significant time periods in culture will be described. Finally, the thesis will conclude with a discussion of the significance and future implications of this research.

### **1.3 General Anatomy**

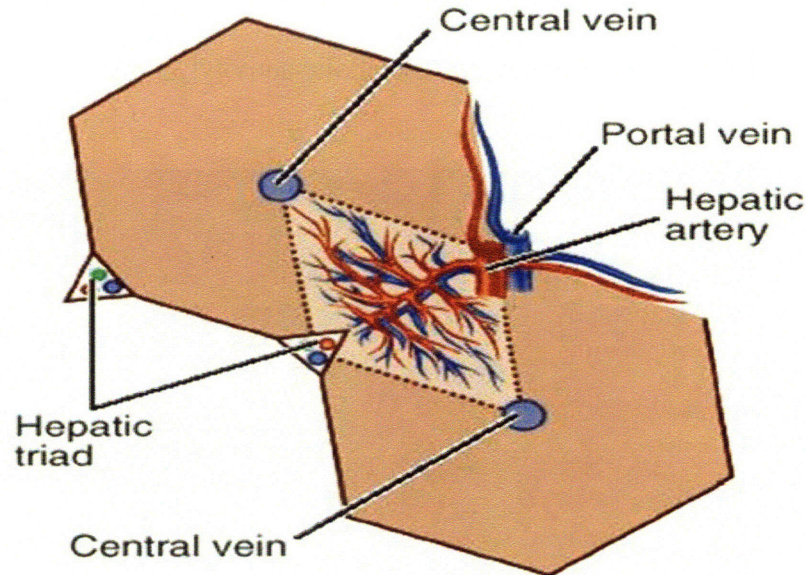
The mammalian liver is an organ whose complex architecture is a reflection of the thousands of vital functions it is required to perform. Macroscopic anatomy divides the human liver into two major (right, left) and two minor (caudate, quadrate) lobes. The liver is supplied with blood from both the portal vein and the hepatic artery. Approximately 80% of the blood entering the liver originates from abdominal tissues (i.e. stomach, intestines, spleen, pancreas). This poorly oxygenated blood travels through the portal vein while the remaining blood is supplied by the hepatic artery. On a microscopic scale these

blood vessels branch off and penetrate through out the liver tissue. Terminal branches of these vessels feed the hepatic sinusoids, fenestrated capillaries which facilitate transvascular exchange between the blood and the functional cells discussed later in this chapter. The blood drains into central veins that eventually merge and empty into the inferior vena cava, a large vein which enters the heart via the right atrium.

Various organizational concepts have been proposed in order to understand both the structural and functional units of the liver. In 1833 Kiernan described the classic hepatic lobule as the structural unit of the liver, the smallest non-repeating structure [31]. Polyhedral in shape, the hepatic lobule consists of a central vein (also known as a terminal hepatic venule) at the center and a portal triad at each corner of the polygonal structure. Each portal triad consists of the portal vein, hepatic artery, and the bile duct (Fig 1-2). As an exocrine gland (which will be discussed later) specific cells within the liver produce bile, a solution composed of detergent-like molecules. The bile is secreted into bile canaliculi, fine canal-like structures. Spread throughout the tissue these structures continually merge to form increasingly larger ducts, culminating in the common bile duct. A portion of this ductwork runs parallel to a branch of the portal vein and the hepatic artery to form a structure known as the portal triad. Single-cell thick layers of hepatocytes form cord-like structures extending from the portal triads to the central venule. Blood entering this unit would travel from the periphery (hepatic artery, portal vein) to the axis where it would drain out through the central vein. In most mammals, the periphery of the hepatic lobule is poorly defined such that the sinusoids from neighboring lobules are connected. Therefore, portal triads are supplying blood to more than one central vein. It was also



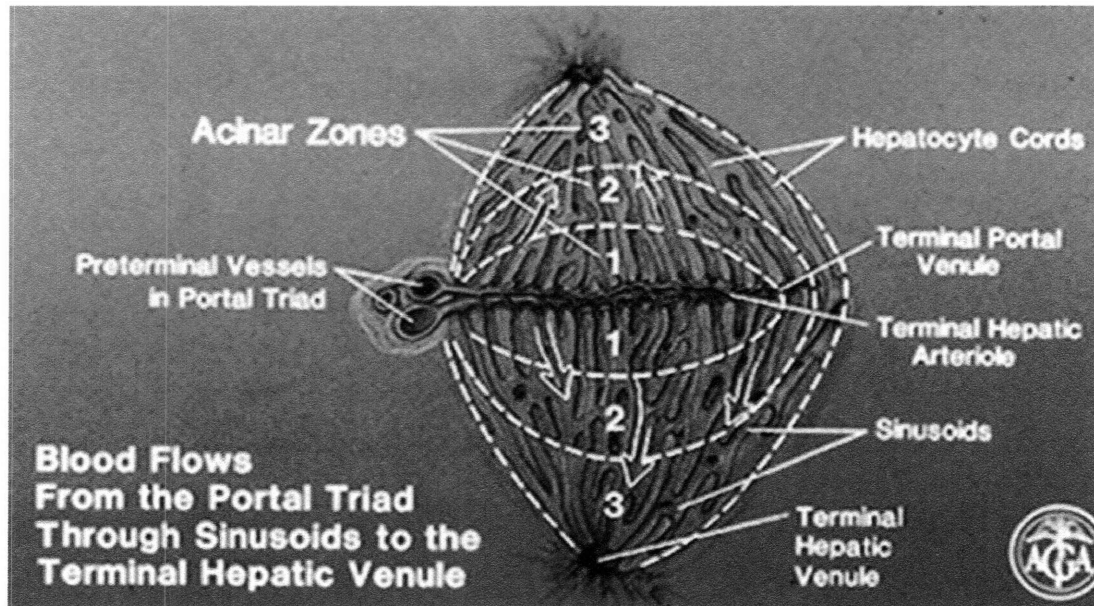
noted that within the same lobule there are differences in oxygenation, metabolic functions, and response to certain diseases depending on the region.



**Figure 1-2.** Classic hepatic lobules are represented by hexagons (solid lines); Rappaport's acinus is represented by rhombus (dotted line). Figure taken from: [http://www.mercksource.com/pp/us/cns/cns\\_health\\_library.jspzQzpgzEzzSzppdocszSzuszSzcnszSzcns\\_health\\_library\\_mainzPzhtm](http://www.mercksource.com/pp/us/cns/cns_health_library.jspzQzpgzEzzSzppdocszSzuszSzcnszSzcns_health_library_mainzPzhtm)

In 1954 this led Rappaport et al. to propose a functional unit of the liver known the acinus [32]. By injecting ink or colored gelatin into the portal vein of various mammals (e.g. rabbit, dogs, humans) they delineated a roughly diamond-shaped area whose four corners consist of two opposing portal triads and two opposing central veins (Fig. 1-2). The axis is formed by a portal tract containing a terminal hepatic venule and hepatic arteriole which branch within the tissue forming sinusoids that eventually drain into the central veins on both ends of the acinus. The acinus is further subdivided into three zones. The zonation reflects the order in which these areas receive blood supply and therefore also reflects different levels of oxygenation. Cells located immediately adjacent to the portal tract (zone 1) receive blood rich in oxygen and nutrients. Zone 2 represents an

intermediate area and zone 3 includes the periphery of the acinus. The greater distance from the incoming blood at the portal tract results in access to less oxygen and nutrients in zones 2 and 3. Hepatocytes located in the different zones have been shown to have different morphology, gene expression, and metabolic activity[33-36].



**Figure 1-3.** Zonation of Rappaport's acinus. Figure taken from [1].

Over the past 30 years several alternative functional units of the liver have been proposed (Table 1-1) because three dimensional studies of lobular angioarchitectures [37, 38] and enzyme distributions [39] have highlighted contradictions to the concept of the acinus.

Taking this additional information into account the functional unit was modified so that now it was actually a subunit of Kiernan's classic hepatic lobule described earlier. In

Evolution of the functional unit of the liver.		
Year	Unit	Proposed By
1665	Lobular architecture	Weppler
1833	Classic hexagonal lobule	Kiernan
1906	Portal lobule	Mall
1954	Liver acinus	Rappaport
1979	Primary lobule	Matsumoto
1988	Single sinusoid	Bloch and McCuskey
1989	Metabolic	Lamers et al.
1989	Zonal circulation	Quistorff and Romert
1993	Choleon	Hofman
1997	Microcirculatory subunit and choleohepaton	Ekataksin and Wake

**Table 1-1.** Different proposals for the functional unit of the liver. Adapted from [2].

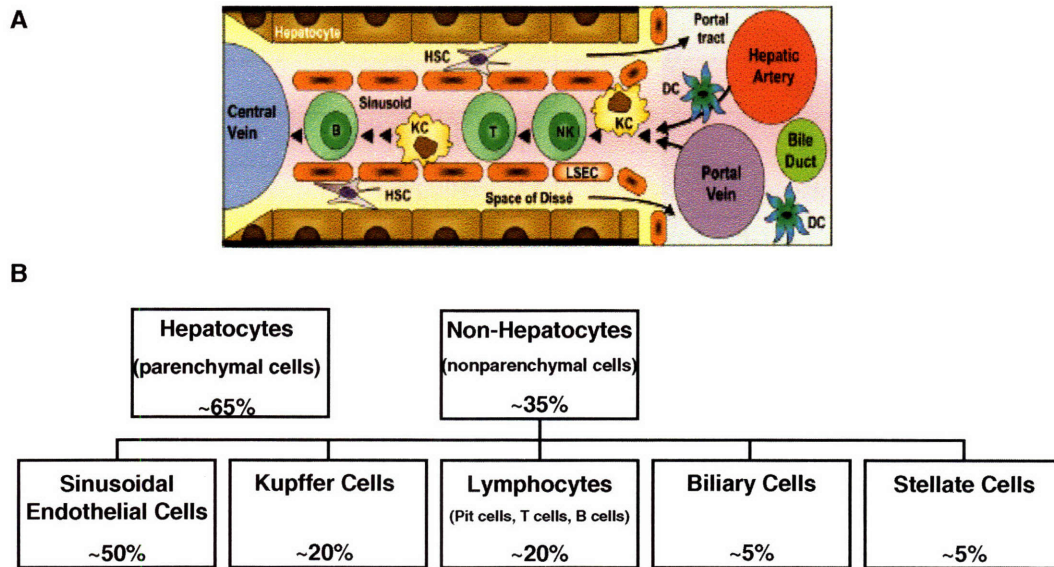
1979 using three-dimensional angioarchitectural reconstructions of human liver

Matsumoto and Kawakami divided each classic lobule into 6-8 cone-shaped primary lobules. The convex surface of the primary lobule is located at the periphery of the classic lobule while the vertex of the primary lobule is located at the central venule (the center of the classic lobule). Other functional units such as the single sinusoid and the choleon are reviewed in MacSween et al. [40]. While the liver has no clear-cut anatomical units, efforts to define such units are useful in understanding the function of the organ in both normal and pathologic states.

#### **1.4 Liver Microenvironments: Sinusoid & Intrahepatic Bile Duct System**

To help illustrate the close relationship between the unique structure and function the main purpose and phenotypic characteristics of each major cell type will be described

in this section. The composition and cellular arrangement within the sinusoidal microenvironment is included in Fig 1-4.



**Figure 1-4.** A) Diagram of sinusoidal microenvironment. B) The percentage of each cell type present in the liver in relation to total number of cells. Image in (A) is taken from [4].

### 1.4.1 Hepatocytes

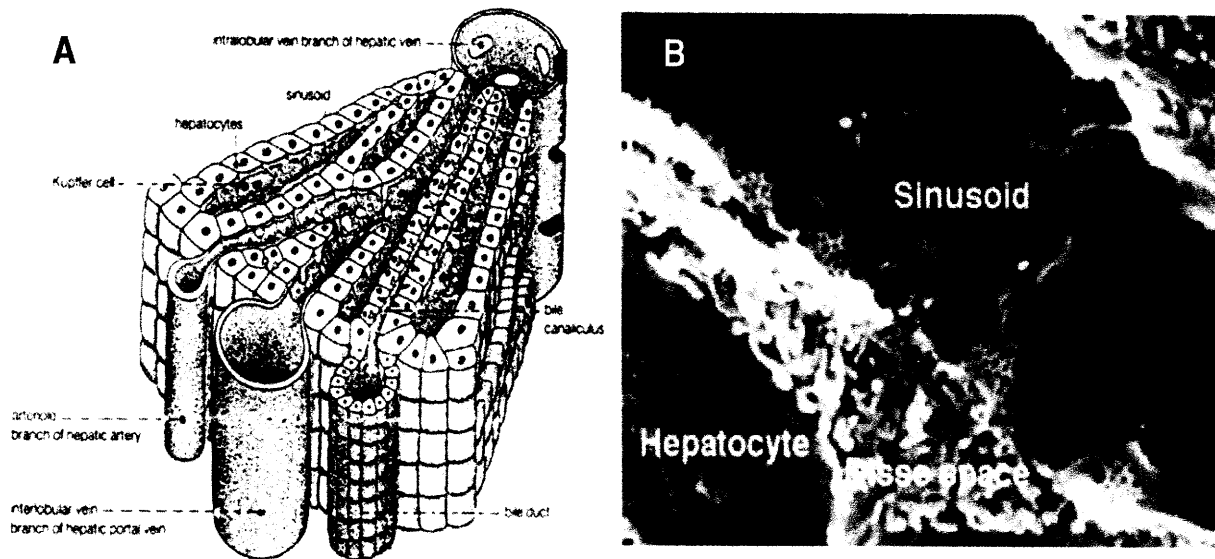
Approximately 65% of the cells in the adult mammalian liver are hepatocytes [41]. These polygonally-shaped cells are arranged in single-cell thick plates which extend from the portal triads to the central vein of the classic hepatic lobule. With regard to surface polarity these cells possess extensive, microvillus-rich basolateral surfaces that take up nutrients and oxygen from passing blood while the canalicular surface, which is ~10% of the hepatocyte surface, is used to secrete bile which aids in the process of digestion. Hepatocyte functions fall into five main categories: 1) carbohydrate metabolism 2) fat metabolism 3) protein metabolism 4) detoxification and 5) storage. One example from the first category is the supplying energy to the organism by the maintenance of normal blood glucose levels. Hepatocytes are able to take up glucose present in the blood following a

meal, store it as glycogen, and later release it when blood concentrations begin to decline. Hepatocytes are also capable of gluconeogenesis, synthesis of new glucose. An example of fat metabolism includes the ability to synthesize cholesterol and phospholipids which is packaged and secreted with lipoproteins which transfer cholesterol between the liver and body tissues. Another important example is the production of bile, a complex aqueous fluid containing water, electrolytes and a battery of organic molecules including bile acids, cholesterol, phospholipids and bilirubin, which all aids in fat digestion as well as elimination of toxic lipophilic compounds. With regard to protein synthesis many blood proteins including clotting factors and albumin are synthesized and secreted by hepatocytes. These cells also remove harmful substances from the blood and break them down or transform them into less harmful compounds. Ammonia, for example, is transformed into urea and excreted into the urine. In terms of storage hepatocytes store fat-soluble vitamins, folate, and minerals such as copper and iron.

#### **1.4.2 Liver Sinusoidal Endothelial Cells**

Based on the brief description of some of the major functions accomplished by hepatocytes it is straightforward to appreciate why about 30% of the total blood passes through the liver every minute [4]. To maximize the access each hepatocyte has to the blood the liver employs a unique microarchitecture. The blood delivered to the liver travels through capillaries known as sinusoids (Fig 1-5). Capillary walls are formed by endothelial cells which comprise ~50% of the non-hepatocyte population in the liver [4]. These endothelial cells have attenuated cytoplasm punctuated with 150 – 175 nm diameter pores known as fenestrae. These fenestrae occur at a frequency of 9 – 13 per  $\mu\text{m}^2$  and occupy 6 - 8% of the endothelial surface using scanning electron microscopy (SEM)





**Figure 1-5.** A) Diagram of sinusoid B) Scanning electron micrograph (SEM) of sinusoidal microenvironment. Fenestrae are  $\sim 100\text{nm}$  in diameter and sinusoid width is  $\sim 5\mu\text{m}$ . Image A taken from [www.tracy.k12.ca.us/thasadvbio/images/sinusoid.gif](http://www.tracy.k12.ca.us/thasadvbio/images/sinusoid.gif) and image B taken from [http://en.wikipedia.org/wiki/Liver\\_sinuosid](http://en.wikipedia.org/wiki/Liver_sinuosid)

[42]. Single-cell thick plates of hepatocytes (i.e. parenchyma) are located adjacent to the sinusoidal wall, separated only by a perisinusoidal space referred to as the space of Disse. There is very little basal lamina associated with the sinusoidal endothelium. Along with the fenestrae it makes the sinusoidal wall a rather permeable structure. Fenestrae are grouped into clusters and act as sieve plates allowing solutes and particles to pass back and forth between the sinusoidal lumen and the space of Disse, thereby gaining access to neighboring parenchymal cells and vice versa. Studies have shown that endothelial cell fenestrae are dynamic structures whose diameter and number can vary in response to factors such as hormones, drugs, hypoxia, virus infection, cirrhosis, fibrosis, and hepatocellular carcinoma [43-50]. In addition to these fenestrae endothelial cells also deliver various macromolecules to the parenchyma via transcytosis. As in Rappaport's

acinus where cells in different zones displayed both morphological and functional heterogeneity sinusoids also demonstrate regional variations. Sinusoids in zone 1 are narrower and more circuitous but become broader and straighter in zones 2 and 3 [51].

### **1.4.3 Kupffer Cells (KCs)**

Within the sinusoidal lumen Kupffer cells, resident macrophages, are amoebid-shaped cells attached to the surface of the endothelium. KCs constitute ~20% of the non-hepatocyte cells in the liver and 80-90% of the tissue macrophages in the body [52]. Viewed as a “front line of defense”, KCs are strategically positioned to encounter foreign particles, tumor cells bacteria, yeast, viruses and parasites in the passing blood. Upon activation by antigen or inflammatory stimuli their major role is the clearance of such material via phagocytosis. KCs are also capable of passing through the space of Disse in order to phagocytose apoptotic hepatocytes. While they are spread throughout the liver there are differences in the population density, cytologic characteristics, and physiologic functions within the different zones of the liver acinus. Larger KCs tend to be located in the periportal region of the acinus where they will encounter incoming pathogen-laden blood [53]. Periportal KCs have been reported to have higher lysosomal enzyme activities and greater phagocytic capacity than the smaller KCs from the midzonal and perivenous regions of the acinus [53]. KCs appear to be derived from bone marrow-derived monocytes circulating in the blood which migrate into various tissues and transform into macrophages [54].

### **1.4.4 Hepatic Stellate Cells (HSCs)**

HSCs, which are also referred to as Ito cells or Fat-storing cells, reside in the space of Disse and account for ~5% of the total cells in the adult liver [55, 56]. In normal liver

they are the principal storage site for vitamin A metabolites within lipid droplets located in the cytoplasm. This storage accounts for 40-70% of the vitamin A within the body [55]. HSCs demonstrate at least two different phenotypic states. In the quiescent state HSCs display a dendritic phenotype in which long cytoplasmic extensions that contact both the neighboring hepatocytes and the adjacent LSECs. These extensions, which vary in range from 60-140  $\mu\text{m}$ , modulate sinusoidal blood flow via contraction and relaxation [57, 58]. Other quiescent activities include synthesizing and releasing extracellular matrix (ECM) components and metalloproteinases, and erythropoietin synthesis. HSC activation following liver injury results in the transformation to the second phenotype and results in changes in the gene expression profile, change from a dendritic-like to a fibroblast-like shape, and a loss of vitamin A-containing lipid droplets [59, 60]. HSC activation is triggered by multiple cytokines and stimuli provided by various cells including hepatocytes, KCs, LSECs, and infiltrating inflammatory cells [57]. Activated HSCs orchestrate the wound healing response.

As with other cell types within the liver, HSCs demonstrate intralobular heterogeneity with smaller, simpler HSCs present at the periphery of the lobule and larger HSCs with more numerous cytoplasmic extensions toward the center of the classic lobule [58]. Vitamin A storage also appears to demonstrate a zone-dependent distribution [58]. Following the resolution of the liver injury it has not been conclusively determined whether activated HSCs revert to the quiescent phenotype or are cleared by apoptosis. However, increasing evidence points to the role of apoptosis in the elimination of activated HSCs [61, 62].

#### **1.4.5 Pit Cells**



Pit cells are located inside the sinusoidal lumen where they adhere to both the KCs and the LSECs. Morphologically, these cells are defined as large granular lymphocytes (LGLs) that are characterized by spherical dense granules and rod-cored vesicles [63, 64]. Functionally, they are defined as natural killer cells that kill target cells by several mechanisms that include the release of cytoplasmic granules containing perforin and granzyme that lyse cells via osmotic rupture, induction of death receptor-mediated apoptosis, and augmentation of other immune cells through interferon-gamma production [63]. Pit cells display a high level of natural cytotoxicity against a variety of tumor cell lines indicating their role in the prevention of metastasis and the suppression of tumor initiation within the liver [63, 65].

#### **1.4.6 Cholangiocytes**

After bile is initially secreted into the bile canaliculus (formed by two adjacent hepatocytes) it travels through ductules formed by cholangiocytes. These biliary epithelial cells are organized into a three-dimensional network of interconnecting ducts of varying size (Table). These cells account for 3-5% of the total liver cell population [66]. In the smaller ductules the cholangiocytes are roughly cubic but as the ductules become larger the cholangiocytes are more columnar in shape. Other morphological differences include the observation that small cholangiocytes have a larger nucleus to cytoplasm ratio which suggests that they are more undifferentiated cells in comparison to large cholangiocytes [67]. Cholangiocytes also display functional heterogeneity. As the bile travels through the duct network it is modified by a series of regulated reabsorptive and secretory events before eventually reaching the small intestine. Small and large cholangiocytes express different enzymes and membrane transporters [68, 69]. The large cholangiocytes which

form the larger ductules have been shown to respond to certain hormones while the small cholangiocytes do not respond which suggests that the small cholangiocytes may form more passive duct structures that deliver the bile from the bile canaliculus to the large hormone-responsive ducts where it is actually modified [70]. However, small cholangiocytes have been shown to compensate for the loss of large cholangiocyte function in certain injury models [67]. The biliary epithelium also demonstrate specific compartments that differentially respond to injury, hepatic toxins, or dietary regimes although the mechanisms by which this occurs are undefined [71-73].

### **1.5 Interactions within the Sinusoidal Microenvironment**

In standard in vitro systems it has been observed that hepatocytes progressively lose a number of liver-specific functions. This dedifferentiation is a result of changes in gene expression and diminished transcription of relevant liver-specific genes. Underlying factors include the ischemia-perfusion stress induced during the isolation process, the disruption of the normal tissue architecture, and the adaptation to the in vitro environment. An in vitro environment that restored fundamental aspects of normal tissue architecture would go a long way in maintaining the liver phenotype.

Normal tissue architecture maintains the various liver phenotypes via cell-matrix interactions, paracrine signaling, and cell-cell interactions within the sinusoidal microenvironment. The loss of such interactions leads to the loss of cellular phenotype and function. Therefore, as highlighted in this section it is important for an in vitro culture system to replicate the critical sinusoidal environmental cues in order to maintain proper cellular function.

#### **1.5.1 Cell-Matrix Interactions**

The sinusoidal surface of hepatocytes are in contact with various extracellular matrix (ECM) components that include type IV collagen, laminin, fibronectin, and heparin sulfate proteoglycans that are located in the space of Disse. When absent from the microenvironment hepatocytes will produce ECM constituents in a negative feedback fashion [74]. Hepatocytes isolated from the liver and cultured on ECM-derived gels have been shown to maintain a differentiated phenotype, expressing liver-specific mRNAs such as serum albumin [75, 76]. Freshly isolated rat heps isolated on Matrigel, a solubilized basement membrane preparation, regained mRNA expression for several constitutive cytochrome P450 (CYP450) proteins, metabolism enzymes used to detoxify and eliminate foreign chemicals introduced into the body [77]. Phenotypic changes occur in various liver cells when there are changes in the microenvironment. For example, during fibrogenesis wherein normal low-density basement membrane in the space of Disse is converted to high-density interstitial type matrix LSECs deposit ECM components and cytokine-activating factors and stellate cells become activated [55]. These results demonstrate the importance of cell-matrix interactions for homeostasis and therefore, the importance to mimic such interactions in an in vitro liver analog.

### **1.5.2 Soluble Ligands**

The coordination of various liver functions requires intercellular communication that is mediated by various molecules including hormones [78, 79], eicosanoids [80-82], reactive oxygen species [52, 83], and cytokines [80, 84]. Liver regeneration following injury (e.g. partial hepatectomy) utilizes multiple interconnected networks of cytokines, growth factors, and metabolic pathways to restore the original organ mass [85]. It has been shown that NPCs synthesize various cytokines and growth factors while hepatocytes

express a variety of receptors for these molecules. Therefore, it is crucial that any in vitro system that aims to reconstruct the sinusoidal microenvironment will need to incorporate these soluble ligands. Adding such ligands directly to the cell culture media is not always ideal since the precise role and concentration of individual ligands are not completely understood. Other approaches have investigated co-culturing hepatocytes with non-parenchymal cells in physiological ratios [86].

### **1.5.3 Cell-Cell Interactions**

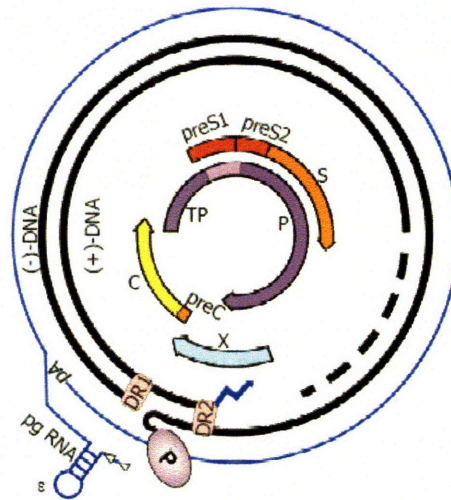
Three main types of cellular junctions include anchoring junctions (adherens junctions & desmosomes), occluding junctions (tight junctions), and communicating junctions (gap junctions). Homotypic interactions within non-parenchymal cell populations vary such that Pit cells display no physical interaction, Kupffer cells demonstrate no physical interaction, LSECs have poorly-defined cellular contacts with each other at their periphery, and stellate cells are interconnected via anchoring junctions and communicating junctions [87]. Hepatocytes demonstrate an abundance of cell junctions which emphasize the need for mutual cooperation in the execution of liver-specific function. Hepatocyte-specific functions that have been shown to require the presence of either adherens junctions or gap junctions include albumin secretion [88, 89], ammonia detoxification [90], glycogenolysis [91], bile secretion [92-95], and xenobiotic biotransformation [96-98]. In order to isolate hepatocytes for in vitro culture the liver is normally subject to the two-step collagenase perfusion technique which chemically and mechanically disrupts normal cell junctions. Efforts to reestablish these junctions in vitro include continuously rotating hepatocytes in suspension or using cell-repelling substrata in order to form multicellular aggregates known as spheroids. Co-culturing has also been

explored [99]. These cell-cell contacts are prerequisites to successfully imitate the natural sinusoidal microenvironment and therefore retain liver-specific function.

## 1.6 Hepatitis B Virus

### 1.6.1 Genome Organization

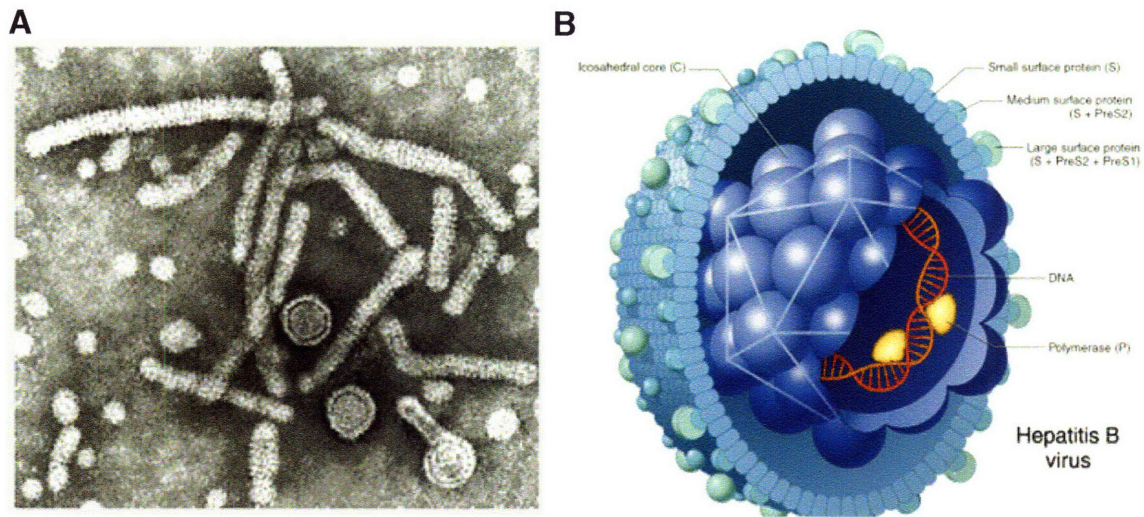
The genome located in infectious human HBV particles is a 3.2kb relaxed, circular, partially double-stranded species (Fig. 1-6). Cohesive 5' ends maintain the circularity of this species. This asymmetric genome includes a minus strand that is unit length and has a protein covalently bound to its 5' end and a plus strand that is less than unit length and has a capped oligoribonucleotide at its 5' end. Although the plus strand has a fixed 5' end the



**Figure 1-6.** HBV genome organization. Relaxed, circular, 3.2kb, partially double-stranded species includes four overlapping open reading frames. Taken from [3].

3' end is variable such that the genome contains a single-stranded region of variable length. The genome is highly compact such that every nucleotide is located within a coding region and more than half the nucleotides are translated in more than one open reading frame (ORF). The genome contains 4 overlapping ORFs: the P ORF that encodes the viral polymerase/reverse transcriptase, the C ORF that encodes the core protein that

forms the nucleocapsid, the S/preS ORF that encodes the envelope glycoproteins, and the X ORF that encodes the X protein whose precise function is not completely elucidated. The main functions of these proteins will be briefly reviewed in the following sections.



**Figure 1-7.** A) Scanning electron micrograph of different HBV particles present during natural infection. Taken from <http://biology.kenyon.edu/slenc/bio38/scuderi/hbv3b.gif>. B) Diagram of Dane particle (infectious particle). Taken from <http://www.rit.edu/~japfaa/HBV.jpg>

### 1.6.2 Envelope Proteins

Cells Infected with HBV produce three types of virus-related particles that include 42nm double-shelled infectious particles referred to as Dane particles, 20nm spheres, and 20nm diameter filaments of variable length (Fig. 1-7). The envelope of all three particles contain three surface glycoproteins and host-derived lipoprotein. The three glycoproteins are all expressed from a single open reading frame. The domain present in all three glycoproteins is referred to as the S domain. The small envelope protein (S) consists of only this 226 amino acid (aa) domain. The two larger envelope proteins contain additional N-terminal domains created by initiation at upstream start codons. The middle envelope protein (M) contains an extra 55 aa domain referred to as preS2. The large envelope

protein (L) contains preS2 and a unique 108 or 119aa domain referred to as preS1. Dane particles contain S, M, and L proteins with M and L present in roughly equal amounts constituting ~30% of the envelope protein content [100]. Sphere particles contain mainly S and M proteins while filaments contain a greater amount of L protein [101]. All three envelope proteins are glycosylated and display a complex transmembrane topology. Interestingly, the L protein demonstrates two different conformations. In the i-preS conformation both preS domains are located in the cytosol while in the e-preS conformation the preS domain are located within the ER lumen of the host cell. Studies have shown that the i-preS conformation is essential for nucleocapsid envelopment [102, 103]. Following translation ~50% of the L proteins switch from the i-preS conformation to the e-preS conformation [104, 105]. In the e-preS conformation the preS domains are exposed on the virion surface and participate in virus receptor binding which will be discussed further in Section 1.7.1.1. The mechanism behind the change in conformation is not well understood but is thought to involve molecular chaperones that include cytosolic Hsc70 and Hsp40 [106]. Studies have also shown that the L protein is myristylated which is not required for virion assembly but is required for infectivity [107-109].

### **1.6.3 Core Protein**

The icosahedral viral capsid is formed by multiple copies of a single protein (C protein; 183 or 185 aa depending on genotype). Assembly requires the initial formation of dimers of core protein stabilized by two disulfide bonds. The final capsid, held together by weak interdimer interactions, appears as two different types that are both found in infected human liver [103]. One type has 90 dimers with a diameter of 30nm and icosahedral T = 3 symmetry. The other type has 120 dimers with a 34nm diameter and icosahedral T = 4



symmetry. The capsid shell is fenestrated with pores ranging from 12-15 Å diameter which allows the free diffusion of nucleotides into and out of the nucleocapsid lumen. An arginine-rich domain located in the C-terminus has been shown to be required for viral nucleic acid packaging implying that this domain is present in the lumen of the fully-assembled nucleocapsid [110]. However, it has been demonstrated that trypsin can remove this domain from ~50% of the C protein chains in recombinant HBV capsids [103]. This suggests the possibility that while some of the arginine-rich domains are located in the lumen another portion of these domains are present on the outer surface of the nucleocapsid.

#### **1.6.4 Viral Polymerase**

The HBV Polymerase (P) is a multifunctional protein that consists of four domains that include the amino terminal protein (TP), the spacer, the polymerase/reverse transcriptase (RT), and the C-terminal RNaseH domain. The RT catalyzes RNA and DNA-dependent DNA polymerization, the RNase H functions to degrade RNA from the RNA-DNA duplexes generated during viral DNA synthesis, the TP is a protein primer necessary to initiate reverse transcription, and the spacer is a highly variable, nonessential tether between the TP and the RT domains [3, 111]. The rate of virion production is estimated to be on the order of  $10^{11}$  virions per day while due to the lack of proofreading/editing ability the error rate of the HBV P has been calculated as  $10^{-7}$  per nucleotide per day [112, 113]. Due to these factors viral populations within the host are a heterogeneous mix known as quasi-species. As mentioned earlier (Section 1.2), mutations in the YMDD motif located in the P gene leads to lamivudine-resistant virions.

#### **1.6.5 HBx protein**



This protein was originally termed X because its unknown function and lack of homology with known proteins. The HBx protein has a molecular mass of 17.5kDa. Little else is known about the protein structure because there is no crystal model currently available. While the precise function is unresolved the HBx protein is regarded as a multifunctional viral regulator that has been shown to transactivate the transcription of a wide range of viral and cellular genes, to stimulate various cytoplasmic signal transduction pathways, and to induce liver cancer in transgenic mice. Some studies have shown that HBV replication is observed both with wildtype HBV and X-defective mutants in both Huh7 and primary rat hepatocyte in vitro culture, suggesting that HBx is not essential for the viral life cycle [114-116].

### **1.7 Animal Models**

Besides humans, chimpanzees are the only animal that is fully permissive to infection by human HBV [117]. Research using chimpanzees has been crucial in safe vaccine development, evaluation of therapeutic agent efficacy, and elucidation of the immune response [117]. There is accumulating evidence of hominoid primates (e.g. gibbons, orangutans, and rhesus monkeys) being susceptible to human HBV but due to the large size, cost, and ethical constraints their use is limited [11]. Based on their phylogenetic closeness to primates and their adaptability to the laboratory environment, tree shrews have been tested for their susceptibility to HBV. Inoculation with HBV-positive human serum resulted in evidence of infection (e.g. viral DNA replication in the liver, HBsAg secretion into serum, production of antibodies to HBsAg and HBcAg) [118, 119]. While this infected proved to be inefficient the full potential of this model is still being investigated.

The use of primary human and primate hepatocytes is restricted by multiple experimental limitations including a rapid loss of susceptibility to infection in culture, lot-to-lot variability in susceptibility to infection, and the necessity of treatment with chemical agents such as DMSO for reproducible infection [107, 108, 120]. Permissive cell lines (e.g. HepG2, Huh7) are capable of supporting viral replication upon transfection with the viral genome. HepG2.2.15, a subline of HepG2, is stably transfected with multiple copies of the HBV genome [121]. HepG2.2.15 cells express all viral RNAs and proteins, produce viral genomes, and secrete virus-like particles. These cell lines have shed greater light on the later events in the viral life cycle (i.e. transcription, encapsidation reverse transcription, virion assembly, export). However, there is less understanding of the early stages that include virus attachment, internalization, uncoating, genome repair, and nuclear transport. These cell lines do not mimic natural infection which limits their usefulness. An in vitro system that will allow researchers to target other aspects of the viral life cycle is needed.

Recently, a cell line known as HepaRG was shown to be susceptible to infection under certain conditions. In the presence of PEG, DMSO, and/or hydrocortisone HepaRG cells exhibit hepatocyte-like morphology, express liver-specific functions (e.g. albumin, aldolase B, CYP3A4), and demonstrate phase I and phase II drug metabolism enzyme activity in the range of normal human hepatocytes [122]. DMSO and hydrocortisone are known inducers of cell differentiation although the underlying mechanism is not known.

Since human HBV demonstrates such a narrow host range with limitations in the previously described models other hepadnaviruses in their natural hosts were investigated. With regard to other non-primate hepadnaviruses none have been found in commonly used laboratory animals such as mice and rats. Research led to the discovery of a hepatitis B

virus in the North American woodchuck. Woodchuck hepatitis B virus (WHV) is ~60% similar to human HBV, it causes chronic hepatitis and hepatocellular carcinoma [123]. This model is useful in studying the fundamental pathogenetic and therapeutic aspects of hepadnaviral infection. Disadvantages of this model include difficulty in handling the animals, difficulty in breeding these animals in captivity, outbred animals that are frequently used are usually infested with other pathogens, and that no experiments can be performed while these animals hibernate. Another disadvantage is the current lack of cell lines that efficiently support replication of cloned WHV DNA. A review of this model is available elsewhere [124].

Hepadnaviruses are subdivided into two categories based on sequence homology; orthohepadnaviruses which infect mammals and avihepadnaviruses which infect birds. Duck HBV (DHBV) was the first avihepadnavirus detected while others have been isolated more recently from grey herons, snow geese, white storks, and cranes. Avihepadnaviruses share little sequence homology with orthohepadnaviruses (~40%). DHBV expresses two major envelope proteins (instead of three) (Section 1.6.2). Similar genome organization, virus structure, and replication characteristics among hepadnaviruses warrant the study of hepadnaviruses found in other species. Many of the principles of hepadnavirus life cycle were elucidated by studying duck hepatitis B virus (DHBV) as a model for HBV. Elucidated principles include the replication by reverse transcriptase [125], cccDNA formation [126], and host-range determinants [127-129]. However, reproducible in vitro infection of primary duck hepatocytes requires culture conditions that incorporate 1.5-2% DMSO whose mechanism of action is unknown [130, 131]. Even with

such artificial additives the kinetics of in vitro infection are slow and inefficient when compared to in vivo infection of neonatal ducklings [132].

### **1.7.1 Host Specificity**

Viral infection begins with the attachment of the viral particle to its receptor/complex on the surface of the host cell. Following receptor binding the enveloped virus is taken into the cell via receptor-mediated endocytosis. Escape from the late endosomal compartment results in the release of the viral nucleocapsid into the cytoplasm. The nucleocapsid is transported to the host cell nucleus whereupon the viral DNA is released into the nucleus. Once inside the nucleus host cell machinery convert the viral DNA into cccDNA which will serve as a master template for all subsequent viral transcripts. As mentioned earlier one of the defining characteristics of all hepadnaviruses is a narrow host range such that only the natural host and those closely related species are susceptible to infection. However, this restriction is not observed when viral genomes are artificially delivered to the nuclei of cell lines derived from a normally non-susceptible species. One interpretation is that it is an early life cycle event (i.e. attachment, entry, fusion) determines the host range for the hepadnavirus and the cellular factors that facilitate later events (i.e. viral genome replication and viral assembly) are not host range determinants. Support for this interpretation comes from a study in which DHBV particles were able to bind to Pekin duck hepatocytes (natural host) but were unable to bind to cells that are not susceptible to DHBV infection including Pekin duck fibroblasts, chicken hepatocytes, and Muscovy duck hepatocytes [133]. The difference in susceptibility corresponded to a difference in the ability to bind the DHBV particles which points to an

early life cycle event such as virus attachment to a cell surface receptor being the host range determinant.

#### **1.7.1.1 Duck Carboxypeptidase D (DCPD)**

To identify possible hepatocyte surface molecules that facilitate viral uptake several groups have studied DHBV infection in ducklings and primary duck hepatocytes (PDH).

Ideally, one would like to do these studies using HBV in human hepatocytes.

Unfortunately, primary human hepatocytes are poorly available and inefficiently susceptible to infection using standard culture methods. Viral infections of the duck model are well-established. Finally, due to the similarity in genome organization and virus structure among hepadnaviruses it has been assumed that they use comparable mechanisms to penetrate the host cell.

DHBV expresses two envelope proteins from a single ORF [134]. The hepatocyte receptor binding domain has been localized to the amino terminal portion of the large (L) envelope protein, a domain usually referred to as “preS”. This domain is not present in the small (S) envelope protein. The S envelope protein is not essential for infectivity [135].

Different groups have identified a 170kDa (p170) or 180kDa (gp180) glycoprotein that binds the preS region of the DHBV large envelope protein [127, 136]. This interaction was shown to be species-specific since the preS region of the HBV large envelope protein failed to bind p170 [127]. Mutagenesis studies using terminally-deleted preS mutants revealed that p170 binds to a stretch of amino acids in a highly conserved region in the preS sequence (aa 87-102) that includes a major neutralizing epitope (site that inhibits viral replication when masked by antibodies). Others studies with substitution mutations identified a larger area of the preS region (aa 43-108) as being involved in gp180 binding.

In more recent studies, the apparent conflict was resolved by using surface plasmon resonance analysis with immobilized DHBV preS polypeptides and soluble duck CPD (aka gp180) to demonstrate that within the larger interaction domain (aa 30 -115) of the preS region that binds gp180 there is a core domain (aa 85-109) that is essential for binding and an N-terminal region (beginning with aa 30) that stabilizes the gp180/preS complex [137]. In addition, they also determined a single preS polypeptide binds to a single sdCPD molecule (1:1) with a dissociation constant,  $K_d=4.6 \times 10^{-8} \text{M}$ .

Sequencing of a gp180 clone predicts a 150kDa non-glycosylated protein with thirteen potential sites for N-linked glycosylation [128]. Significant sequence homology was found between gp180 and members of the basic carboxypeptidase family; particularly carboxypeptidase H (CPB-H). gp180 is approximately three times the size of CPB-H and thought to consist of tandem carboxypeptidase homology domains. Basic carboxypeptidases specifically remove basic amino acids (e.g. lysine, arginine) from the COOH terminus of polypeptide chains. gp180 is now designated as duck carboxypeptidase D (DCPD). Of the three carboxypeptidase-like domains identified within DCPD, the first and second domains were shown to demonstrate enzymatic activity [138]. The third domain, which has been shown to be highly conserved (~82%) among the rat and human homologs of DCPD, is enzymatically inactive but binds the preS region of DHBV [138].

Various studies give evidence to support DCPD as the host cell receptor for DHBV. Reconstitution experiments demonstrated that certain cell lines (e.g. 293 (human embryonic kidney cell line), COS (monkey kidney cells), LMH (chicken hepatoma cells)) transfected with DCPD are able to bind and internalize DHBV particles [139]. However,

no viral replication was observed in DCPD-reconstituted LMH cells which, prior to reconstitution, are normally permissive for DHBV replication when transfected with cloned DHBV DNA [139]. Neutralizing antibodies against the DCPD contact site of the preS region of the viral envelope protein inhibit DHBV binding to DCPD-reconstituted cells. PreS peptides covering the DCPD binding site were also shown to inhibit DHBV infection of PDH as well as block DHBV binding to DCPD-reconstituted cells [139]. Antibodies generated against a soluble form of DCPD have been shown to inhibit DHBV infection in PDHs [140]. However, it was noted that attempts to block infection with antibodies recognizing only primary sequence elements or denatured soluble DCPD were unsuccessful. These observations suggest that the tertiary or quaternary structure of the virus binding site within the receptor is crucial for virus recognition. Breiner et al. demonstrated that HuH7 cells, which are normally non-permissive for infection, internalized fluorescein-labeled DHBV particles when transfected with DCPD (via a pUC plasmid with CMV promoter) [141]. Confocal microscopy revealed that the viral particles were internalized and in some cases were co-localized with DCPD. None of the cells were productively infected as determined by the absence of core antigen. In the same study, they demonstrated that soluble recombinant DCPD (including only the extracellular domain) is able to inhibit DHBV infection of PDH cultures in a dose-dependent manner. Finally, DCPD has been detected in both tissues capable of DHBV replication and in tissues that have shown no evidence of DHBV replication [127, 136].

DCPD has been found on both internal and surface membranes of PDHs [128, 141]. DCPD localizes to an intracellular compartment rather than the cell surface in PDHs [141]. Further studies using HuH-7 cells confirmed that gp180 localizes to a Golgi-like

compartment. Further mutagenesis studies identified sequences in the cytoplasmic tail of DCPD that are involved in its retention in the trans-golgi network or retrieval from the endosomal-lysosomal pathway [142]. Consistent with its presence in these various compartments, DCPD has been shown to be active within a broad pH range (pH 5-7).

Aware of other viruses (e.g. measles) that down-regulate their host cell receptors, Breiner et al. have found that the DHBV L envelope protein specifically down-regulates DCPD expression in infected hepatocytes [143]. Decreased DCPD expression was found only in liver and not in other tissues. Pulse-chase analysis demonstrated that DCPD was being synthesized at similar rates in both infected and uninfected PDHs. In studies done with HepG2.18 cells (human hepatoma cell line) stably expressing DCPD under control of CMV promoter investigators also found that expression of the L envelope protein resulted in a decrease in DCPD steady-state levels, whereas levels of other Golgi-resident proteins remained unchanged. In their pulse-chase analysis with these L-transfected HepG2.18 cells they found that L envelope protein expression prevented the complete maturation of DCPD, which led to the accumulation of the precursor (p170), which was subsequently degraded. gp180 was localized to perinuclear compartments and occasional small vesicles in DHBV-infected PDHs that were induced to overexpress gp180. DHBV L protein showed a similar cellular distribution in a parallel experiment. According to the authors, these results support the hypothesis that the DHBV L envelope protein binds gp180 in a pre-Golgi compartment, thereby preventing its maturation (leading to degradation). The down-regulation of the host cell receptor in DHBV-infected cells could serve several purposes that include preventing gp180 from inappropriately interacting with maturing progeny virions which have to traffic through the same secretory pathway. Another reason



to down-regulate gp180 would be to prevent the re-infection of cells that are already infected.

The aforementioned body of evidence does point to DCPD being necessary for DHBV susceptibility. However, as mentioned earlier in this section the non-susceptibility of DCPD-transduced cell lines that are normally permissive for viral replication indicate that DCPD is not sufficient to re-establish susceptibility. One possibility is that DCPD is but one component of a receptor complex that the large envelope protein interacts with on the host cell surface. One or more additional factors could be necessary to confer DHBV susceptibility. Another possibility is that DCPD is both necessary and sufficient to overcome the host specificity constraint and that other liver-specific factors (e.g. transcription factors) are necessary for the complete viral life cycle to take place. The following section will review some of the evidence that points to the necessity of a more differentiated liver phenotype for productive DHBV infection.

### **1.7.2 Liver Specificity**

In terms of other cellular molecules that may be involved in binding DHBV, Li et al. have identified a 120kDa non-glycosylated protein (p120) that binds cleaved DHBV preS polypeptides with high affinity [144]. While not proven to occur in vivo, such cleavages are possible. The p120 binding motif covers a neutralizing epitope and is conserved among all DHBV strains that have been sequenced. Further importance of p120 binding was established by the reduced infectivity of DHBV with mutations in the preS region that binds p120. Increasing doses of synthetic preS peptides that bind p120 reduced DHBV infectivity of PDHs but not as effectively as preS peptides that bind DCPD which may reflect a sequential interaction with dCPD followed by p120. Finally, the tissue-

specific distribution of p120 matches DHBV hepatotropism. Therefore, depending on the site of cleavage, p120 may be a component of the receptor complex necessary for DHBV infection or an intracellular binding partner that aids in disassembly of viral particles.

More recently, Li et al. have confirmed p120 to be the duck p protein component of the glycine decarboxylase complex (DGD) [145]. Sequence homology, unique binding patterns to truncated DHBV preS and mutants, and identical tissue distribution established that p120 and DGD as the same protein. Although DGD is known to reside on the mitochondrial inner membrane, Li et al. detected it both in the cytoplasm and on the cell surface using indirect immunofluorescence analysis [145]. Studies have also shown a correlation between the loss of susceptibility to DHBV and the loss of DGD expression over time in PDH cultures [146]. Reconstitution experiments in which 17 day-old PDH cultures were transfected with DGD demonstrated increased viral replication markers (e.g. DHBV envelope protein, core protein, viral DNA). Antisense RNA was employed in order to block DGD expression in PDH cultures. The antisense RNA constructs blocked the translation initiation codon of DGD protein which resulted in reduced levels of productive infection markers. DGD antibodies that do not interfere with DCPD binding to the full-length preS domain demonstrated reduced levels of productive DHBV infection markers. The precise role of DGD during the natural DHBV infection process is yet unknown but Li et al propose that it might be involved in the proteolytic cleavage of the viral envelope proteins which is known to occur for many other enveloped proteins within the lumen of the secretory pathway [146]. Since circulating DHBV particles do not display processed envelope proteins they suggest that DCPD serves to direct the particles to the secretory pathway where the large envelope protein may be processed. Following

proteolytic processing the cleaved viral particles may then interact with DGD. However, recently it has been reported that a DHBV mutant with a point mutation R101H is fully infectious even though this mutation abolishes binding to DGD [147].

Tang & McLachlan [148] have also identified liver-enriched transcription factors that support DHBV replication in nonhepatoma cells. Upon transfection of a replication-competent DHBV genome and various liver-enriched transcription factors it was shown that the combined expression of HNF3 and HNF4 support viral replication of DHBV DNA and RNA intermediates. HNF4 $\alpha$  is considered to be a master transcription factor due to its ability to regulate the expression of a disproportionately large number of hepatic genes that include fatty acid, cholesterol and glucose metabolism, urea biosynthesis, apolipoprotein synthesis, liver development, and other transcription factors (e.g. HNF1 $\alpha$  and HNF6) [149-152]. Multiple genes encoding hepatic and pancreatic enzymes, serum proteins, and hormones (e.g. glucagon) have been shown to contain HNF3-binding sites. HNF3 has been shown to play a critical role in the regulation of metabolism and in the differentiation of metabolic tissues including the liver [153].

To conclude, DCPD is necessary for DHBV infection although the exact role for this molecule is not completely understood. It has been shown to act as the attachment receptor which internalizes DHBV particles. Evidence also suggests that there are additional factors necessary to initiate DHBV infection. Likely candidates include DGD and HNF4. Our studies (discussed in Chapters 3 and 4) indicate that these factors restrict DHBV infection to specific tissues but do not necessarily restrict DHBV to a particular host.

## **1.8 Objectives & Specific Aims**

Hepatocytes rapidly lose liver-specific functions in standard in vitro culture systems. Loss of susceptibility to Hepatitis B Virus (HBV) infection, a hepatotropic virus, is attributed to the loss of both the attachment receptor and various liver-specific factors necessary for viral replication. The main objective of this thesis is to test the hypothesis that hepatocytes cultured in a more physiological in vitro culture system, that maintains a more highly-differentiated liver phenotype, remain susceptible to DHBV infection after extended culture periods. Such a demonstration would provide the foundation for the future development of a chronic human HBV infection model in which various aspects of the viral life cycle can be studied and therapeutic targets identified.

DHBV is an ideal virus to employ in this thesis rather than human HBV. Culture conditions have been established to achieve repeatable DHBV infection in primary duck hepatocytes. This system has been used to elucidate various aspects of the hepadnavirus life cycle. One of the most important discoveries is the identification of the host attachment receptor that internalizes the virus. However, culture of primary duck hepatocytes requires the addition of factors such as DMSO and hydrocortisone which maintain a more differentiated state. The mechanism by which these factors bring about such maintenance is also not completely understood. Combined with practical limitations of housing ducks, the use of primary duck hepatocytes is not ideal. Fortunately, earlier studies have demonstrated that freshly-isolated primary rat hepatocytes are capable of supporting DHBV replication upon transfection of the DHBV genome. Our lab has extensive experience in maintaining highly-differentiated primary rat hepatocyte cultures without such additives (e.g. DMSO, hydrocortisone). Therefore, research efforts were

focused on developing strategies to render primary rat hepatocytes susceptible to DHBV infection.

In order to overcome the species barrier it was necessary to give the rat hepatocyte the internalization receptor for the DHBV. Recombinant adenoviruses are commonly used as transgene delivery vectors. Therefore, recombinant adenoviral vectors carrying the attachment receptor for DHBV were generated. Research efforts focused on characterizing the transient receptor expression in order to identify the optimal adenoviral concentration necessary for DHBV infection.

Once cultures were rendered susceptible to DHBV infection it was necessary to measure evidence of DHBV infection. As discussed earlier in this chapter natural DHBV infection presents several challenges to studying in an in vitro culture. Factors including the large ratio of non-infectious subviral particles to infectious Dane particles and the multiple viral DNA forms present during the infectious cycle required several methods to be incorporated in order to convincingly affirm active viral replication taking place.

Finally, this thesis will discuss efforts to compare the ability of different culture systems ability to sustain susceptibility to DHBV infection, once transfected with the attachment receptor. Following extended culture periods (~2 weeks) primary rat hepatocytes maintained in the three-dimensional perfused culture system developed in our lab remained susceptible to infection. This research confirms that after overcoming the species barrier, primary rat hepatocytes are able to support DHBV replication. This represents a novel system in which early events in the life cycle (i.e. prior to viral DNA arriving in the nucleus) can be studied. Extending this research further this system could

be used to study the ability of putative human HBV receptors to initiate viral replication in a highly-differentiated liver phenotype.

## **Chapter 2.**

### **Development of 3D Perfused Liver Microenvironment**

The ongoing goal of this research group is to develop an in vitro system that recreates a perfused liver capillary bed structure in order to study different aspects of liver physiology. To that end, it is necessary to understand the key aspects of the liver microenvironment that need to be mimicked in an in vitro system.

As mentioned earlier there is an unmet need in the field of HBV research for in vitro culture systems that maintain a more differentiated liver phenotype. (mention hepatoma cell lines not being able to be infected) Such a system would facilitate the dissection of the dynamic virus-cell interactions that are difficult to study in whole animal models.

The following chapter briefly reviews the development and characterization of the 3D perfused liver microreactor used in this thesis. The key aspects of the liver microenvironment that will influence the design parameters will be covered. Comprehensive reviews of the design parameters, fabrication, and characterization of the multiple reactor systems are available elsewhere [5, 6].

#### **2.1 Key aspects of the liver microenvironment**

Like most tissues the liver is composed of multiple cell types that are infiltrated by blood vessels. As discussed in Section 1.5 signaling that includes direct cell-cell interactions, cell-matrix interactions, and soluble molecules are necessary to achieve normal tissue function.

A wide array of models exist that culture the different cell types of the liver together in various ratios [154-158]. A crucial feature that many of these models fail to incorporate is physiological perfusion at the length scale of the capillary bed microenvironment.

## **2.2 Fostering tissue morphogenesis in vitro**

It has been shown that within a mixture of various cell types reorganization into a functional tissue will occur given the appropriate length scales and time scales [159-161]. Cell adhesion is one of the key processes underlying the way that cells are organized into tissues. The differential adhesion hypothesis proposed by Steinberg states that when cells of differing adhesive properties are mixed, stronger, more stable interactions will supplant weaker interactions resulting in cells separating themselves into different populations [159, 162]. Those with the strongest interactions will aggregate towards the center of the overall aggregate and the weaker interacting cells accumulating at the surface of the aggregate. These inherent affinity differences can account for the reorganization of cells and tissues that have been disrupted and mixed together in culture. Morphogenesis is also affected by the differential adhesion cell types demonstrate for various matrix substrata. Predominantly mediated by integrins, cell-matrix adhesion can determine the reorganization of multiple cells types based on their differential adhesion to the given substratum present [163].

The design of an in vitro system that fosters the reorganization of dissociated cells into tissue will require some manipulation of these differential cell-cell and cell-matrix adhesion properties. The development of this microreactor focused on the manipulation of homotypic interactions between hepatocytes and the cell-matrix interactions between the

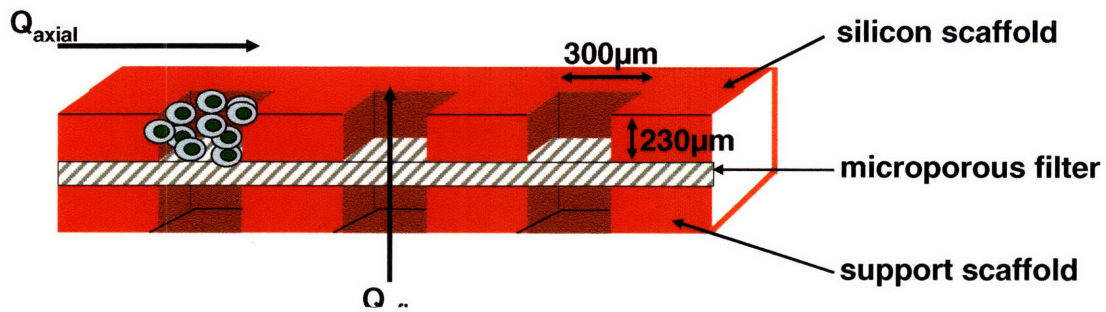


hepatocytes and collagen type I matrix component. The control of heterotypic interactions between hepatocytes and other cell types found in the liver is not addressed. While these non-parenchymal cells are present in the prepared cultures it is likely that they are present at sub-physiological ratios with respect to the hepatocytes. It should also be noted that the development of this system does not attempt to control soluble signaling mechanisms either.

### **2.3 Microscopic design parameters**

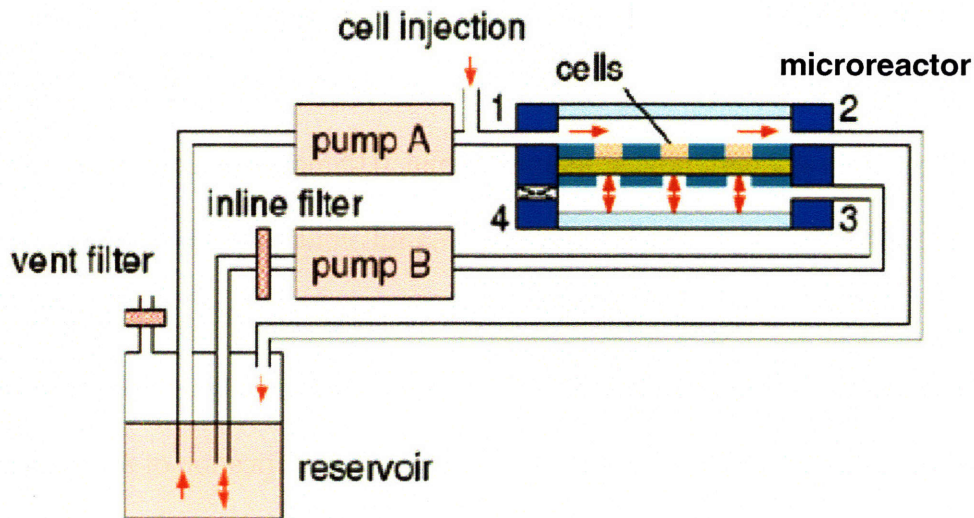
The central part of the in vitro system is the scaffold (~230 $\mu$ m thick) that contains a regular array of channels into which the cells are seeded. Each individual channel represents a functional unit of the microreactor similar to a functional unit of the liver described earlier (Section 1.3). This scaffold is positioned on a microporous filter that is mechanically supported by a second scaffold. Tissue morphogenesis is influenced in the channels of the upper scaffold by several factors that include the adhesion to the channel walls that are coated with collagen (cell-matrix adhesion), the physical dimensions of the channels, and the rate of media perfusion through the channel. The microscopic design parameters are illustrated in Figure 2-1. The cross section of each square channel was set at 300 $\mu$ m as an appropriate length scale to allow for cells to reorganize once seeded into the channels [161]. The depth of the channel (i.e. the thickness of the scaffold) was set at 230 $\mu$ m in order to mimic the length of the hepatic acinus. The depth was also chosen based on the ability of oxygen and various nutrients to penetrate the depth of the tissue using flow rates within the desired operating range. The filter material was used in order to create a large pressure drop across the filter in order to establish a uniform crossflow of media through all the channels independent of the differing number of cells and/or tissue

structures present in each channel. The media crossflow rate was chosen to be  $50\mu\text{L}/\text{min}$  in order to meet oxygen demand throughout the depth of the tissue and to simulate physiological shear stresses. The axial flow was set at  $0.5\text{mL}/\text{min}$  in order to minimize oxygen concentration gradients along the length of the scaffold [6].



**Figure 2-1.** Diagram of scaffold, microporous filter, and support scaffold. Channel dimensions were chosen based on several factors that include the length scales over which cells tend to reorganize, the length of the hepatic acinus, and the ability of oxygen and other nutrients to penetrate the entire depth of the channel. Flow rates were set taking into account oxygen demand of tissue within the channels and the need to stimulate physiological shear stresses.

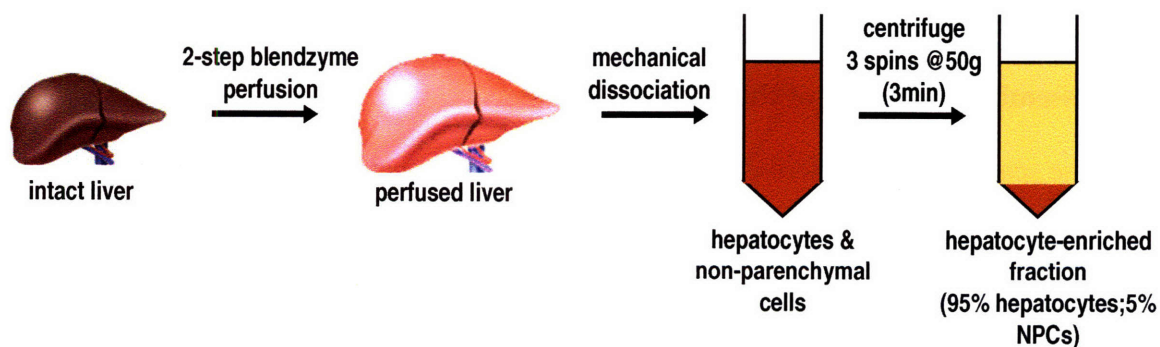
The fluidic system that was employed is diagrammed in Figure 2-2. It features a  $30\text{mL}$  reservoir with a customized lid containing multiple connectors and silicone tubing to attach the microreactor to the reservoir. Two miniperistaltic pumps were employed in order to establish the crossflow and the axial flow in the system. Tubing with different diameter was used in each pump to establish the different axial and crossflow rates.



**Figure 2-2.** Schematic of the microreactor and the fluidic system.

## 2.4 Isolation of primary rat hepatocytes

Figure 2-3 diagrams the procedure used to isolate a population enriched for hepatocytes. Enriched primary hepatocytes were isolated from male Fischer F344 rats (150 – 230g) using a modified version of Seglen’s two-step collagenase perfusion procedure [164] as previously described [165]. Tissue dissociation was accomplished using Liberase Blendzyme 3 (Roche). Final cell viability was  $\geq 89\%$  based on trypan blue exclusion.



**Figure 2-3.** Schematic of isolation procedure for hepatocyte-enriched fraction.

The final cell pellet (~95% hepatocytes) was re-suspended in supplemented DMEM (GIBCO) that includes 0.03g/L proline, 0.10g/L ornithine, 0.305g/L niacinimide, 2.0g/L glucose, 2.0g/L galactose, 2.0g/L bovine serum albumin, 0.05mg/mL gentamycin, 5mg/L insulin, 5mg/L transferrin, 5ug/L sodium selenite, 20ng/mL epidermal growth factor, 1mM L-glutamine, 0.1uM dexamethasone, and trace metals (5.44mg/mL ZnCl<sub>2</sub>, 7.5mg/mL ZnSO<sub>4</sub>·7H<sub>2</sub>O, 2.0mg/mL CuSO<sub>4</sub>·5H<sub>2</sub>O, 2.5mg/mL MnSO<sub>4</sub>) collectively referred to as Hepatocyte Growth Media (HGM). This medium is a minor modification of the medium formulation described by Block and coworkers [166].

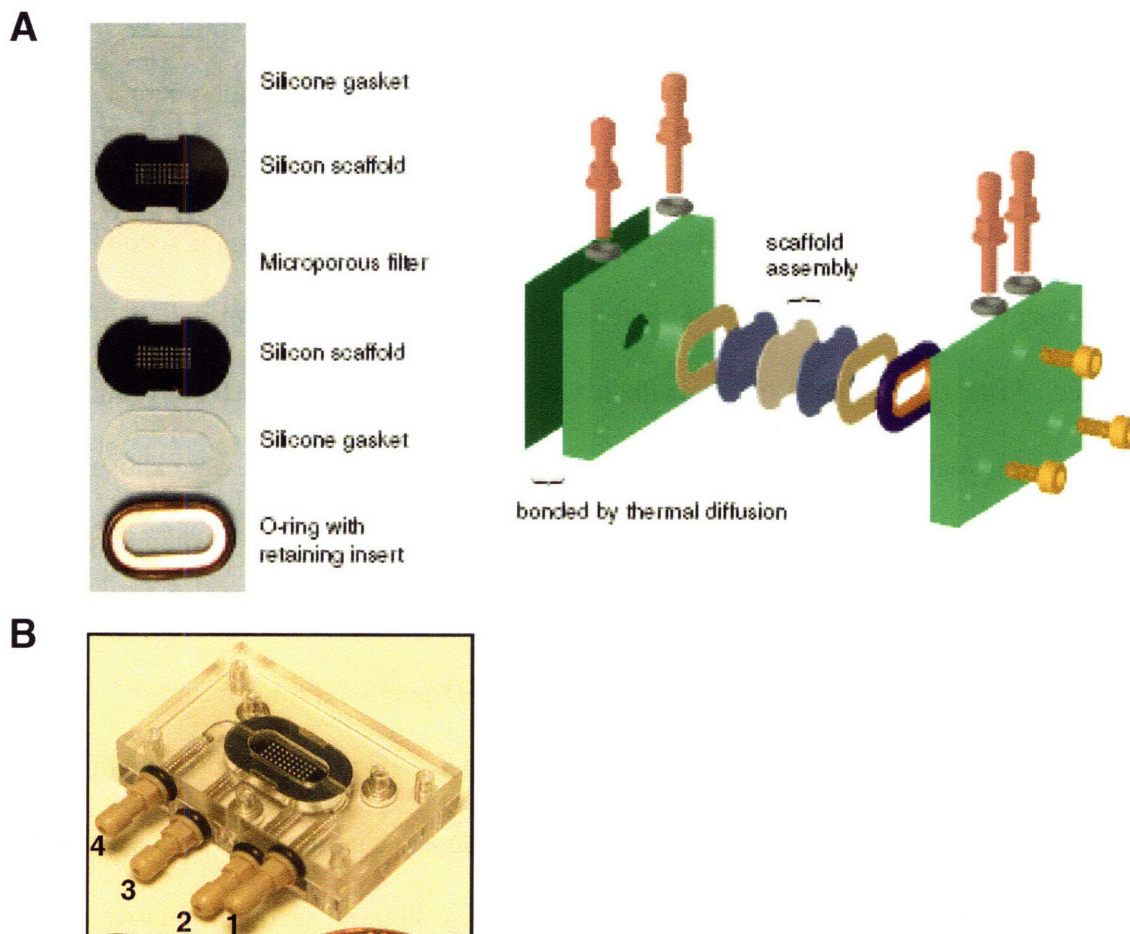
#### **2.4.1 Formation of spheroidal aggregates**

Spheroidal cell aggregates were formed in suspension as previously described [164]. Briefly, freshly isolated hepatocytes were seeded into a 500mL spinner flask (BellCo, NJ, USA) at  $3 \times 10^5$  hepatocytes/mL HGM and cultured on a spinner table at 84rpm (37°C and 8.5% CO<sub>2</sub>) to induce spheroid formation. Following a 24h culture period, 50- to 300- $\mu$ m spheroids were collected by filtering through 50- and 300- $\mu$ m nylon meshes (SEFAR America, Kansas City, MO), pelleting (50xg, 3min), and resuspending in 10 – 15mL HGM. Previous work has shown that a better functional tissue phenotype was achieved by seeding spheroidal aggregates into the microreactor instead of single cell suspensions [9].

#### **2.5 Assembly & seeding of the 3D perfused microreactor**

The scaffold setup described in Section 2.3 is housed between two polycarbonate compartments (Figure 2-4). The design and assembly of the microreactor have been previously described [9, 164]. The assembly protocol used in this thesis is

included in Appendix 1. Following assembly, the microreactor is primed with HGM in order to passivate all the surfaces in the system and to remove air bubbles from all the flow



**Figure 2-4.** A) Schematic of the arrangement of the different components that constitute microreactor. B) Picture of fully-assembled microreactor. Images taken from [6].

paths in the systems. In order to seed the spheroidal aggregates into the fully assembled microreactor a 1-mL syringe was connected to the outlet port of the upper chamber (port#1) (Figure 2-4b) and the peristaltic pump was activated in order to fill the syringe with ~1mL of HGM. A syringe filled with 1-mL of filtered spheroidal aggregates was connected to the inlet of the upper chamber (port#4). The cross-flow tubing was



unclamped and then the spheroid suspension was manually injected into the upper chamber of the microreactor slowly (~0.5mL/min). The spheroidal aggregates go into the channels through a combination of settling and flow of HGM from the upper chamber into the lower chamber. Once the channels are full the resistance to flow in this direction becomes greater than the resistance provided by the syringe attached to the outlet and the piston of the syringe will begin to move. Both syringes are removed and the tubing is reconnected and the media is set to flow in a downward fashion, from the upper chamber to the lower chamber. After 1h, the HGM in the media reservoir is replaced with fresh HGM in order to remove residual cells and cellular debris from the system. Flow rates were chosen based on simulating physiological sheer stress conditions and satisfying tissue oxygen demand (as discussed in Section 2.4). A detailed seeding protocol is provided in Appendix 2.

## **2.6 Evaluation of the hepatic phenotype in the 3D perfused microreactor**

In order to determine the capability of the 3D perfused microreactor to maintain a well-differentiated liver phenotype in vitro it is necessary to characterize various aspects of the liver phenotype such as biochemical production (e.g. albumin secretion), tissue morphology, mRNA expression, and drug metabolism. Such analysis has been published elsewhere [9, 10]. The remaining portion of this section will summarize some of the key findings.

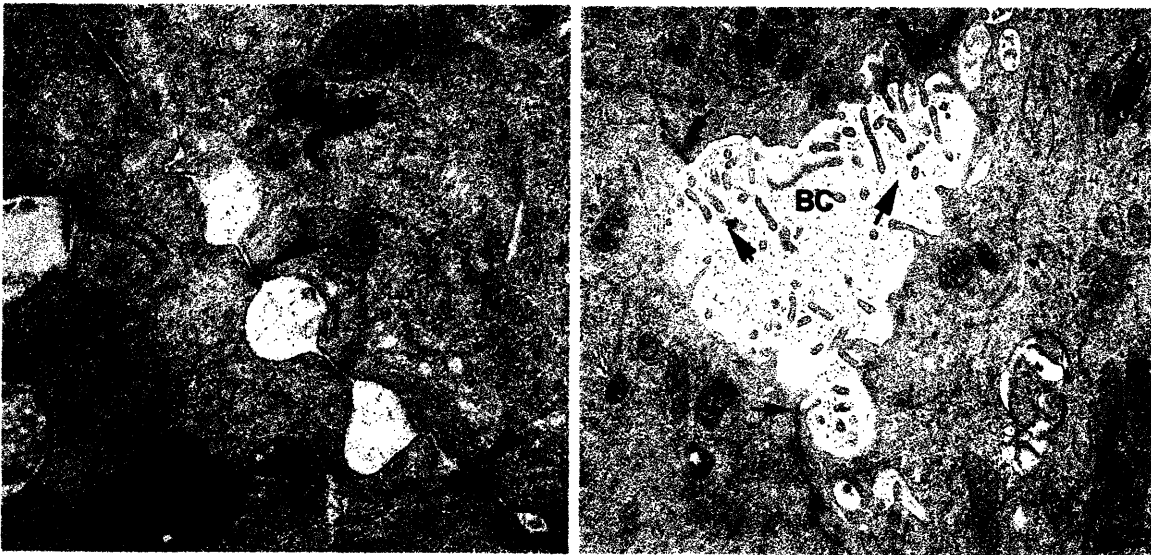
### **2.6.1 Analysis of albumin and urea secretion**

Earlier work was done in the group to evaluate liver-specific function in the microreactor media samples from the reservoir were assayed for both serum albumin and urea[6, 9, 10]. Serum albumin concentrations were determined by a sandwich enzyme-linked immunosorbent assay (ELISA) [167]. Urea concentrations were measured by

Berthelot determination methods (urea nitrogen kit from Sigma, procedure 640). Both the albumin and urea data were normalized to total DNA measured in the microreactor. These analyses revealed a long-term microreactor albumin secretion rate of ~150pg/cell/day and urea synthesis rate of ~700-900 pg/cell/day for reactors seeded with spheroidal aggregates. These rates are an order of magnitude higher than comparable static cultures [9].

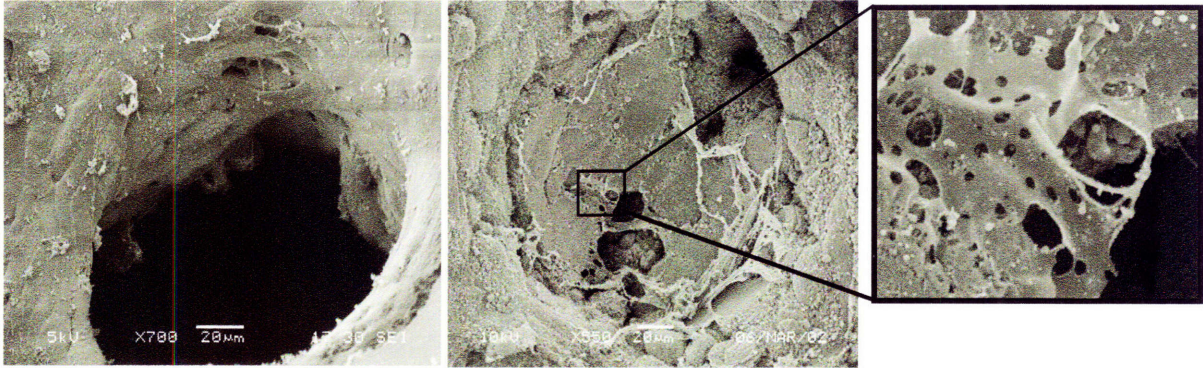
### 2.6.2 Tissue morphological analysis

Figure 2-5 shows representative transmission electron micrographs (TEM) of fixed microreactor tissue sections. One will note the presence of cell-cell junctions and bile canaliculi. As discussed in Section 1.5 it is the loss of such cell-cell interactions that are involved in the loss of liver function in standard culture. Their presence in the microreactor during extended culture indicates some success in recapitulating liver structure.



**Figure 2-5.** Transmission electron micrographs (TEMs) of tissue structures formed in microreactor channels. Left image shows a series of canaliculi bound by desmosomes (arrowheads) between adjacent hepatocytes. Right image includes a large bile canalicula containing microvilli (large arrows) located at junction of three hepatocytes and bounded by tight junctions (small arrows). MT = mitochondria, BC = bile canaliculi. Images taken from [9].

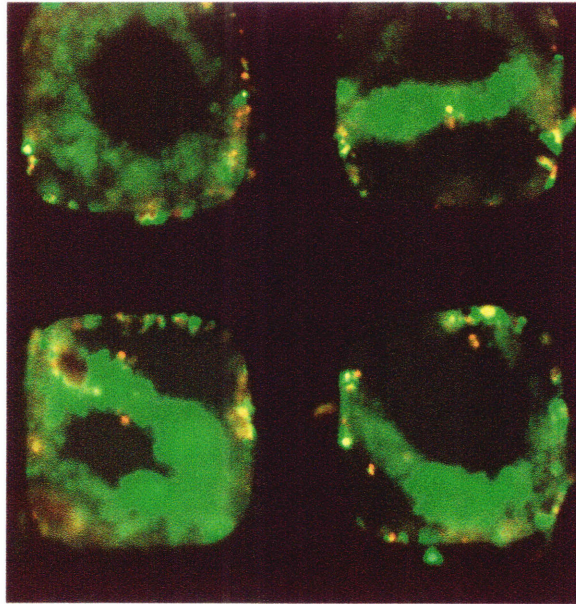
Figure 2-6 includes representative scanning electron micrographs in which endothelial-like cells are located at the tissue-fluid interface in the channel. Such organization is suggestive of the sinusoidal environment, wherein endothelial cells form the porous walls of the sinusoid (described in Section 1.4.2), through which blood travels.



**Figure 2-6.** Scanning electron micrographs of tissue structures formed in microreactor channels.



Cell viability within the microreactor was assessed using a Calcein AM-ethidium homodimer stain (Figure 2-7). The Calcein AM (green fluorescence) is actively taken up by live cells while ethidium homodimer (red fluorescence) is only able to penetrate dead cells. These long-term (13 days) microreactor cultures demonstrate that the majority of the cells are still viable. There has also been significant tissue reorganization considering that these cultures were seeded with spheroidal aggregates.



**Figure 2-7.** Live-dead cell images in the microreactor. Calcein AM-ethidium homodimer stain of cells maintained in microreactor for 13 days. Channel width = 300 $\mu$ m.

### 2.6.3 Liver-enriched mRNA & protein expression

It was mentioned in the previous chapter (Section 1.4.1) that detoxification is among the many vital functions performed by hepatocytes. The conversion of foreign chemicals (e.g. drugs, toxins) into more water-soluble forms (a.k.a. biotransformation) allows them to be removed from the organism (via feces or urine) requires many enzymes. Although present in various tissues these enzymes are highly concentrated in the liver. Earlier work done in the group focused on the expression of cytochrome p450 (CYP450) enzymes, a system of enzymes that are responsible for the biotransformation of a wide variety of foreign chemicals. RT-PCR analysis revealed that among the genes for enzymes studied (including CYP450s) most of them were either unchanged or only slightly down-regulated in the microreactor after 7 days in culture. By comparison, collagen gel sandwich culture (a static 2D culture) demonstrated strong down-regulation for the same genes. Studies looking at particular CYP protein activity (e.g. rates of testosterone hydroxylation) found trends similar to those at the mRNA level such that the microreactor cultures can maintain activity levels closer to physiological levels than conventional 2D cultures [10].

mRNA data was also collected for various key transcription factors. As discussed in the previous chapter (Section 1.5) the loss of the differentiated liver phenotype is a result of changes in gene expression and diminished transcription of liver-specific genes. Many liver-specific genes, including the CYP450s, contain multiple consensus Hepatocyte Nuclear Factor (HNF) binding sites [168, 169]. Therefore, a differentiated liver phenotype requires the expression of multiple HNF transcription factors. Previously published studies in our group used RT-PCR analysis to demonstrate that the expression of multiple

HNFs remained unchanged in the microreactor [10]. However, significant down-regulation was observed in the collagen gel sandwich cultures for those same HNFs. HNF4 $\alpha$  is considered to be a master transcription factor due to its ability to regulate the expression of a disproportionately large number of hepatic genes that include fatty acid, cholesterol and glucose metabolism, urea biosynthesis, apolipoprotein synthesis, liver development, and other transcription factors (e.g. HNF1 $\alpha$  and HNF6) [149-152]. It was demonstrated that in microreactor cultures HNF4 $\alpha$  is better maintained over seven days at both the mRNA and the protein level than in collagen gel sandwich culture.

## **2.7 Scaling up the microreactor**

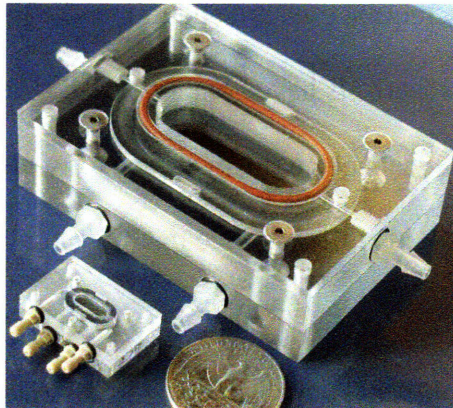
Each individual channel of the microreactor represents a functional unit. Different experimental applications may require greater cell numbers or multiple treatment conditions. To meet these needs efforts have gone into scaling up the microreactor system by 1) increasing the number of channels in the microreactor scaffold and 2) developing a high-throughput format that would allow multiple microreactors to be operated in parallel (i.e. simultaneous dosing of twelve different microreactors with separate compounds). In the following section the development and characterization of these two different scaled up systems are reviewed.

### **2.7.1 Development of the giant microreactor**

The microreactor described in these earlier sections of this chapter was designed to maintain liver cells in long-term 3D culture that could be assessed via in situ optical imaging and spectroscopy for structure and function. This system can hold ~100,000 cells at maximum capacity. However, some applications (described in later chapter) will require greater cell numbers. By keeping the microenvironment constant (i.e. the channel

dimensions and flow rates) the system can be scaled up by adding more channels in the overall array on the scaffold. Such a system was developed and the details of its design and fabrication are available elsewhere [7].

The giant microreactor contains one-thousand  $300 \times 300 \times 230 \mu\text{m}$  square channels in the scaffold as compared to forty such channels in the previous microreactor (Fig 2-8). These additional channels allow the giant microreactor to culture  $1 \times 10^6$  cells which will satisfy the sensitivity requirements of various assays described in later chapters. Flow rates (using the same dual pump fluidic set up) were linearly scaled up in order to maintain the same per channel flow and residence time in the upper chamber as in the earlier model. For a detailed assembly, seeding, and maintenance protocol please see Appendix 3.



**Figure 2-8.** Giant microreactor. In this scaled up model there are a total of 1000 channels ( $300 \times 300 \times 230 \mu\text{m}$ ) which will hold  $\sim 1 \times 10^6$  cells upon seeding.

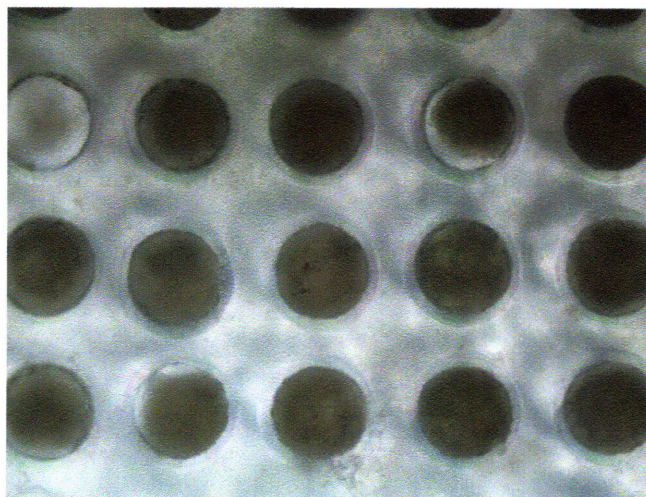
While the components for the giant reactor are similar to the earlier model there are some key differences in working with the giant reactor. In the earlier model silicon worked well as the scaffold material. However, in the giant microreactor silicon presented a number of disadvantages. Fabrication of silicon scaffolds for the giant microreactor was costly and tedious because only 2 scaffolds could be machined at the same time. The top



cell-containing scaffold and the bottom support scaffold must be perfectly aligned in the assembled microreactor in order to insure uniform flow through the channels. Therefore, the scaffolds were machined to exactly fit the dimensions of the pocket in the middle polycarbonate microreactor compartment. Inserting the scaffolds into the pocket proved difficult and would result in either breaking the scaffolds or significantly extending the assembly time. Polycarbonate proved to be a suitable scaffold material. Drilling methods were developed by Jim Serdy to fabricate circular channels with a 300 $\mu$ m diameter (to allow for cell sorting). Additional changes including increased tubing diameter, additional filters in the crossflow line, different geometries at the inlet and outlet ports of the microreactor are discussed in detail elsewhere [7].

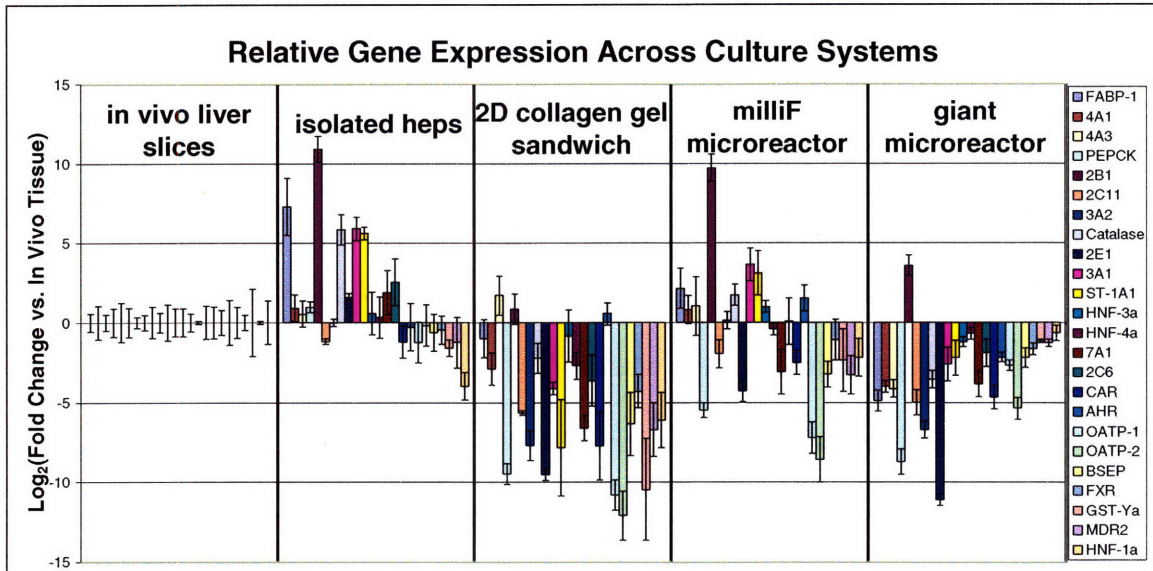
### 2.7.2 Characterization of the giant microreactor

To characterize the ability of the giant microreactor to foster an *in vivo*-like liver phenotype both tissue morphology and gene expression were studied. These studies would also allow a comparison of this scaled up system to the earlier model. Tissue morphology was evaluated via light microscopy. As shown in Fig 2-9 tissue structures formed by day 14 are comparable to those seen in the earlier microreactor system.



**Figure 2-9.** Phase contrast image of tissue structures in channels of giant microreactor. Spheroids (24h in spinner flask) were seeded into the channels. 5x objective

A number of liver-specific genes were analyzed by real-time RT-PCR and compared across multiple cultures that included in vivo liver slices, isolated hepatocytes, 2-D collagen gel sandwiches, milliF microreactor, and the giant reactor. In Fig 2-10 the relative gene expression levels reveal that the giant microreactor and the milliF microreactor



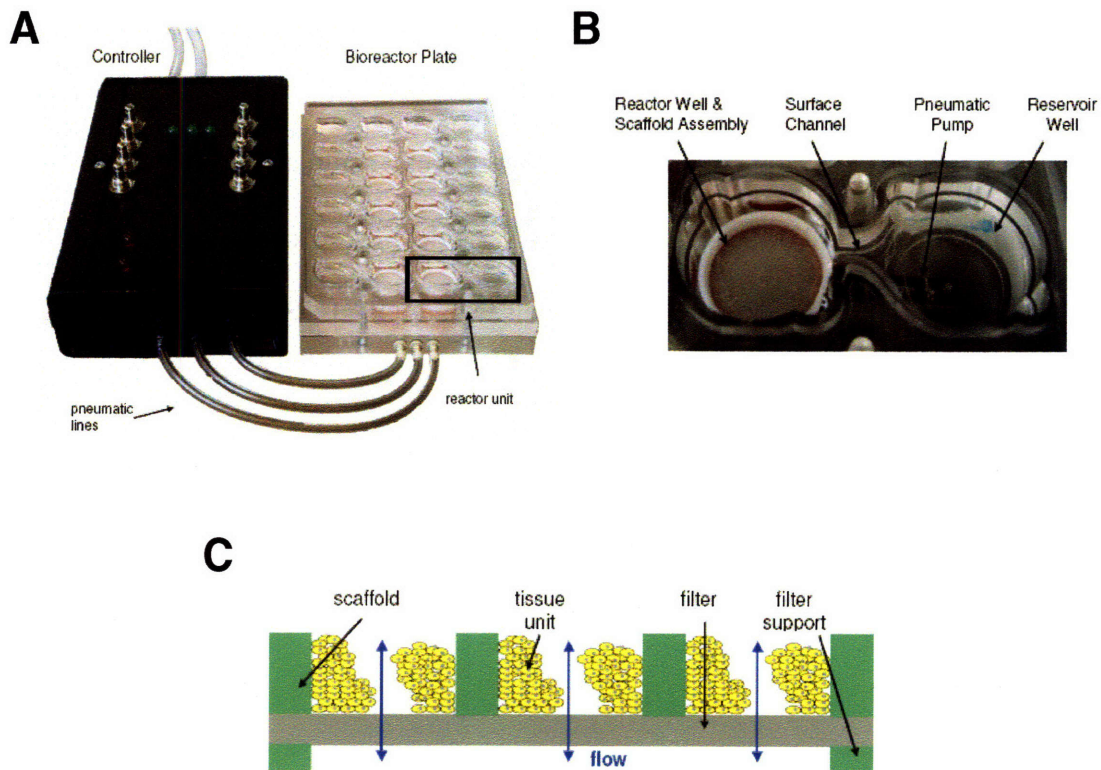
**Figure 2-10.** Relative gene expression across culture systems. Real-time RT-PCR analysis was used in order to measure gene expression in different culture systems and compare it to gene expression within in vivo liver slices. The baseline represents the gene expression of in vivo liver slices. Figure taken from [7].

display similar expression patterns with a few exceptions [7]. Both systems showed better maintenance of gene expression than the 2-D collagen gel sandwich cultures. This indicates that the changes made in order to scale up the microreactor did not significantly alter the microreactor's ability to maintain a more in vivo-like liver phenotype.

### 2.7.3 Development of the multi-well microreactor

A newer generation microreactor has been developed in the Griffith laboratory that builds on earlier models. Whereas earlier models employed 2 relatively bulky peristaltic pumps to generate the necessary fluid flow the latest model uses significantly smaller pneumatic pumps which allow multiple microreactors to be fabricated on a single 24-well standard tissue culture plate format. This newer generation (a.k.a. multi-well microreactor) represents a more high-throughput system in which 12 microreactors, each capable of culturing ~800,000 cells, are fabricated on a single plate.

The reactor is a multilayered structure whose design and assembly have been previously described (Fig 2-11) [170].



**Figure 2-11.** Multi-well microreactor diagram. A) Fully assembled micoreactor with controller for pneumatic pump connected. B) Image of individual reactor unit. C) Cross-sectional diagram of scaffold assembly. Images taken from [5].



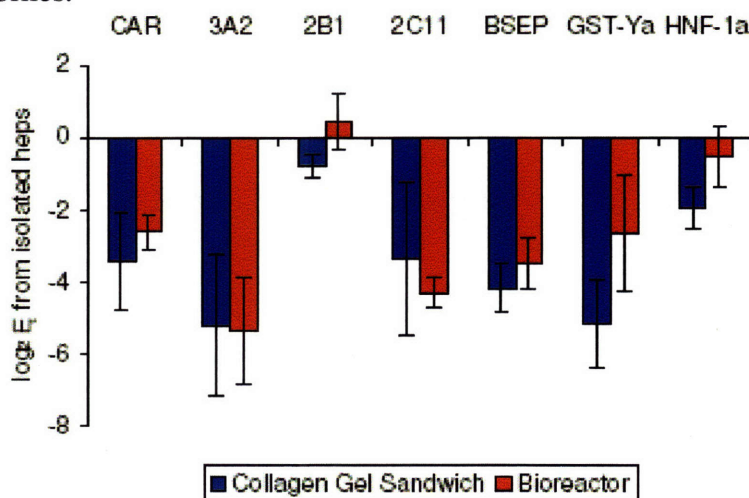
Briefly, there are 12 reactor units on a single fluidic plate. Each reactor unit consists of a scaffold assembly and a media reservoir. The polycarbonate scaffold has an array of 800 circular channels (diameter = 300 $\mu$ m, depth = 230 $\mu$ m). Cells in the scaffold channels are continuously perfused with culture media from the reservoir via a pneumatic pump which is then recirculated across a surface channel back to the reservoir (Figure 2-11b). Each reactor unit is fluidically isolated but all pumps are simultaneously driven by pneumatic control lines connected to sources of positive and negative air pressure. Physiological rates of media perfusion are achieved by controlling the frequency of the pulses of air pressure. Primary scaffold channels are coated with collagen type I (30 $\mu$ g/mL) to allow for cellular attachment.

The greatest advantage of the multi-well microreactor is the relative ease by which several reactor units can be manipulated. This allows various parameters such as multiple dosing concentrations to be studied in the same experimental setup and therefore minimizes animal-to-animal or instrument variation. A detailed discussion of the assembly, seeding, and maintenance is available elsewhere [171]. The protocol used in this thesis is available in Appendix 4.



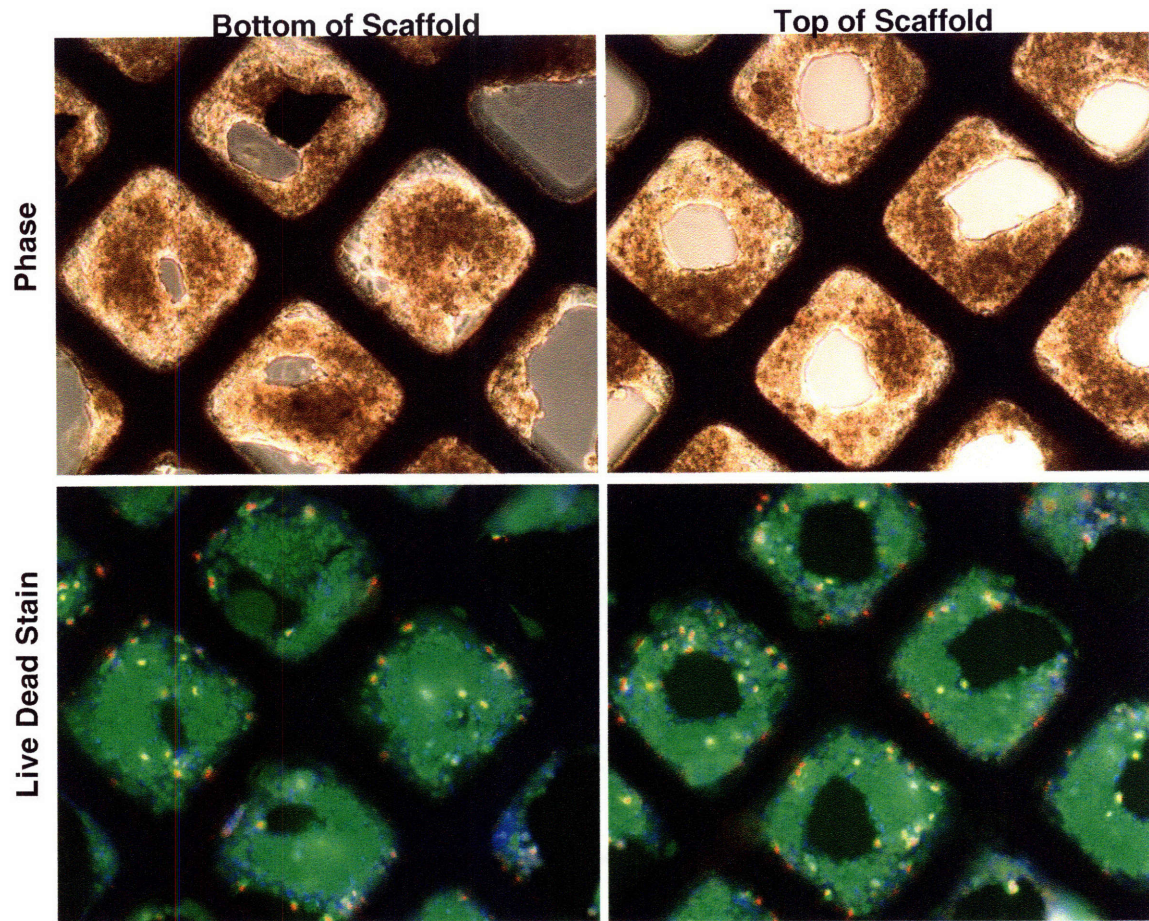
## 2.7.4 Characterization of multi-well microreactor

Relative gene expression data indicate that the multi-well behaves similarly to the earlier microreactor system (Fig. 2-12, [5]). The genes being measured include those that transcribe Phase I and Phase II enzymes, surface proteins, and transcription factors. Overall, the milliF, giant, and multi-well microreactor systems demonstrate similar gene expression profiles.

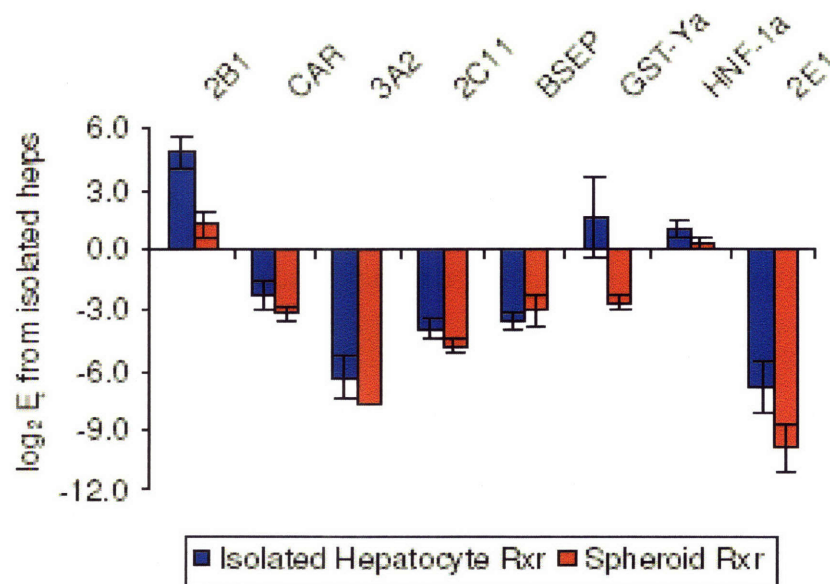


**Figure 2-12.** Relative gene expression analysis in multi-well. 72h spheroids were seeded into multi-well (“bioreactor”). This data represents day 7 post cell isolation gene expression. Expression levels are normalized to freshly isolated hepatocytes. Taken from [5].

The incorporation of single cell seeding immediately following the perfusion was revisited. Earlier studies done in the milliF had demonstrated that spheroidal cell aggregates performed better over the length of the culture [164]. As shown in Figure 2-13 phase contrast and live-dead staining indicate healthy tissue structures present by 5 days in culture. Relative gene expression data (Fig. 2-14, [5]) confirm that single cells perform similarly to spheroidal aggregates and represent a viable option when seeding the multi-well microreactor. Further characterization of drug metabolism via metabolite accumulation and specific p450 induction is available elsewhere [5].



**Figure 2-13.** Tissue structures formed after 5 days in culture in multi-well microreactor. Calcein AM-ethidium homodimer stain indicates good cell viability that is comparable to viability measured in earlier microreactor system. These are silicon scaffolds with square channels (300×300×230μm). *Images courtesy of Dr. Sharon Karackattu.*



**Figure 2-14.** Comparison of relative gene expression levels in multi-well cultures seeded with either single cells or 72h spheroids. Data represents day 7 post cell isolation. Taken from [5].

## Chapter 3.

# A Novel Method to Render Primary Rat Hepatocytes Susceptible to Duck Hepatitis B Virus

### 3.1 Introduction

Human HBV is the prototype member of the family *Hepadnaviridae* that consists of enveloped, partially double-stranded DNA viruses that specifically target hepatocytes for viral replication [111]. Although a vaccine has been available for more than 20 years chronic hepatitis B afflicts ~5% of the world's population [11]. All hepadnaviruses display a narrow host range. Besides humans, chimpanzees and, more recently, *Tupaia belangeri* tree shrews are the only animals that are susceptible to infection [11, 111]. The use of primary human and primate hepatocytes is restricted by multiple experimental limitations including a rapid loss of susceptibility to infection in culture, lot-to-lot variability in susceptibility to infection, and the necessity of treatment with chemical agents such as DMSO for reproducible infection [107, 108, 120]. There is also low efficiency of HBV infection in primary human and *Tupaia belangeri* hepatocytes [117, 172]. Along with the lack of susceptible cell lines or small animal models these factors have hampered research into many aspects of hepadnavirus biology.

Permissive cell lines (e.g. HepG2, Huh7), capable of supporting viral replication upon transfection with the viral genome, have shed greater light on the later events in the viral life cycle (i.e. transcription, encapsidation reverse transcription, virion assembly, export). However, there is less understanding of the early stages that include virus attachment, internalization, uncoating, genome repair, and nuclear transport. These cell



lines do not mimic natural infection which limits their usefulness. An in vitro system that will allow us to target other aspects of the viral life cycle is needed.

Similar genome organization, virus structure, and replication characteristics among hepadnaviruses warrant the study of hepadnaviruses found in other species. Many of the principles of hepadnavirus life cycle were elucidated by studying duck hepatitis B virus (DHBV) as a model for HBV. Elucidated principles include the replication by reverse transcriptase [125], cccDNA formation [126], and host-range determinants [127-129]. However, reproducible in vitro infection of primary duck hepatocytes requires culture conditions that incorporate 1.5-2% DMSO whose mechanism of action is unknown [130, 131]. Even with such artificial additives the kinetics of in vitro infection are slow and inefficient when compared to in vivo infection of neonatal ducklings [132].

Putative host receptors for DHBV have been defined. The amino terminal portion of the large envelope protein (preS domain) has been shown to be involved in virus uptake [136, 173]. Studies have demonstrated that hepatocyte penetration of DHBV occurs via the attachment of a highly conserved region in the preS domain to an enzyme known as carboxypeptidase D (cleaves C-terminal basic residues) [128, 136, 141, 174]. Current evidence from multiple groups has shown that DCPD serves a crucial role in DHBV infection: 1) reconstitution experiments demonstrate that permissive cell lines (e.g. LMH cells) transfected with DCPD are able to internalize DHBV particles; 2) recombinant DHBV preS peptides covering the DCPD binding site inhibit DHBV infection of PDH as well as block DHBV binding to DCPD reconstituted cells; 3) soluble recombinant DCPD (including only the extracellular domain) is able to inhibit DHBV infection of PDH cultures in a dose-dependent manner; 4) antibodies against DCPD block DHBV infection

5) DCPD expression is specifically downregulated in DHBV-infected hepatocytes and not in other tissues 6) reconstitution of PDH with DCPD mutants lacking the cytoplasmic TGN-retrieval signal abolishes DHBV infection in those cells. However, it has not been possible to render non-susceptible cell lines that fully support DHBV replication after transfection with cloned DHBV DNA susceptible via DCPD expression. DCPD is also found on tissues not susceptible to DHBV infection [136]. Taken together these data suggests that either there are additional host-specific factors necessary or that there are tissue-specific factors that only exist in a more highly differentiated state.

We report here the use of recombinant adenovirus vectors to transfer DCPD to primary rat hepatocytes in order to study the ability of a normally non-susceptible species to support DHBV replication. Earlier studies have shown that primary rat hepatocytes are capable of supporting DHBV replication upon adenoviral transfection of the viral genome, confirming that the later events of the viral life cycle are not rigidly host-restricted [175]. We generated recombinant vectors in which both DCPD and green fluorescent protein (GFP) are incorporated in the adenoviral genome. DHBV replication was initiated in primary rat hepatocytes when DCPD was transduced via adenoviral delivery. In this study we provide the first evidence that DCPD is sufficient to cross the species barrier and establish a DHBV infection in primary rat hepatocytes. We also report DCPD transduction in primary rat hepatocytes cultured in a microfluidic device that promotes a more highly-differentiated liver phenotype than conventional culture systems (e.g. collagen-coated polystyrene, collagen gel sandwich).

## **3.2 Materials and Methods**

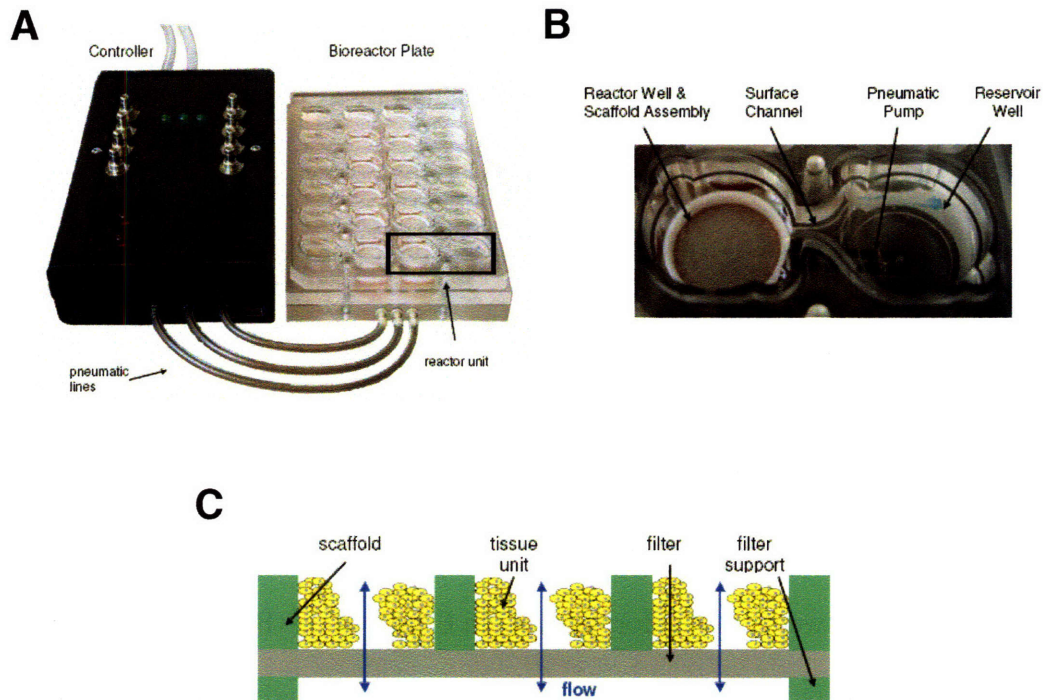
### **3.2.1 Primary rat hepatocyte isolation and culture**

Primary liver cells were isolated from male Fischer rats (150 – 230g) using a modified version of Seglen's two-step collagenase perfusion procedure [164] as previously described [165]. Tissue dissociation was accomplished using Liberase Blendzyme 3 (Roche). Final cell viability was in the range of 89-94 % based on trypan blue exclusion. The final cell pellet (~95% hepatocytes) was re-suspended in supplemented DMEM (GIBCO) that includes 0.03g/L proline, 0.10g/L ornithine, 0.305g/L niacinimide, 2.0g/L glucose, 2.0g/L galactose, 2.0g/L bovine serum albumin, 0.05mg/mL gentamycin, 5mg/L insulin, 5mg/L transferrin, 5ug/L sodium selenite, 20ng/mL epidermal growth factor, 1mM L-glutamine, 0.1uM dexamethasone, and trace metals (5.44mg/mL ZnCl<sub>2</sub>, 7.5mg/mL ZnSO<sub>4</sub>·7H<sub>2</sub>O, 2.0mg/mL CuSO<sub>4</sub>·5H<sub>2</sub>O, 2.5mg/mL MnSO<sub>4</sub>) collectively referred to as Hepatocyte Growth Media (HGM). This medium is a modified version of that described by Block et. al. [166]. Resuspended hepatocytes were plated on polystyrene plates coated with collagen type I (30 µg/mL) (BD Biosciences) at a plating density of 50,000 cells/cm<sup>2</sup>. Cultures were maintained at 37°C and 5% CO<sub>2</sub> with media changes every 48h.

### **3.2.2 Multi-well microreactor culture**

A schematic of the reactor and fluidic circuit is shown in Figure 1. The reactor is a multilayered structure whose design and assembly have been previously described [170]. Briefly, there are 12 reactor units on a single fluidic plate. Each reactor unit consists of a scaffold assembly and a media reservoir. The polycarbonate scaffold has an array of 800 circular channels (diameter = 300µm, depth = 230µm). Cells in the scaffold channels are

1



**Figure 3-1.** Diagram of multi-well microreactor. A) Image of microreactor connected to controller device for pneumatic pumps. B) Image of individual reactor unit consisting of media reservoir and a reactor well containing the scaffold assembly which is connected by a surface channel and a pneumatic pump. C) Illustration of scaffold assembly with tissue in channels. Taken from [5].

continuously perfused with culture media from the reservoir via a pneumatic pump which is then recirculated across a surface channel back to the reservoir. Each reactor unit is fluidically isolated but all pumps are simultaneously driven by pneumatic control lines connected to sources of positive and negative air pressure. Physiological rates of media perfusion are achieved by controlling the frequency of the pulses of air pressure. Primary scaffold channels are coated with collagen type I ( $30\mu\text{g}/\text{mL}$ ) to allow for cellular attachment. Prior to seeding, the microreactor system is primed with HGM in order to passivate the surfaces and remove any air bubbles in the fluidics. Primary cells isolated from the rat perfusion are pipetted directly into the channels of the scaffold and adhere to

the collagen coating the channel walls. During the first 8h the media perfuses the channels in a downward direction in order to pull the cells into the channels. To eliminate any residual cell debris that might clog the filter the media flow is reversed (lower chamber to upper chamber) after 8h and fresh media is added to the reservoir. Reactors were maintained at 37°C and 5% CO<sub>2</sub> with daily media changes.

### **3.2.3 Generation of recombinant adenovirus vectors**

The adenovirus constructs were generated using the AdEasy vector system and has been previously described [146]. Briefly, a shuttle vector containing the gene of interest (DCPD) and an adenovirus backbone plasmid that includes the Ad5 genome with both E1 and E3 genes deleted were co-transformed into an E. coli strain (BJ5183). The highly efficient homologous recombination machinery within the bacteria produce recombinant adenovirus constructs containing the gene of interest. These constructs are linearized and transfected into the 293 packaging cell line which constitutively express E1 gene products, necessary for propagation of all recombinant adenoviruses. Successful viral production is monitored via the GFP reporter gene which is also incorporated into the adenovirus backbone plasmid. Further tests were done to confirm that there were no replication-competent adenovirus constructs present in the final preparations. The final recombinant adenovirus containing the DCPD gene is designated Ad-eGFP-DCPD. This vector was kindly provided by the Wands laboratory at Brown University. Further amplification and purification was performed by Puresyn, Inc.

### **3.2.4 DHBV-positive serum isolation**

Mammoth White Pekin ducklings were obtained from a commercial supplier (Ridgway Hatchery), housed at the Liver Research Center at Brown University, and given



ad libitum access to food and water. Three-day old ducklings were injected in a foot vein with 200uL of highly viremic duck serum. Five days later the duck was sacrificed by pentobarbital overdose (Abbott Laboratories) and the total blood volume was collected via cardiac puncture. Total blood was kept at room temperature for ~6hrs and then spun (3000 rpm) for 5 min. The serum was collected and tested for DHBV particles via dot blot analysis. Briefly, total DNA was isolated using QIAamp DNA MicroKit (Qiagen), boiled at 100C for 10 min and placed immediately on ice. DNA was spotted onto nylon membrane (Schleicher & Schuell) and fixed using UV exposure. A <sup>32</sup>P-radiolabeled DHBV DNA probe was added overnight (45C). Following multiple washes, the blot was exposed to a phosphor screen that was developed on a Cyclone Imaging Station (Packard Bioscience).

### **3.2.5 DHBV infection**

Approximately 6h after plating, cultures were exposed to adenovirus vectors diluted in HGM to achieve the proper multiplicity of infection (MOI). Cells were cultured with the adenovirus for ~24h at 37C prior to being removed with multiple washes of Phosphate Buffered Saline (PBS). DHBV-positive duck serum was diluted (1/5) in HGM and added to the cultures for 24 incubation at 37C. The diluted serum contained ~  $7.2 \times 10^8$  virus genome equivalents (vge)/mL as determined by PCR analysis. Non-adsorbed virus particles in the culture were removed with multiple PBS washes. Cells were maintained at 37C with media changes every 48h.

### **3.2.6 Sodium dodecyl sulfate-polyacrylamide gel electrophoresis (SDS-PAGE) and western blot analysis**

Cell samples were lysed with 100uL RIPA buffer on ice for 20 minutes and total protein was determined by BCA protein assay (Pierce). SDS-PAGE was done using 7.5 or 12% polyacrylamide gels (BioRad). Prior to loading the gel, samples were adjusted so that equal amounts of total protein were loaded onto the gel. Following electrophoresis, proteins were transferred to a polyvinylidene difluoride (PVDF) membrane (BioRad, USA). The PVDF membrane was probed with primary antibodies that included: polyclonal rabbit anti-duck carboxypeptidase D (1:10000 dilution), polyclonal rabbit anti-DHBV preS (1:5000 dilution) and rabbit polyclonal anti-actin (1:10,000 dilution) (Santa Cruz). Primary antibodies were detected with goat anti-rabbit HRP-conjugated secondary antibody (1:5000 - 1:10000 dilution) (Jackson ImmunoResearch, USA). Detection and quantification were done using enhanced chemiluminescence (ECL) (Amersham, USA) and a Kodak Image Station (Eastman Kodak).

### **3.2.7 Isolation and detection of DHBV DNA in primary rat hepatocytes**

Cell samples were analyzed for the presence of DHBV DNA as previously described [175]. Briefly, samples were lysed in TEN Buffer (150mM NaCl, 50mM Tris-HCl (pH 8.0), 10mM EDTA, 1% SDS) and 0.5mg/mL proteinase K overnight at 37C. Residual protein was removed via phenol-chloroform extraction.

Nucleic acids were precipitated using ethanol and dissolved in TE buffer. Nucleic acid samples were subjected to electrophoresis in a 1% agarose gel. DNA was fragmented with 0.25N HCl-0.6M NaCl, denatured with 0.5N NaOH-1.0M NaCl, and neutralized with 1.0M Tris-HCl (pH 7.0)-1.0M NaCl. Samples were then transferred to a nylon membrane overnight at room temperature. Hybridization was done overnight at 42C using a nick-translated <sup>32</sup>P-labelled DHBV probe (MegaPrime DNA Labelling System, Amersham

Biosciences). The blot was exposed to x-ray film with an intensifying screen (Biomax, Eastman Kodak Co.) for 72h at -80C. The film was developed on an X-OMAT 100A processor (Kodak).

### **3.2.8 Fluorescence Activated Cell Sorting (FACS) analysis.**

After plating, hepatocytes were exposed to adenovirus at different MOI for ~24h. Non-adsorbed particles were washed out with multiple PBS washes. Several samples were collected using 10mM EDTA and fixed in 2% paraformaldehyde. Other samples were exposed to DHBV serum diluted in HGM ( $\sim 3 \times 10^8$  vge) for ~24h. Following multiple PBS washes to remove nonadsorbed DHBV particles the samples were collected using dispase (50U/mL, BD Biosciences) and fixed in 2% paraformaldehyde. Some fixed cell samples were permeabilized using ice cold 100% MeOH. Samples were blocked with 1% bovine serum albumin for 1h and then exposed to primary antibodies that include polyclonal rabbit anti-duck carboxypeptidase D (1:250 dilution) and polyclonal rabbit anti-DHBV preS (1:250 dilution). Primary antibodies were detected with highly cross-adsorbed goat anti-rabbit AlexaFluor 647 secondary antibody (1:250 dilution) (Invitrogen). Labeled cells were analyzed using a FACSCalibur dual laser flow cytometer system (BD Biosciences).

### **3.2.9 Fluorescence & Immunofluorescence analysis**

Cultures maintained on collagen-coated polystyrene dishes were imaged using a Zeiss Axiovert 100 microscope. GFP expression was imaged using a fluorescein isothiocyanate (FITC) filter. To analyze DCPD expression in the tissue structures formed in the multi-well cultures, cells were fixed in 2% paraformaldehyde and permeabilized using 0.1% Triton X-100. Following a 1h incubation in normal goat serum (1:20 dilution) the rabbit anti-duck DCPD Ab was added overnight at 4C (1:1000 dilution). Alexa Fluor

568-conjugated highly cross adsorbed goat anti-rabbit secondary antibody (Invitrogen) was incubated with the cells for 1h at room temperature. Confocal images were collected using a Nikon TE2000 microscope equipped with a Yokagawa spinning disk confocal head (McBain Instruments) and processed using Metamorph Offline 6.1r0 software.

### **3.2.10 Statistical analysis**

Statistical significance of results was analysed using GraphPad Prism Version 4.0 for Windows (GraphPad Software, San Diego, CA). One-way analysis of variance (ANOVA) tests were used to compare mean cell numbers present at a given timepoint for increasing adenovirus concentration. The difference in means was considered statistically significant when probability values were  $<0.01$ .

### **3.3 Results**

#### ***3.3.1 DCPD expression in primary rat hepatocytes (PRH) in standard tissue culture***

Following plating on collagen I-coated tissue culture plates, replicate PRH cultures were exposed to Ad-eGFP-DCPD at select MOI ranging from 0-50. Recombinant adenoviral infection is known to cause transient transgene expression. Fluorescence images were taken every 24h for 5 days to follow GFP expression. At the initial timepoint (24h following Ad exposure), GFP expression can only be observed at the higher MOI (MOI 20, 50) (Fig. 3-2a). By 48h in culture significant cell spreading has occurred in all conditions and cultures appear to be confluent. Increasing transfection efficiency is observed for increasing Ad MOI. Individual cells within each condition appear to exhibit different GFP intensities indicating the possibility of differential adenovirus uptake and/or differential protein translation capability. By 72h in culture GFP intensity has reached a maximum level. Some cell death is observed in the MOI=50 cultures but all lower MOI are comparable to the control (No Ad) cultures. By 96h the percentage of GFP-positive cells have declined in all MOI conditions. Similar percentages seen at 120h suggest that a baseline level of GFP expression is being observed.

The expression of DCPD was investigated by western blot analysis (Fig. 3-2b). Following Ad-eGFP-DCPD MOI=10 exposure, relatively equal levels of DCPD expression were measured over 9 days in culture. Equal loading of total protein in the blot suggests that cells being lost over the culture period were not expressing significant DCPD or that DCPD expression increases over time in order to compensate. Western blot

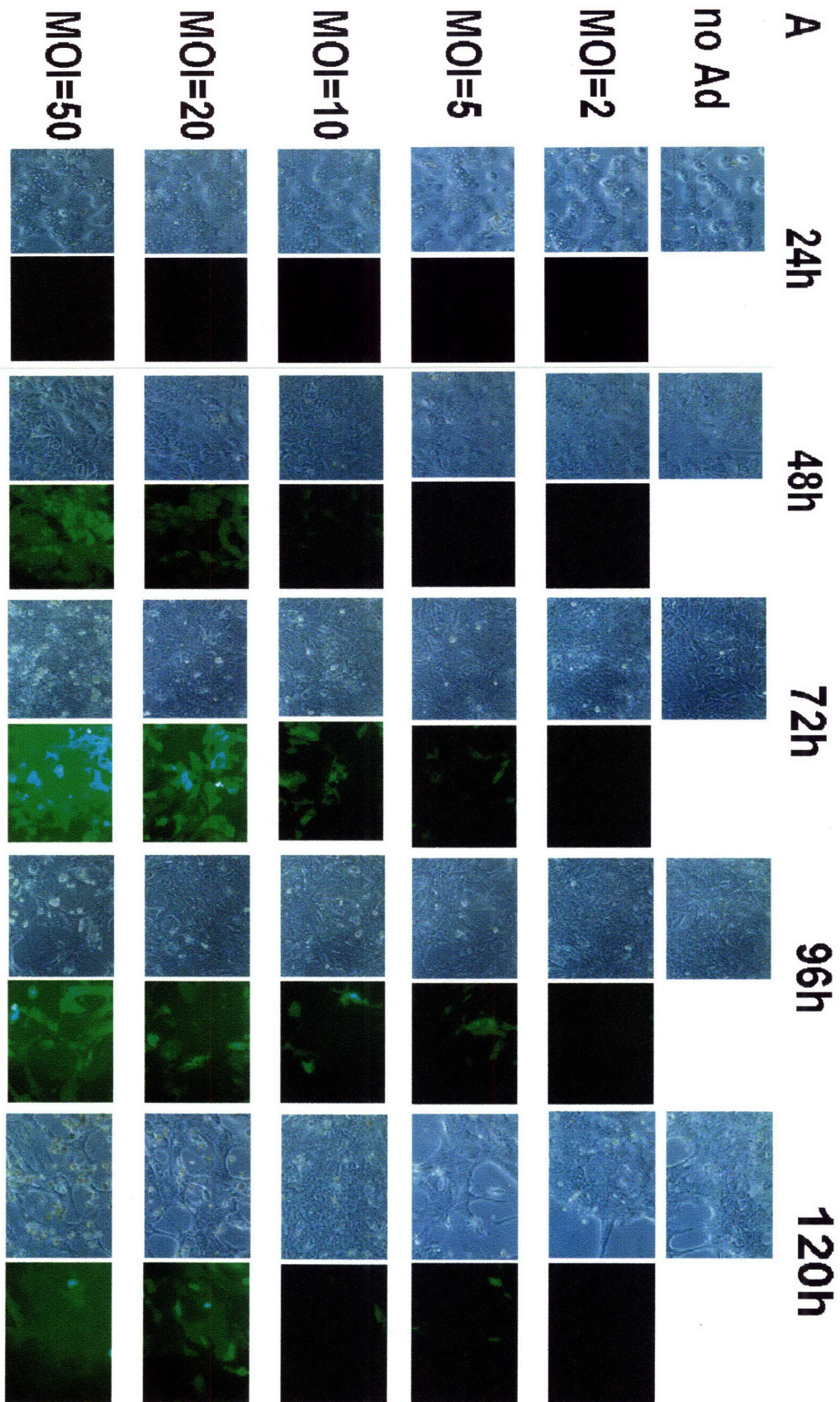
analysis also established that increased DCPD expression is achieved by exposure to increased Ad MOI. This analysis demonstrates DCPD maintenance for ~2weeks.

It is interesting that DCPD appears as two separate bands (Fig. 3-2c) which has been observed in primary duck hepatocyte cultures [141]. This doublet could represent the membrane-bound form (180kDa) and a truncated form (170kDa). Another group showed that upon transfection with DCPD (via baculovirus expression vectors) insect Sf9 cells secreted a soluble 170kDa version that behaved similarly with regard to enzymatic activity, activation, and optimum pH [138]. It was suggested that the 170kDa version was likely missing the putative transmembrane domain and cytoplasmic tail because it does not react strongly with an antiserum raised against the C-terminal tail. It was concluded that such a truncation resulted either from proteolysis or from differential mRNA splicing. A variety of smaller versions of carboxypeptidase D (CPD), some of which are soluble, have been observed in both bovine and rat tissues [176]. It is interesting to note that for lower Ad MOI (MOI=2) there appears to be a loss in the truncated form of the DCPD over time in culture. For the higher Ad MOI (MOI=5, MOI=10) both forms are present for ~2weeks.

At 72h following Ad exposure, parallel PRH samples were fixed in 2% paraformaldehyde in order to analyze DCPD expression on an individual cell basis via FACS analysis. DCPD is located both intracellularly and on the plasma membrane and it has been shown to traffic back and forth from the *trans*-Golgi network (TGN) to the cell surface [177]. Half of the fixed samples were permeabilized to determine the total (surface & intracellular) levels of DCPD. As expected, greater levels of DCPD are detected in primary rat hepatocytes infected with increasing Ad MOI (Fig 3-3a). Comparing permeabilized hepatocytes and non-permeabilized hepatocytes for a given Ad MOI it

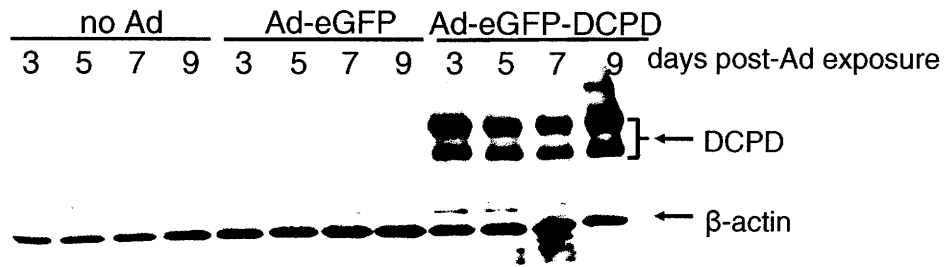
appears that the majority of the DCPD ( $\geq 70\%$ ) is available on the cell surface (Fig. 3-3b, Table 3.1). Previous studies using CPD-transfected AtT-20 cell line (murine pituitary tumor) have shown that a small fraction ( $\sim 10\%$ ) of CPD is available at the cell surface [178, 179]. Mutational analysis in these earlier studies demonstrated that a cytoplasmic domain functions in TGN retention inside cell compartment.

It is interesting to note that for increasing Ad MOI a growing subpopulation appeared that is negative for GFP expression but positive for DCPD expression. This could explain the apparent discrepancy between timecourse expression of GFP and DCPD seen in Figure 3-2. This DCPD+/GFP- population could account for the sustained DCPD expression. As mentioned earlier the two transgenes carried in the adenoviral vector (DCPD and GFP) are contained within two independent CMV-driven transcription units. Differential translational and post-translational regulation may account for the two distinct subpopulations. Comparing the permeabilized vs non-permeabilized DCPD within this particular population also indicates that the majority of the DCPD ( $\geq 50\%$ ) is available on the cell surface.

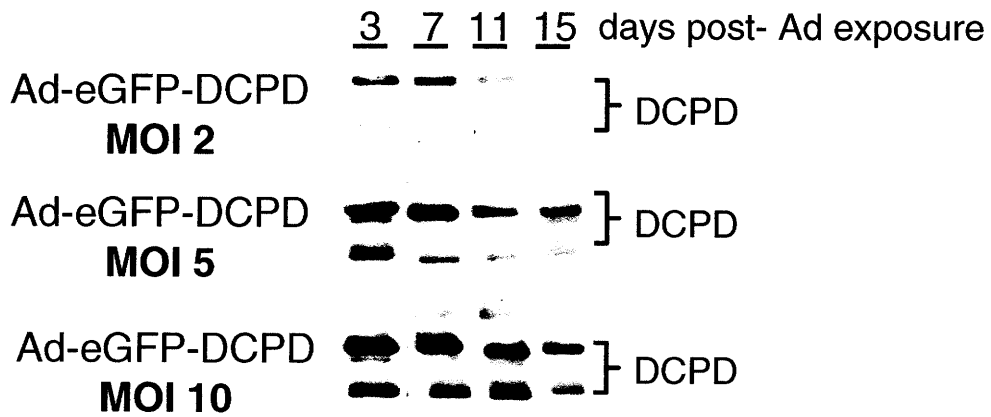




**B**



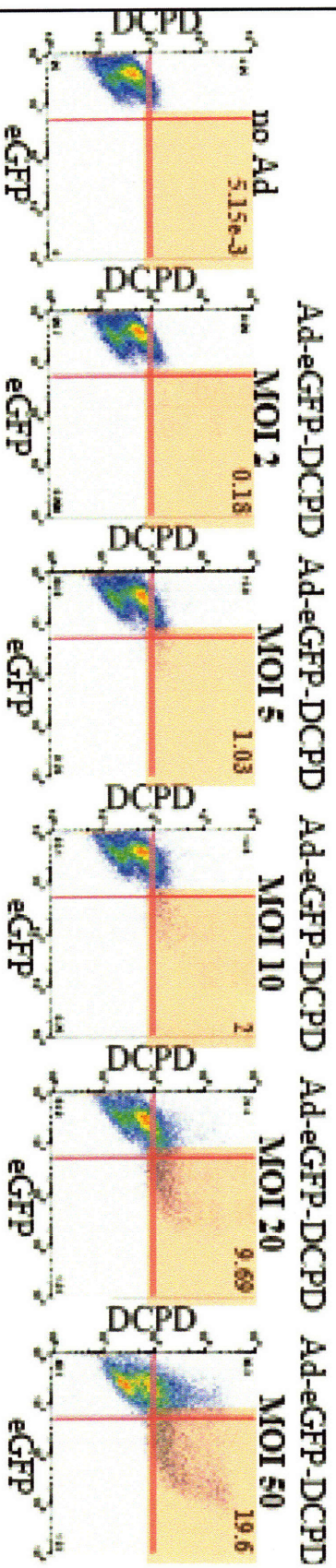
**C**



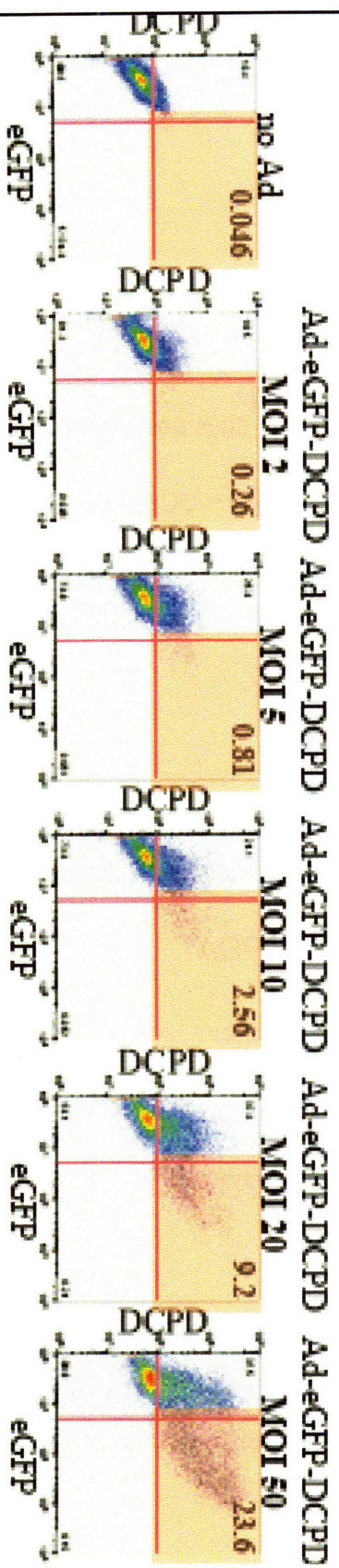
**Figure 3-2.** DCPD transfection of PRHs in monolayer culture. A) Phase contrast and GFP expression images following Ad-eGFP-DCPD exposure (24h, 48h, 72h, 96h, 120h). B) Western blot image of DCPD expression in DCPD-transfected cultures (Ad MOI=10). C) Western blot image of PRHs exposed to different Ad-eGFP-DCPD MOI.

A

non-permeabilized cells:

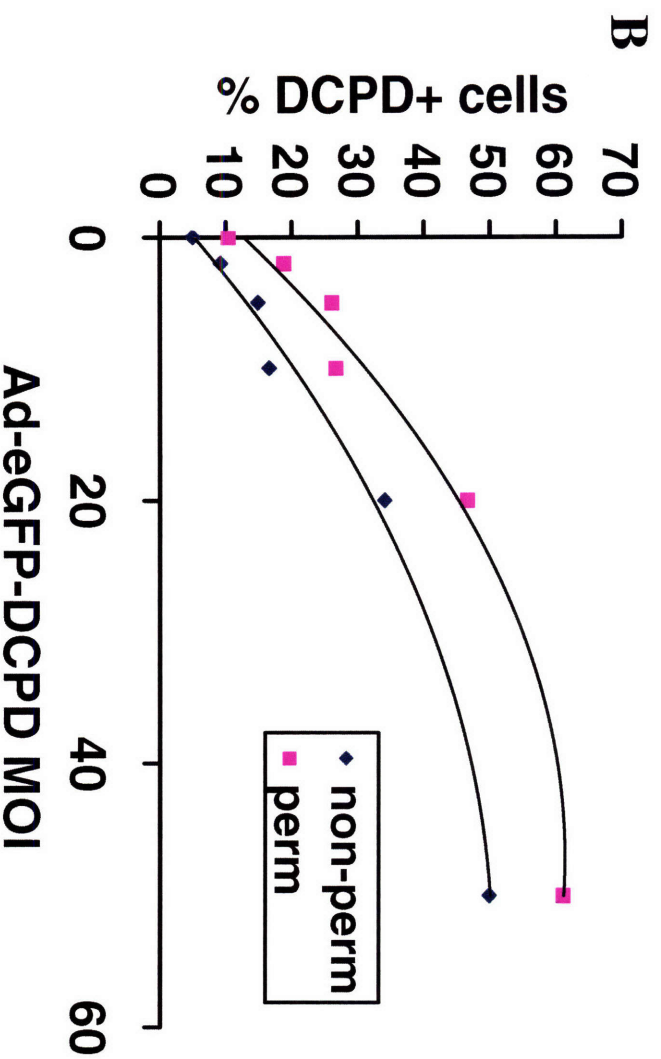


permeabilized cells:



	DCPD+ & GFP+ (72h)		DCPD+ & GFP- (72h)		DCPD- & GFP+ (72h)	
	non-perm. % FACS (% of total pop.)	perm. % FACS (% of total pop.)	non-perm. % FACS (% of total pop.)	perm. % FACS (% of total pop.)	non-perm. % FACS (% of total pop.)	perm. % FACS (% of total pop.)
No Ad	0.0 (0.0)	0.0 (0.01)	5.0 (0.59)	10.4 (1.97)	0.0 (0.0)	0.0 (0.0)
Ad-eGFP-DCPD MO12	0.2 (0.04)	0.3 (0.04)	9.0 (1.71)	18.5 (2.92)	0.098 (0.02)	0.036 (0.01)
Ad-eGFP-DCPD MO15	1.0 (0.17)	0.8 (0.13)	13.9 (2.40)	25.3 (4.01)	0.29 (0.05)	0.051 (0.01)
Ad-eGFP-DCPD MO110	2.0 (0.34)	2.6 (0.43)	14.6 (2.51)	24.1 (4.01)	0.25 (0.04)	0.062 (0.01)
Ad-eGFP-DCPD MO120	9.7 (1.67)	9.2 (1.59)	24.4 (4.19)	37.4 (6.46)	1.01 (0.17)	0.24 (0.04)
Ad-eGFP-DCPD MO150	19.6 (3.32)	23.6 (3.95)	30.3 (5.14)	37.5 (6.28)	1.02 (0.17)	0.15 (0.03)

**Table 3-1.** FACS Analysis of DCPD-transfected PRHs 72h following Ad exposure






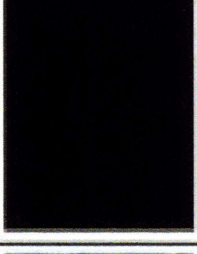

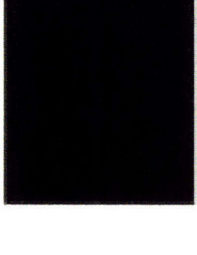


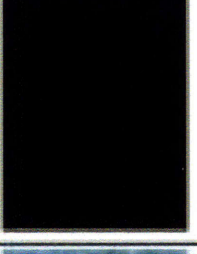

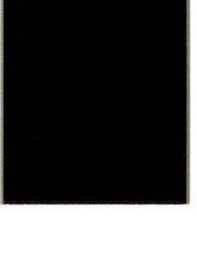


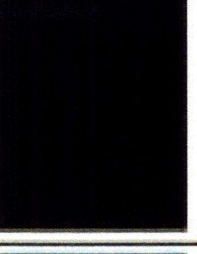

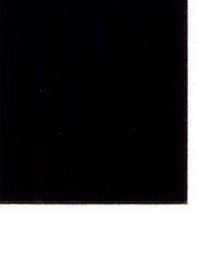
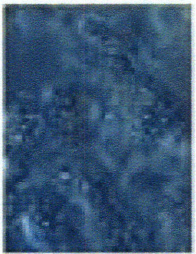

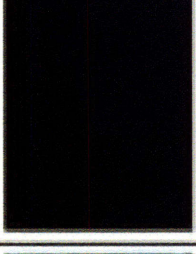

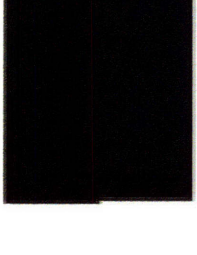

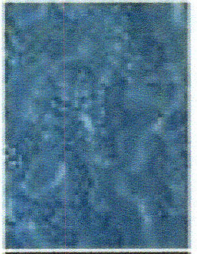
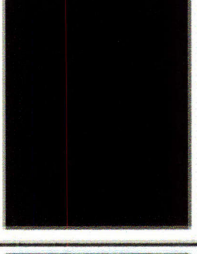
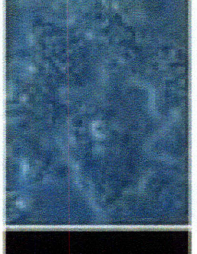
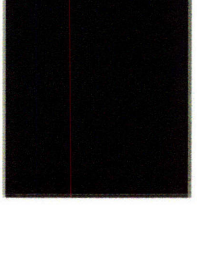
**Figure 3-3.** FACS Analysis of DCPD-transfected PRHs. A) Density plots of PRHs exposed to increasing Ad MOI. 72h following Ad exposure cells were fixed (2% PFA) and/or permeabilized (100% MeOH), and labeled with primary DCPD Ab and AlexaFluor 647-conjugated secondary Ab. B) Plot of % of FACS cell population staining DCPD-positive in permeabilized (perm.) and non-permeabilized (non-perm) conditions.

### ***3.3.2 DCPD protects against Ad-mediated cytotoxicity***

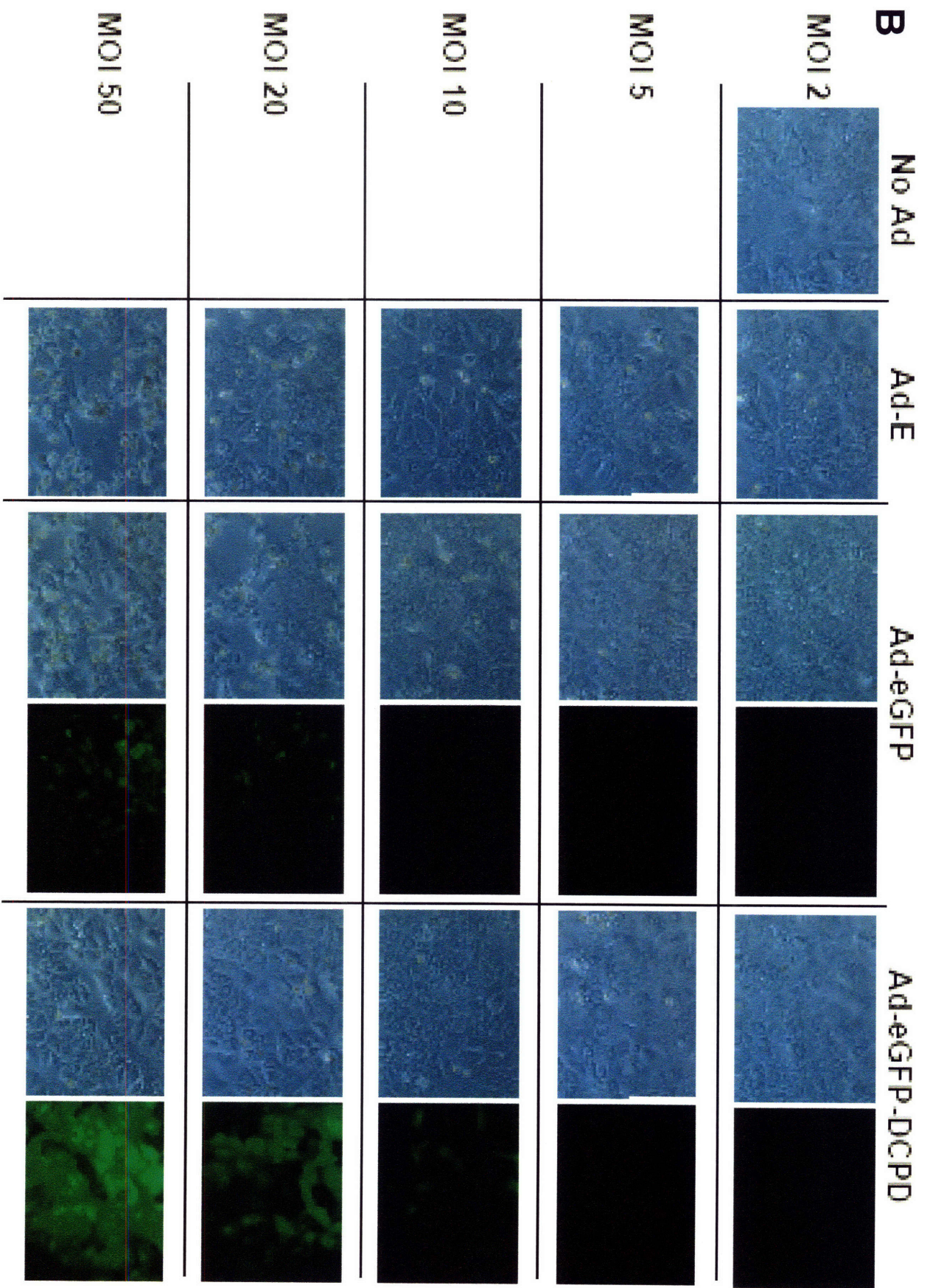
A striking morphological difference was consistently observed between cultures exposed to control vectors (Ad-e or Ad-eGFP) compared to the Ad-eGFP-DCPD vectors (Fig. 3-4). Control Ad vectors appeared more toxic at moderate MOI (MOI =5, MOI=10, MOI=20) than did Ad-eGFP-DCPD vector as assessed by substantial number of cells with a condensed apoptotic appearance (Fig. 3-4b, 3-4c, 3-4d, 3-4e). The apparent toxicity seen in light micrographs was quantified by measurement of total protein as an indicator of cell number. Statistical analysis revealed that cell loss over the 5-day culture period was significantly greater in cultures exposed to Ad-e MOI=50, Ad-eGFP MOI=20, Ad-eGFP MOI=20, and Ad-eGFP MOI=50 than the control, no Ad, case at the later timepoints (72, 96, and 120h) (p values <0.01) (Fig. 3-4f, 3-4g). In contrast no significant cell loss greater than the control (no Ad) case was observed for any of the PRH cultures exposed to any Ad-eGFP-DCPD MOI (Fig. 3-4h). Adenovirus-mediated toxicity is a well-known phenomenon. Underlying mechanisms include adenovirus-mediated sensitization to TNF-induced apoptosis [180]. The PRH cultures in our study are enriched for hepatocytes but ~5% of the culture consists of NPCs that include macrophages which can efficiently take up adenovirus and subsequently release TNF to eliminate surrounding infected cells in an inflammatory response. Earlier work has shown that upon infection E1/E3-deleted adenovirus vectors can still cause low level expression of other wild-type gene products such as E4 that can induce apoptosis [181]. Such mechanisms are likely to be involved in the cell loss observed in these experiments. Ad-e and Ad-eGFP stock preparations have nominal ratios of non-infectious to infectious units of 11:1 and 12:1, respectively, while Ad-eGFP-DCPD stock preparation has a ratio of 6:1. As demonstrated in Figure 3-5a and

3-5b the observed cell loss in Ad-e and Ad-eGFP can not be solely explained by differences in total virus particles. It appears that expression of DCPD protects cells against adenovirus-mediated toxicity, a result not previously reported in the literature.

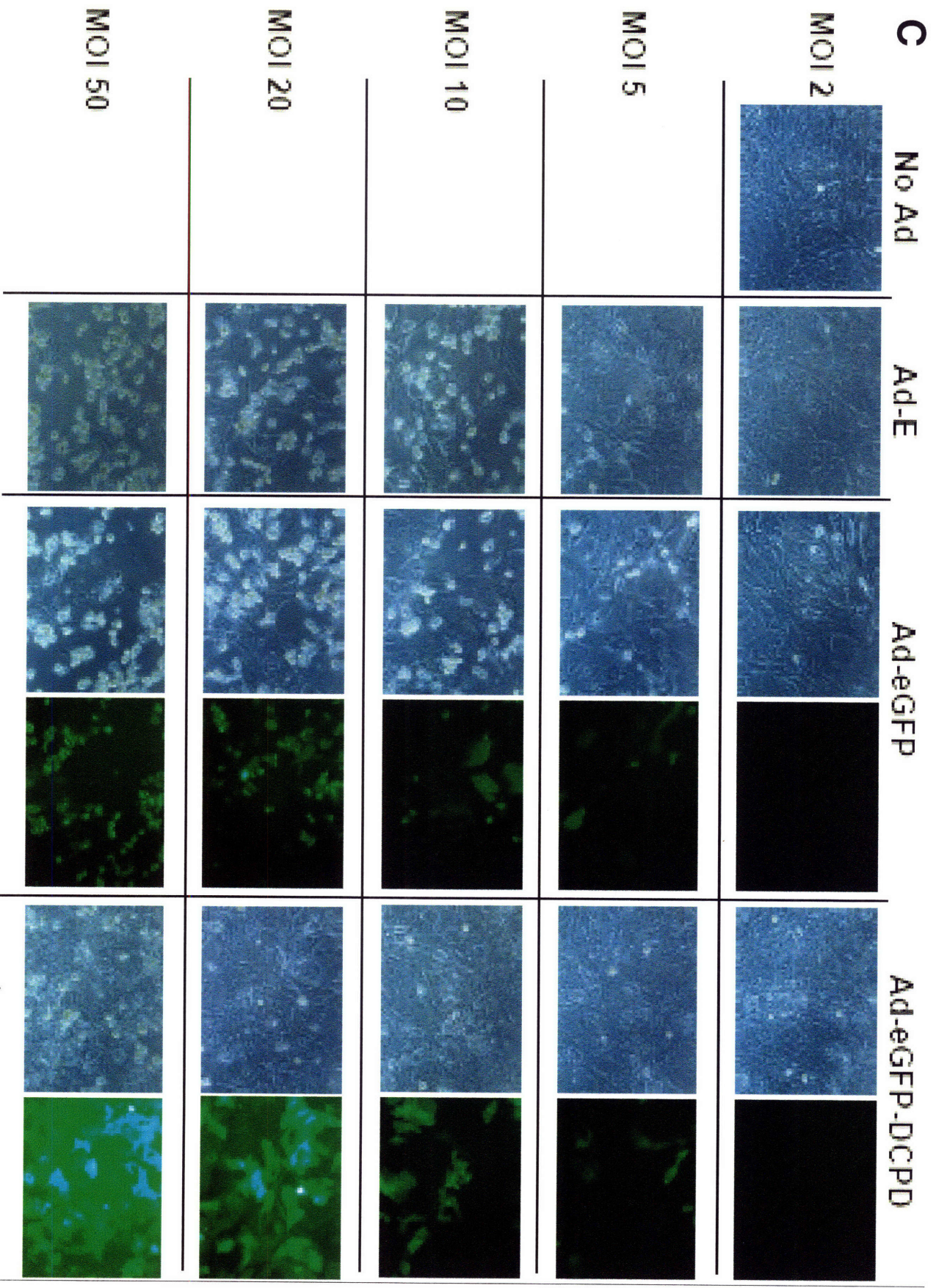


<b>A</b>	No Ad	Ad-E	Ad-eGFP	Ad-eGFP-DCPD
MOI 2			 	 
MOI 5			 	 
MOI 10			 	 
MOI 20			 	 
MOI 50			 	 




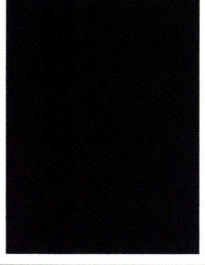



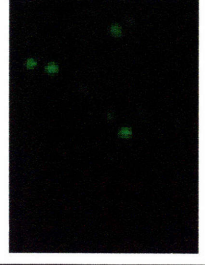


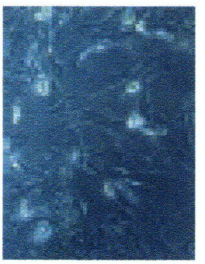
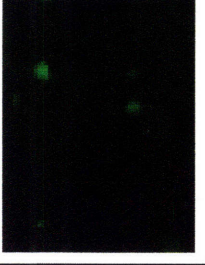

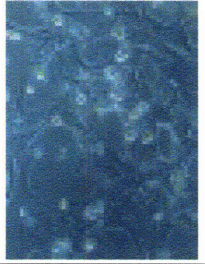
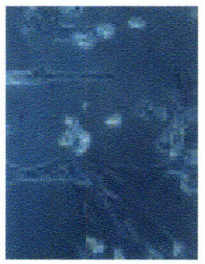
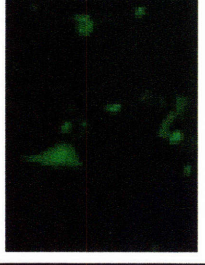



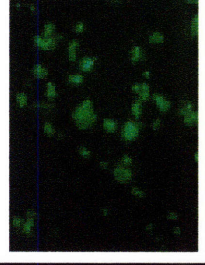






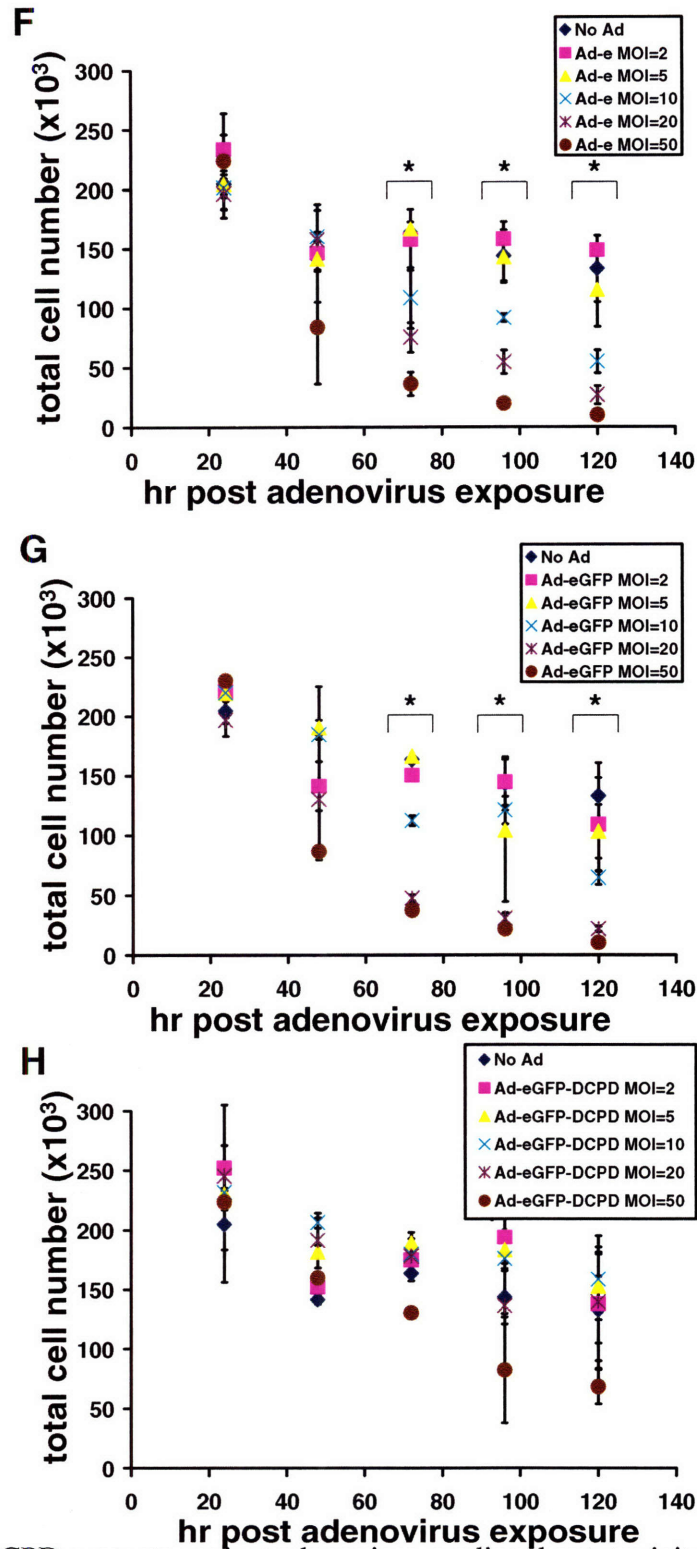




<b>D</b>	<b>No Ad</b>	<b>Ad-E</b>	<b>Ad-eGFP</b>	<b>Ad-eGFP-DCCPD</b>
MOI 2				
MOI 5				
MOI 10				
MOI 20				
MOI 50				

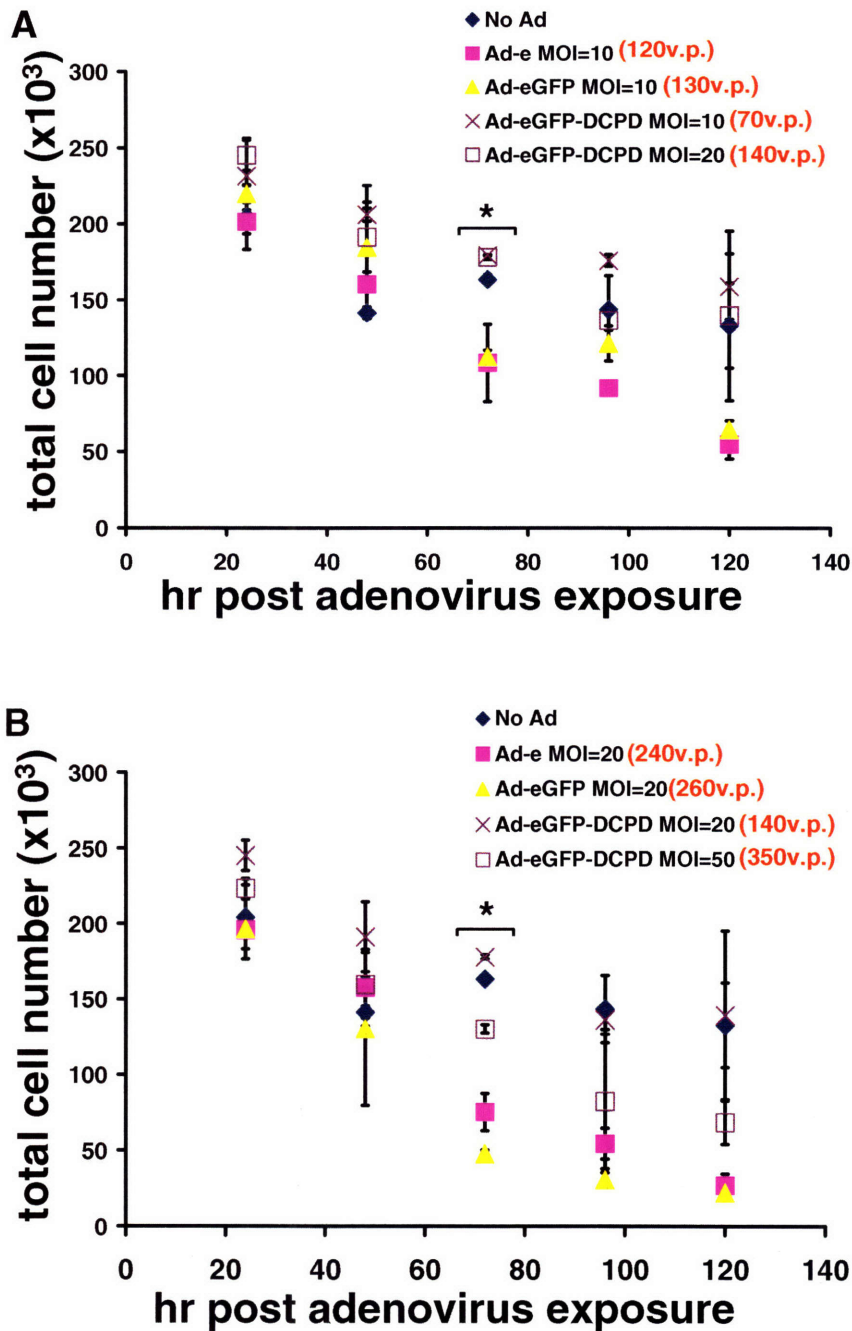


<b>E</b>	<b>No Ad</b>	<b>Ad-E</b>	<b>Ad-eGFP</b>		<b>Ad-eGFP-DCCPD</b>	
<b>MOI 2</b>						
<b>MOI 5</b>						
<b>MOI 10</b>						
<b>MOI 20</b>						
<b>MOI 50</b>						



**Figure 3-4.** DCPD protects against adenovirus-mediated cytotoxicity. A)-E) Phase-contrast and GFP expression images of PRHs following Ad exposure (24h, 48h, 72h, 96h, 120h). Total protein values were determined following adenovirus exposure. F) PRHs exposed to Ad-e vectors. G) PRHs exposed to Ad-eGFP vectors. H) PRHs exposed to Ad-eGFP-DCPD vectors. Data represents mean  $\pm$  SD of 2 biological replicates (2 technical replicates per biological replicate). \*  $P < 0.01$ , significantly different from No Ad control.





**Figure 3-5.** Differences in total viral particles per culture. Total protein measurements made following Ad-exposure (24h, 48h, 72h, 96h, 120h). Rearrangement of data from Figure 3-4. Comparable levels of total viral particles are compared for the three different adenoviral vectors. A) 120-140 virus particles (v.p.) per adenoviral construct. C) 240-350 v.p. per adenoviral construct. Data represents mean  $\pm$  SD of 2 biological replicates (2 technical replicates per biological replicate). \*  $P < 0.01$ , significantly different from No Ad control.

### ***3.3.3 Evidence of DHBV internalization and replication in DCPD-transfected rat hepatocytes***

The influence of DCPD expression levels on DHBV uptake was assessed by immunofluorescence staining of permeabilized cells for DHBV preS envelope protein. Approximately 72h following adenovirus exposure cells were incubated with DHBV for 24h, washed, fixed (2% PFA), and permeabilized (100% MeOH). Immunofluorescence staining for DHBV preS was followed by flow cytometry. As shown in Fig 3-6A, those hepatocytes expressing more DCPD via adenovirus transfection demonstrated greater DHBV binding as evidenced by detection of DHBV preS envelope protein. For increasing Ad-eGFP-DCPD MOI the percentage of DHBV preS-positive cells appears to plateau around ~4.5% (Table 3.2), a value significantly smaller than the percentage of cells that appear to express DCPD. Several factors may account for the relatively low percentage of cells observed to express preS envelope protein. Several groups have determined that DHBV internalization in PDHs occurs in <3h [182, 183]. Once internalized, preS protein is unstable and is rapidly cleared by cellular proteases [184]. Production of viral proteins begins ~96h following DHBV uptake and therefore one would not expect to observe novel preS production at this 48h timepoint [182]. Hence, the preS protein detected in cells at 48h following DHBV exposure reflects the amount remaining after 20-45h of proteolytic digestion.

Western blot analysis of cells subjected to the same DHBV infection protocol as those analyzed by flow cytometry also indicates that DHBV protein is being internalized as evidenced by DHBV preS envelope protein (Fig 3-6b). These cultures were exposed to Ad-eGFP-DCPD MOI=10. Although flow cytometry measured relatively few cells

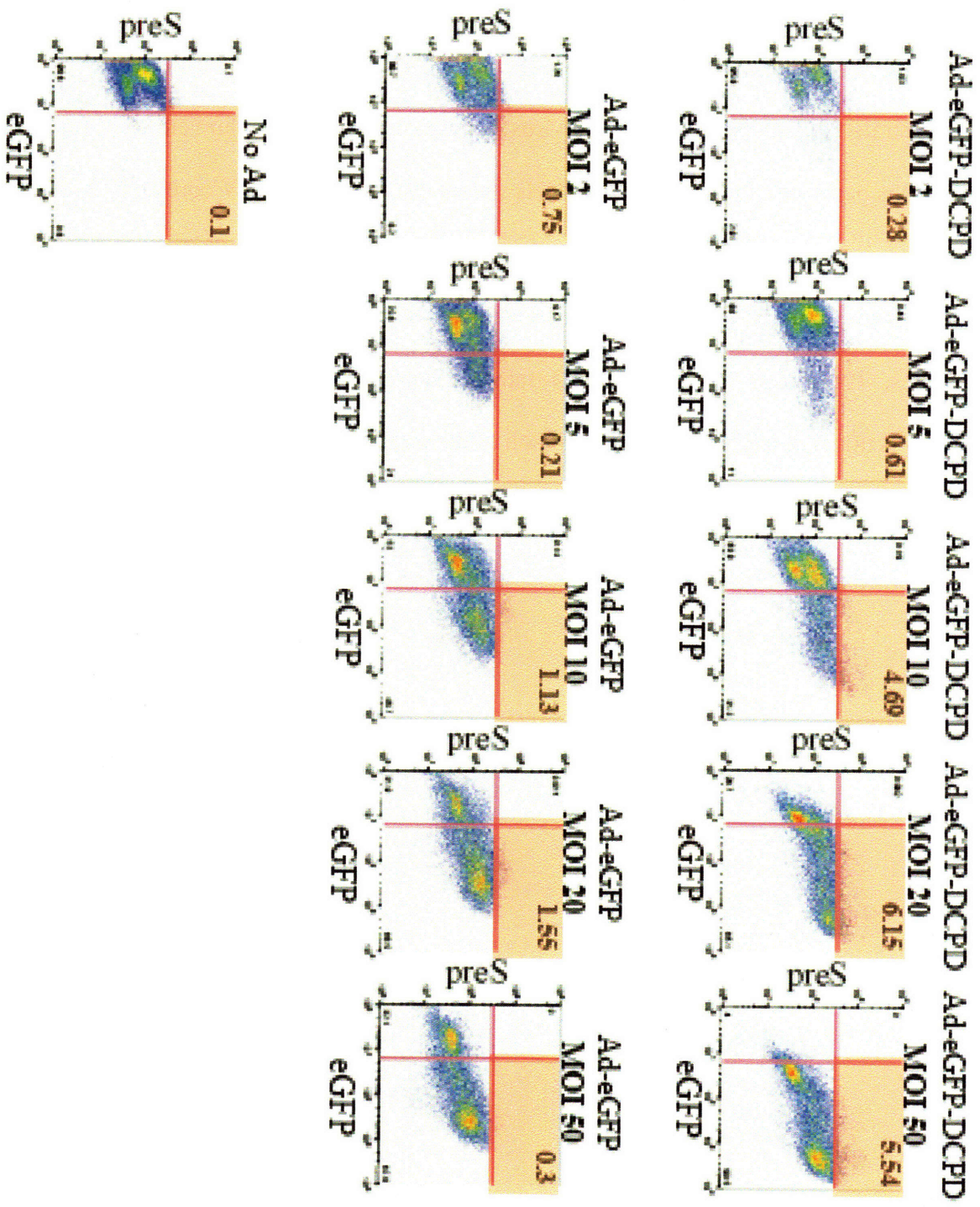
expressing DHBV preS at 48h following DHBV exposure the western blot analysis reveals that preS expression was maintained for over 13 days following DHBV exposure. Such maintenance is consistent with viral replication taking place within these cells. Western blot analysis of supernatant samples collected from the same experiment demonstrate preS envelope protein in the media of DCPD-transfected cultures which is consistent with viral particles being secreted (Fig 3-6c). Equal amounts of total protein is loaded per lane. Band intensity analysis indicate that 5 days after DHBV exposure there is ~200% increase in preS protein in the supernatant in comparison to preS levels present by day 1 post DHBV exposure. This is consistent with other studies that report viral progeny in the media of infected duck hepatocytes ~4 days following DHBV infection [182].  $\beta$ -actin was not detected in the blot (data not shown) confirming that the observed preS envelope protein in the media was not associated with cells present in the media. It should be noted that these blots are representative of several experiments.

There is also evidence of DHBV particles being internalized in the control condition (i.e. Ad-eGFP) (Fig. 3-6c). However, it should be noted that unlike DCPD-transfected hepatocytes, DHBV preS protein is being lost over the culture period in the control condition. The absence of DHBV preS protein in the media samples confirms that the viral uptake does not lead to any evidence of viral replication (Fig. 3-5d).

Recombinant adenovirus particles have been shown to mediate uptake of non-viral macromolecules (e.g. proteins, dextrans, DNAs) possibly through macropinocytosis [185-187]. However, this phenomenon was transient and occurred within minutes following adenovirus exposure. In the present study DHBV was added to the media approximately

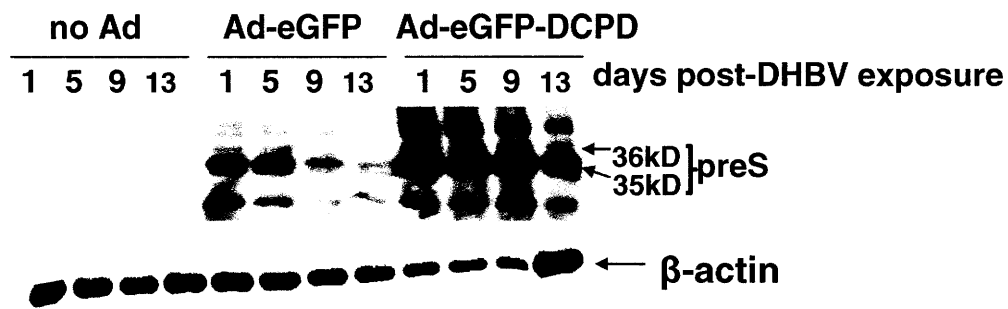
48h following adenovirus being washed out of the system which most likely excludes adenovirus-mediated uptake.

DHBV infection on in vitro PDHs is an inefficient process. It has been demonstrated that under synchronized virus adsorption with an inoculum enriched for infectious particles as few as 10% of PDHs stained positive for DHBV core antigen by 7 days post-inoculation. DCPD-transfected PRHs in the present work were exposed to asynchronous viral adsorption using an inoculum that was not enriched for infectious particles. Therefore, ~5% of the DCPD-transfected population staining positive for preS protein is not necessarily low in comparison to the inefficient infection seen during in vitro PDH infection.

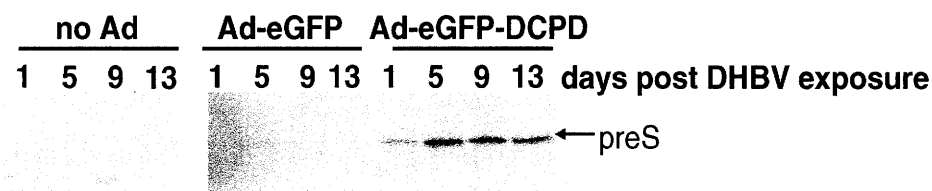
**A**



**B**



**C**

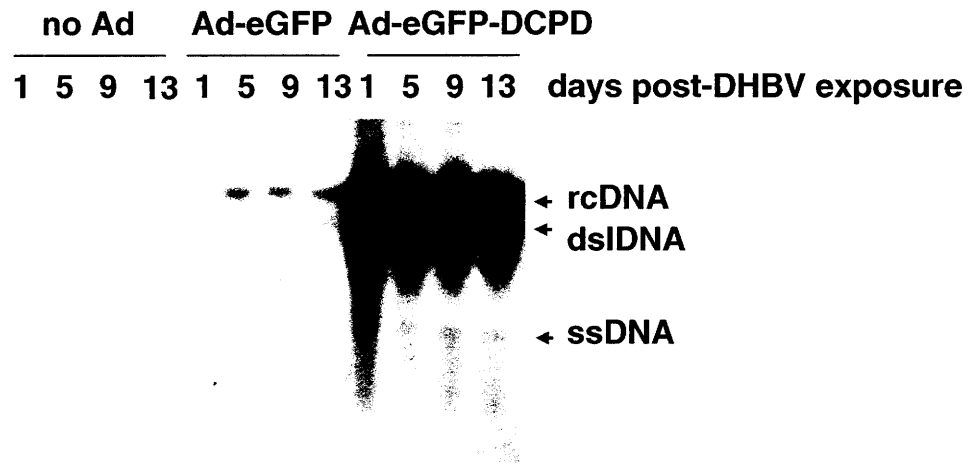


**Figure 3-6.** DHBV preS envelope protein demonstrates evidence of viral replication in DCPD-transfected PRHs. A) Density plots of PRHs exposed to increasing Ad MOI followed by DHBV exposure. Fixed and permeabilized samples represent 120h culture period (48h post DHBV-exposure). For increasing DCPD+ cell population the percentage of cells expressing DHBV preS plateaus at ~5%. B) Representative western blot of preS protein expression in DCPD-transfected PRHs (Ad MOI=10). Maintenance of preS protein is consistent with active viral replication. C) Representative western blot demonstrates freely available preS protein in media of DCPD-transfected PRHs which is consistent with virus being secreted into media.

	preS+/GFP+ (120h)	preS-/GFP+ (120h)
	perm % FACS (% of total pop.)	perm % FACS (% of total pop.)
No Ad	0.10 (0.04)	0.60 (0.24)
Ad-eGFP-DCPD <b>MOI2</b>	0.28 (0.04)	8.20 (2.33)
Ad-eGFP-DCPD <b>MOI5</b>	0.61 (0.19)	24.00 (8.10)
Ad-eGFP-DCPD <b>MOI10</b>	4.69 (1.18)	46.70 (27.23)
Ad-eGFP-DCPD <b>MOI20</b>	6.15 (1.73)	66.50 (~100)
Ad-eGFP-DCPD <b>MOI50</b>	5.54 (3.18)	67.60 (~100)
Ad-eGFP <b>MOI2</b>	0.75 (0.21)	2.91 (0.43)
Ad-eGFP <b>MOI5</b>	0.21 (0.07)	11.00 (3.43)
Ad-eGFP <b>MOI10</b>	1.13 (0.66)	31.30 (7.87)
Ad-eGFP <b>MOI20</b>	1.55 (2.78)	65.10 (18.33)
Ad-eGFP <b>MOI50</b>	0.30 (1.23)	90.50 (51.93)

**Table 3-2.** FACS Analysis of DCPD-transfected PRHs 48h following DHBV exposure

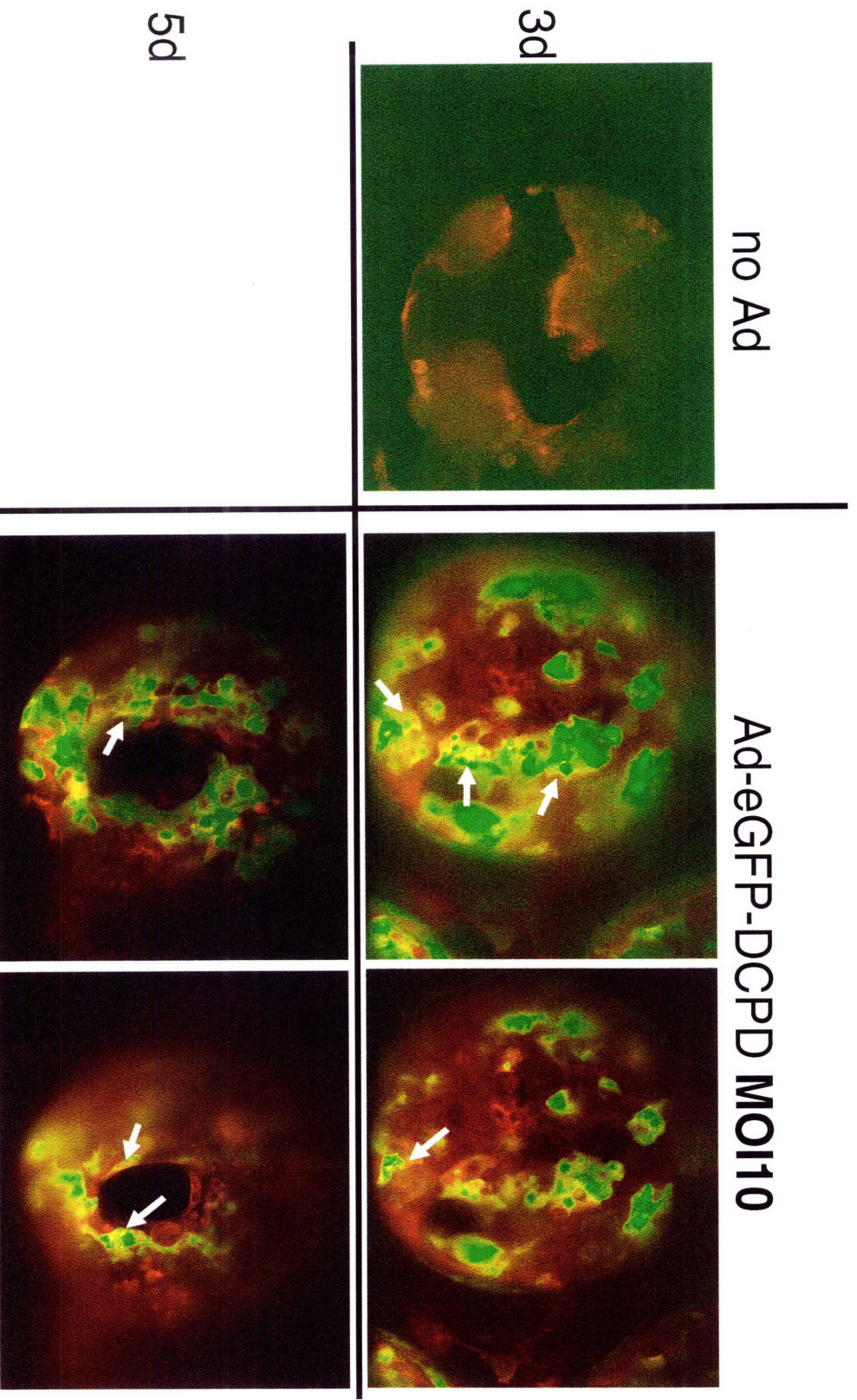
In addition to viral protein, DCPD-transfected cultures exposed to DHBV were also analyzed for DHBV DNA. Southern blot analysis reveals evidence of DHBV DNA intermediates in DCPD-transfected PRHs (Fig. 3-7). Among the many forms in which DHBV DNA exists, single-stranded DHBV DNA (ssDNA) is not present in a mature secreted particle. ssDNA appears during the viral life cycle when the viral pregenomic RNA (pgRNA) is being converted into relaxed circular DNA (rcDNA). Its presence indicates active viral replication taking place in these DCPD-transfected rat hepatocytes. There are relatively small amounts of DHBV rcDNA and dsDNA present in the Ad-eGFP control cultures. These DNA forms are found in the mature infectious DHBV particle. As mentioned in the previous section the adenovirus could be mediating DHBV uptake in these controls but the absence of ssDNA intermediates suggests that the virus is not undergoing viral replication. This is a representative blot demonstrating the typical results that are observed. It should be noted that this representative southern blot was not run with equally loaded DNA in each well. Due to the loss of cells over the course of these experiments, as discussed earlier, attempts to load equal DNA led to signals that were lower than the detection sensitivity of southern blot analysis.



**Figure 3-7.** Representative southern blot image of DCPD-transfected PRHs (Ad MOI=10) demonstrates presence of multiple DHBV DNA replicative intermediates. Lanes are not equally loaded.

### ***3.3.4 DCPD expression in rat hepatocytes maintained in multi-well microreactor***

Adenoviral-mediated transfer of DCPD initiated DHBV replication in freshly isolated PRHs. This phenomenon was lost if PRHs were cultured for a few days prior to DCPD transfection (data not shown). The loss is most likely attributed to the decrease in liver-specific factors necessary for the initiation of viral replication when primary hepatocytes are cultured on collagen-coated polystyrene [146]. A three-dimensional perfused culture system that recapitulates key aspects of the liver microenvironment has been previously described [164]. Previous characterization has demonstrated that the 3-D perfused culture system maintains a liver phenotype closer to that of native liver than other standard culture systems (e.g. collagen-coated polystyrene, collagen gel sandwich) [9, 10]. To investigate the possibility of applying a similar infection strategy in this system adenovirus was added directly to the media in the reservoir. Following a 24h incubation the adenovirus was washed out. At different timepoints following Ad exposure the scaffolds, containing the cells, were removed from the microreactor, fixed, permeabilized and stained for DCPD expression. Confocal imaging reveals DCPD expression throughout the tissue formed in the channels (Fig 3-8). Co-localization of the GFP and the AlexaFluor 568-conjugated secondary antibody to detect the DCPD reveals mainly cell surface expression of the DCPD. As with the FACS analysis in Fig 3-3 there are also cells present in the channel which are positive for the DCPD and negative for the GFP. These data indicate that the PRHs maintained in the microreactor can be transfected with DCPD. Differential DCPD expression throughout the tissue structures suggests differential Ad exposure within the tissue.



**Figure 3-8.** Confocal images of DCPD-transfected microreactors at 2 different timepoints following adenovirus exposure (3d & 5d). Tissues were fixed and permeabilized. Primary DCPD Ab binding was detected via AlexaFluor 568-conjugated secondary. Overlay of GFP and RFP image stacks reveal DCPD+/GFP+ cells. DCPD expression tends to localize at cell periphery although there are some examples of diffuse intracellular staining (arrows). Adjacent images for each condition represent different depths in same channel. 20x objective.

### 3.4 Discussion

Previous research has demonstrated that freshly isolated PRHs are capable of producing infectious viral progeny upon transfection of the DHBV genome. DHBV was able to cross the species barrier and effectively replicate using following the artificial delivery of the viral genome to the host cell nucleus. In this study we have established that PRHs are capable of supporting viral replication upon transfection of DCPD, the known internalization receptor for DHBV.

In this study the E1/E3-deleted recombinant Ad5 vectors carrying both DCPD and GFP transgenes under separate CMV promoters were generated. Although GFP is generally used as a marker for expression of both transgenes our analysis revealed the presence of subpopulations that differentially express GFP and DCPD. Fluorescence micrographs showed that the percentage of GFP-positive cells noticeably declined over 5 days following Ad exposure, DCPD expression was maintained for ~ 2 weeks via western blot analysis. This differential expression could be due to an adenovirus-mediated retention of the DCPD. FACS analysis revealed that the majority of DCPD was available at the cell surface in the DCPD-transfected cultures. This is in contrast to other studies in which DCPD is only transiently available at the cell surface. A 20-residue region within the cytoplasmic tail of CPD binds Protein Phosphatase 2A (PP2A). It has been shown that when the binding of PP2A to DCPD is inhibited or competed with via microinjection of the CPD cytoplasmic tail the rate of movement of CPD from the cell surface to the TGN is greatly slowed [188]. This suggests that PP2A plays an important role in the intracellular trafficking of CPD. E1/E3-deleted Ad vectors still express low levels of wild-type gene products that include E4 [189]. Studies have shown that the primary target of E4 ORF4 is

PP2A [190]. It is possible that E4 ORF4 protein is competing with DCPD to bind PP2A and effectively “trapping” the 180kDa DCPD at the cell surface.

The 2 separate DCPD proteins (180kDa and 170kDa) detected in DCPD-transfected PRHs has been also been observed in primary duck hepatocytes in other studies. While the 180kDa probably represents the full-length membrane-bound form the 170kDa protein could be a truncated soluble version as seen in other studies [138, 191]. Such smaller soluble versions have also been seen in bovine and rat tissues [176, 192]. Other groups have shown that following DCPD-transfection the resulting 170kDa protein demonstrated similar DCPD enzymatic activity, activation, and pH optimum. However, the 170kDa protein demonstrated a lack of reactivity to antiserum raised against the C-terminal tail which suggested that it was missing a significant portion of the transmembrane domain and cytoplasmic tail [176]. This truncated protein could be the result of proteolysis or differential mRNA splicing.

Another interesting finding of this study is the increased cell death in control cultures observed with increasing Ad MOI which was not observed in DCPD-transfected cultures. This cytotoxicity could not be explained by the overall difference in total viral particles present in the adenovirus stock preparations. This suggests that DCPD appears to be protective against Ad-mediated apoptosis. CPDs cleave individual amino acids (specifically Arg or Lys) from the COOH-terminal portion of peptides and proteins. DCPD is primarily located in the TGN and is thought to function in protein processing along the secretory pathway. Cell surface CPD has been shown to mediate nitric oxide (NO) production, via inducible NO synthase (iNOS induction), in both isolated perfused rat lungs and rat lung microvascular endothelial cells [193]. Cell-surface CPD was shown



to cleave various substrates and release extracellular Arg, which upon cellular uptake, triggered NO production through iNOS. As the present data shows the majority of DCPD being expressed in the DCPD-transfected PRHs is available at the cell surface. Various media components (e.g. albumin, EGF) could serve as substrates for cell surface DCPD.

NO has a complex biological role that can be either beneficial or detrimental to a cell. iNOS mediated NO has been shown to protect against hepatic apoptotic cell death seen in models of sepsis and hepatitis [194]. Factors that determine whether NO protects or injures include the amount, duration, and source of NO production. Therefore, it is possible that DCPD being expressed at the PRH-surface is mediating sufficient NO production for a sufficient time period that is protecting against adenovirus-mediated apoptosis.

Although flow cytometry data revealed a low percentage of cells staining for preS envelope protein these cells are demonstrating active viral replication. The combined maintenance of intracellular preS levels and the increase in extracellular preS protein detected at 5days post DHBV exposure is consistent with the secretion of viral progeny that occurs during natural infection. Viral replication in DCPD-transfected PRHs was also substantiated by the appearance of DHBV ssDNA, a viral form that appears during viral replication. Southern blot analysis used unequally loaded total DNA but it has been previously establish in this study that there is cell loss over the culture period. Therefore, it is not possible to extract conclusions about trends seen in ssDNA expression. Although control cultures did demonstrate some evidence of DHBV binding the loss of preS expression over time and the absence of extracellular preS levels is consistent with the



viral protein being degraded. The minimal levels of rcDNA most likely represent the non-specific binding of DHBV particles.

Recombinant adenovirus particles trigger receptor-mediated endocytosis concomitant with macropinocytosis which is thought to mediate uptake of non-viral macromolecules (e.g. proteins, dextrans, DNAs) available in the extracellular fluid [185-187]. Macropinocytosis, a major endocytic pathway involved in non-specific bulk fluid phase uptake, has been described in murine hepatocytes [195]. Recently, macropinocytosis has been suggested as a possible pathway for uptake of Vesicular stomatitis virus/HCV pseudotyped viruses in HepG2 cells. One possible scenario would be that in addition to the control Ad vectors causing increased cell death it also triggers macropinocytosis such that DHBV particles could gain non-specific entry. However, Ad-triggered macropinocytosis is transient and occurred within minutes following adenovirus exposure in previously published studies using HeLa cells [187]. In the present study DHBV was added to the media approximately 48h following residual adenovirus being washed out of the culture. Whether this phenomenon can still take place by this 48h timepoint is unknown.

The strategy to render PRHs susceptible to DHBV infection was lost once freshly isolated cells were cultured for a few days (data not shown). Such a loss is likely due to the loss in expression of liver-specific factors necessary for the initiation of viral replication when primary hepatocytes are cultured on collagen-coated polystyrene. Confocal imaging demonstrates that DCPD expression via adenoviral delivery is feasible in a more liver-like culture system. In standard culture the adenovirus has to diffuse through the media to reach the layer of hepatocytes. It is assumed that with a well-mixed

medium that the hepatocytes lining the dish have equal access to the adenovirus particles. In multiwell culture diffusive and convective transport through the tissue in each channel will affect the adenovirus exposure for hepatocytes such that the MOI seen by hepatocytes at the fluid-tissue interfaces differs from the MOI experienced by hepatocytes located adjacent to the channel wall. Such considerations represent a more physiological condition in which cells with closer proximity to incoming blood experience greater access to oxygen and nutrients than cells located closer to the exiting blood as in the metabolic zonation of the hepatic acinus [33-35]. It was demonstrated in this study that PRHs cultured in the multi-well microreactor can be transfected with DCPD. Differential DCPD expression throughout the tissue does suggest differential exposure as well as differential translational machinery.

DCPD-transfected PRHs do represent a novel system in which to study the early steps of the DHBV life cycle. Viral markers indicate a relatively slow infection process but similar inefficiency is seen during DHBV infection of in vitro cultures of PDHs. We have also demonstrated that recombinant adenoviral vectors can mediate an alternative mechanism by which DHBV can non-specifically penetrate primary rat hepatocytes although it does not seem to result in active replication.

## Chapter 4.

# Prolonged Susceptibility to DHBV Infection in Rat Hepatocytes Maintained in a 3D Perfused Culture System

### 4.1 Introduction

Human Hepatitis B Virus (HBV) is the prototype member of the family *Hepadnaviridae* that consists of enveloped, partially double-stranded DNA viruses that specifically target cells in the liver for viral replication. Although a vaccine has been available for more than 20 years chronic hepatitis B afflicts ~5% of the world's population (350 – 400 million) [11]. It is estimated that 500,000 to 1.2 million people die each year from HBV-attributable cases of chronic hepatitis, cirrhosis, and hepatocellular carcinoma [12, 13].

Currently available therapeutics include interferon alpha (IFN $\alpha$ ). This naturally occurring cytokine has a dual mode of action; the first being the inhibition of viral replication and the second being the enhancement of the immunological response of the host against the virus. The disadvantages associated with IFN $\alpha$  include a limited efficacy rate, undesirable side effects, and an inconvenient dosing regimen (3 injections per week). Studies have shown that the addition of a polyethylene glycol (PEG) molecule to IFN $\alpha$  significantly increases the half-life and leads to more sustained activity[21, 22]. Other therapeutics include nucleoside analogues (e.g. lamivudine) which are synthetic molecules that, following conversion into nucleoside triphosphate equivalents, compete with natural nucleoside triphosphates for incorporation into viral DNA by the viral DNA polymerase. Since these analogues lack a bond site necessary to link it to an adjacent nucleoside their

incorporation effectively terminates the elongation of nascent viral DNA chains and therefore inhibits viral replication. Lamivudine which is administered orally has minimal side effects. However, it does display a modest efficacy rate of 20-30% following a 12 month dosing regimen [23]. Following therapy termination most patients experience a relapse evidenced by the detection of viral DNA and HBeAg in the serum [24].

Continuous lamivudine treatment is necessary for a sustained therapeutic effect. This is a major drawback when combined with the observation that lamivudine-resistant HBV species emerge during long-term treatment [23, 24]. These therapeutics interfere with viral replication but it is prudent to develop novel therapeutics which target earlier events in the viral life cycle (i.e. viral attachment, viral uptake, fusion, delivery to the host cell nucleus). Combined antiviral therapies that target both early and late viral life cycle events may be more effective in suppressing viral replication and preventing relapses observed when current drug therapies are discontinued [196, 197].

Future antiviral drug therapy is dependent on the development of better cell culture systems. To date, no successful in vitro system has been developed for chronic HBV infection wherein the entire viral life cycle can be studied. The use of primary human and primate hepatocytes is restricted by multiple experimental limitations including a rapid loss of susceptibility to infection in culture, lot-to-lot variability in susceptibility to infection, and the necessity of treatment with chemical agents such as DMSO for reproducible infection [107, 108, 120]. Permissive cell lines (e.g. HepG2, Huh7) are capable of supporting viral replication upon transfection with the viral genome. HepG2.2.15, a subline of HepG2, is stably transfected with multiple copies of the HBV genome [121]. HepG2.2.15 cells express all viral RNAs and proteins, produce viral genomes, and secrete

virus-like particles. These cell lines have shed greater light on the later events in the viral life cycle (i.e. transcription, encapsidation reverse transcription, virion assembly, export). However, there is less understanding of the early stages that include virus attachment, internalization, uncoating, genome repair, and nuclear transport. These cell lines do not mimic natural infection which limits their usefulness. An in vitro system that will allow us to target other aspects of the viral life cycle is needed.

Recently, a cell line known as HepaRG was shown to be susceptible to infection under certain conditions. In the presence of PEG, DMSO, and/or hydrocortisone HepaRG cells exhibit hepatocyte-like morphology, express liver-specific functions (e.g. albumin, aldolase B, CYP3A4), and demonstrate phase I and phase II drug metabolism enzyme activity in the range of normal human hepatocytes [122]. DMSO and hydrocortisone are known inducers of cell differentiation although the underlying mechanism is not known.

Hepadnaviruses are subdivided into two categories based on sequence homology; orthohepadnaviruses which infect mammals and avihepadnaviruses which infect birds. Duck HBV (DHBV) was the first avihepadnavirus detected while others have been isolated more recently from grey herons, snow geese, white storks, and cranes. Avihepadnaviruses share little sequence homology with orthohepadnaviruses (~40%). DHBV expresses two major envelope proteins (instead of three) (Section 1.6.2). However, similar genome organization, virus structure, and replication characteristics among hepadnaviruses warrant the study of hepadnaviruses found in other species. Many of the principles of hepadnavirus life cycle were elucidated by studying duck hepatitis B virus (DHBV) as a model for HBV. Some of these principles include the replication by reverse transcriptase [125], cccDNA formation [126], and host-range determinants [127-129].

However, reproducible in vitro infection of primary duck hepatocytes requires culture conditions that incorporate 1.5-2% DMSO whose mechanism of action is unknown [130, 131]. Even with such artificial additives the kinetics of in vitro infection are slow and inefficient when compared to in vivo infection of neonatal ducklings [132].

Our group has developed an in vitro system that recreates a perfused liver capillary bed structure. This perfused three-dimensional culture system recapitulates key aspects of the liver microenvironment in order to maintain a well-differentiated liver phenotype as evidenced by multiple criteria (e.g. biochemical production, tissue morphology, liver-enriched mRNA expression, and drug metabolism) [9, 10]. Using a novel method to render PRHs susceptible to DHBV this study demonstrates that PRHs cultured in this microreactor remain susceptible to DHBV infection at longer timepoints in culture than in standard tissue culture.

## **4.2 Materials & Methods**

### **4.2.1 Primary rat hepatocyte isolation and culture**

Primary liver cells were isolated from male Fischer rats (150 – 230g) using a modified version of Seglen's two-step collagenase perfusion procedure [164] as previously described [165]. Tissue dissociation was accomplished using Liberase Blendzyme 3 (Roche). Final cell viability was in the range of 89-94 % based on trypan blue exclusion. The final cell pellet (~95% hepatocytes) was re-suspended in supplemented DMEM (GIBCO) that includes 0.03g/L proline, 0.10g/L ornithine, 0.305g/L niacinimide, 2.0g/L glucose, 2.0g/L galactose, 2.0g/L bovine serum albumin, 0.05mg/mL gentamycin, 5mg/L insulin, 5mg/L transferrin, 5ug/L sodium selenite, 20ng/mL epidermal growth factor, 1mM L-glutamine, 0.1uM dexamethasone, and trace metals (5.44mg/mL ZnCl<sub>2</sub>, 7.5mg/mL

ZnSO<sub>4</sub>·7H<sub>2</sub>O, 2.0mg/mL CuSO<sub>4</sub>·5H<sub>2</sub>O, 2.5mg/mL MnSO<sub>4</sub>) collectively referred to as Hepatocyte Growth Media (HGM) [166]. Resuspended hepatocytes were plated on polystyrene plates coated with collagen type I (30 μg/mL) (BD Biosciences) at a plating density of 50,000 cells/cm<sup>2</sup>. Cultures were maintained at 37°C and 5% CO<sub>2</sub> with media changes every 48h.

#### **4.2.2 Preparation of spheroidal cell aggregates in spinner flasks**

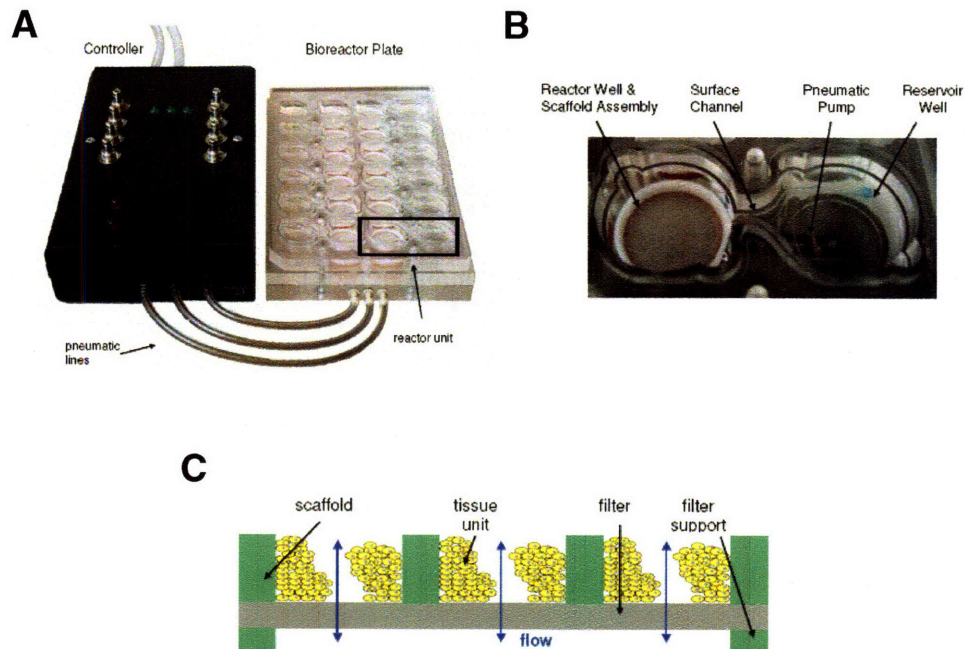
Spheroidal cell aggregates were formed in suspension as previously described [9, 164]. Briefly, freshly isolated hepatocytes were added to spinner flasks (BellCo, USA) at 3x10<sup>5</sup> hepatocytes/mL HGM and cultured on a spinner table at 84rpm (37°C and 8.5% CO<sub>2</sub> with humidity) to induce spheroid formation. Following a 24hr culture period, 50- to 300-μm spheroids were collected by filtering through appropriately sized nylon meshes (SEFAR America, Kansas City, MO), pelleting (50xg, 3min), and resuspending in HGM.

#### **4.2.3 Giant microreactor culture**

The giant microreactor is a multilayered structure whose design and assembly have been described elsewhere [7]. Briefly, the main portion of the microreactor is a polycarbonate scaffold (~230μm thick) that contains a regular array of channels into which cells are seeded. The scaffold is positioned on a microporous filter that is mechanically supported by a second scaffold. Cooled drilling methods were employed to make the array of evenly spaced channels (1000 total channels), each with a 300μm diameter. The primary scaffold channels are coated with collagen type I (30μg/mL) to allow for cellular attachment. The fully assembled microreactor was primed with HGM to passivate the reactor, connector, and tubing surfaces, and to remove air bubbles from the flow paths. Immediately prior to seeding, fresh HGM was added to the media reservoir. Seeding was

accomplished by removing the top polycarbonate window and pipetting ~1mL of spheroidal cell aggregate suspension onto the polycarbonate scaffold. A downward crossflow was maintained during seeding in order to pull the spheroidal aggregates into the channels. The microreactor was also gently rocked back and forth to ensure even seeding across all the channels. Excess spheroids were carefully aspirated off the scaffold. After replacing the top window the peristaltic pumps were used to set flow rates which were chosen based mainly on physiological shear stress conditions [9, 164]. During the first 24h the media perfuses the channels in a downward direction to pull the cells into the channels. After 24h the media crossflow is reversed in order to eliminate cellular debris from the channels and fresh media is added to the reservoir. Microreactors were maintained at 37°C, 8.5% CO<sub>2</sub> with media changes every 72h.

#### 4.2.4 Multi-well microreactor culture



**Figure 4-1.** Diagram of multi-well microreactor. A) Image of microreactor connected to controller device for pneumatic pumps. B) Image of individual reactor unit consisting of media reservoir and a reactor well containing the scaffold assembly which is connected by a surface channel and a pneumatic pump. C) Illustration of scaffold assembly with tissue in channels.



A schematic of the microreactor and fluidic circuit is shown in Figure 4-1. The microreactor is a multilayered structure whose design and assembly have been previously described [170]. Briefly, there are 12 reactor units on a single fluidic plate. Each microreactor unit consists of a scaffold assembly and a media reservoir. The polycarbonate scaffold has an array of 800 circular channels (diameter = 300 $\mu$ m, depth = 230 $\mu$ m). Cells in the scaffold channels are continuously perfused with culture media from the reservoir via a pneumatic pump which is then recirculated across a surface channel back to the reservoir. Each reactor unit is fluidically isolated but all pumps are simultaneously driven by pneumatic control lines connected to sources of positive and negative air pressure. Physiological rates of media perfusion are achieved by controlling the frequency of the pulses of air pressure. Primary scaffold channels are coated with collagen type I (30 $\mu$ g/mL) to allow for cellular attachment. Prior to seeding, the microreactor system is primed with HGM in order to passivate the surfaces and remove any air bubbles in the fluidics. Primary cells isolated from the rat perfusion are pipetted directly into the channels of the scaffold and adhere to the collagen coating the channel walls. During the first 8h the media perfuses the channels in a downward direction in order to pull the cells into the channels. To eliminate any residual cell debris that might clog the filter the media flow is reversed (lower chamber to upper chamber) after 8h and fresh media is added to the reservoir. Microreactors were maintained at 37°C and 5% CO<sub>2</sub> with daily media changes.

#### **4.2.5 Generation of recombinant adenovirus vectors**

The adenovirus constructs were generated using the AdEasy Vector System as previously described [146]. Briefly, a shuttle vector containing the gene of interest

(DCPD) and an adenovirus backbone plasmid that includes the Ad5 genome with both E1 and E3 genes deleted were co-transformed into an *E. coli* strain (BJ5183). The highly efficient homologous recombination machinery within the bacteria produce recombinant adenovirus constructs containing the gene of interest. These constructs are linearized and transfected into the 293 packaging cell line which constitutively express E1 gene products, necessary for propagation of all recombinant adenoviruses. Successful viral production is monitored via the GFP reporter gene which is also incorporated into the adenovirus backbone plasmid. Further tests were done to confirm that there were no replication-competent adenovirus constructs present in the final preparations. The final recombinant adenovirus containing the DCPD gene is designated Ad-eGFP-DCPD. This vector was kindly provided by the Wands laboratory at Brown University. Further amplification and purification was performed by Puresyn, Inc.

#### **4.2.6 DHBV-positive serum isolation**

Mammoth White Pekin ducklings were obtained from a commercial supplier (Ridgway Hatchery), housed at the Liver Research Center at Brown University, and given ad libitum access to food and water. Three-day old ducklings were injected in a foot vein with 200uL of highly viremic duck serum. Five days later the duck was sacrificed by pentobarbital overdose (Abbott Laboratories) and the total blood volume was collected via cardiac puncture. Total blood was kept at room temperature for ~6hrs and then spun (3000 rpm) for 5 min. The serum was collected and tested for DHBV particles via dot blot analysis. Briefly, total DNA was isolated using QIAamp DNA MicroKit (Qiagen), boiled at 100C for 10 min and placed immediately on ice. DNA was spotted onto nylon membrane (Schleicher & Schuell) and fixed using UV exposure. A <sup>32</sup>P-radiolabeled

DHBV DNA probe was added overnight (45C). Following multiple washes, the blot was exposed to a phosphor screen that was developed on a Cyclone Imaging Station (Packard Bioscience).

#### **4.2.7 DHBV infection**

##### **4.2.7.1 Standard 2D culture**

Approximately 6h after plating, cultures were exposed to adenovirus vectors diluted in HGM to achieve the proper multiplicity of infection (MOI). Cells were cultured with the adenovirus for ~24h at 37C prior to being removed with multiple washes of Phosphate Buffered Saline (PBS). DHBV-positive duck serum was diluted (1/5) in HGM and added to the cultures for 24h incubation at 37°C. The diluted serum contained  $\sim 4 \times 10^8$  virus genome equivalents (vge) as determined by PCR analysis. Non-adsorbed virus particles in the culture were removed with multiple PBS washes. Cells were maintained at 37°C with media changes every 48h.

##### **4.2.7.2 Multi-well microreactor**

Approximately 6h following seeding single cells into the multi-well cultures were exposed to adenovirus vectors diluted in HGM to achieve the proper multiplicity of infection (MOI). Cells were cultured with the adenovirus for ~24h at 37C followed by multiple HGM washes to remove excess vectors. DHBV-positive duck serum was diluted (1/5) in HGM and added to the cultures for 24h incubation at 37°C. The diluted serum contained  $\sim 4 \times 10^8$  virus genome equivalents (vge)/mL as determined by PCR analysis. Excess virus particles in the culture were removed with multiple PBS washes. Cells were maintained at 37°C with media changes every 24h.

#### **4.2.8 Sodium dodecyl sulfate-polyacrylamide gel electrophoresis (SDS-PAGE) and Western blot analysis**

Cell samples were lysed with 100uL RIPA buffer on ice for 20 minutes and total protein was determined by BCA protein assay (Pierce). SDS-PAGE was done using 7.5 or 12% polyacrylamide gels (BioRad). Prior to loading the gel, samples were adjusted so that equal amounts of total protein were loaded onto the gel. Following electrophoresis, proteins were transferred to a polyvinylidene difluoride (PVDF) membrane (BioRad, USA). The PVDF membrane was probed with primary antibodies that included: polyclonal rabbit anti-DGD (1:20000 dilution), polyclonal rabbit anti-actin (1:5000 dilution; Santa Cruz) and polyclonal goat anti-HNF4 $\alpha$  (1:5000 dilution) (Santa Cruz). Primary antibodies were detected with either goat anti-rabbit HRP-conjugated secondary antibody (1:5000 - 1:10000 dilution) (Jackson Immunoresearch) or rannit anti-goat HRP-conjugated secondary (1:500 – 1:1000 dilution) (Santa Cruz). Detection and quantification were done using enhanced chemiluminescence (ECL) (Amersham, USA) and a Kodak Image Station (Eastman Kodak).

#### **4.2.9 Isolation and detection of DHBV DNA in primary rat hepatocytes via quantitative real-time PCR analysis**

Frozen cell samples were thawed to room temperature and total DNA was extracted with the DNeasy Tissue Kit (Qiagen). Using a strategy adapted from Kock & Schlicht [198] we developed a real-time PCR assay in which a primer/probe set is targeted for a region in the DHBV genome that is common to all viral DNA forms (Table 4-1). For dsDNA, the region targeted by the primer/probe set is unaffected by the linear nature of the viral DNA. It should be noted that the ssDNA includes the complete (-) strand and

would be detected by the probe and the forward primer of Set A. However, since the (+) strand is absent, ssDNA would not be amplified during the PCR and therefore would not contribute significantly to the fluorescent signal. The second primer probe set (Table 4-1) is designed to converge upon the gap region in the (-) strand of the DHBV genome. This gap is present in rcDNA but not in cccDNA. Again, ssDNA would not contribute significantly to the signal for the reason mentioned earlier. dsDNA is also not detected by the second primer/probe set because the gap region is effectively infinite due to the linearity of the viral DNA form. Therefore the second primer/probe set is selective for cccDNA.

Standard curves were established by isolating total DNA from DHBV+ Pekin duck liver (Qiagen DNeasy Tissue Kit and QIAamp DNA Micro Kit). Almost full-genome length DHBV DNA fragments were amplified via PCR consisting of thermostable DNA polymerases with proofreading activity and DHBV-specific primers (Expand High Fidelity PCR System, Roche). The amplified product was run on 1% agarose gel and the DHBV DNA band (~3kb) was excised and purified (QIAquick Spin Kit, Qiagen). This purified DHBV DNA was quantified spectrophotometrically (Nanodrop) and represents total DHBV DNA. In the literature it has been found that cccDNA represents ~2% of total intracellular viral DNA [199]. Using these data, real-time PCR assays using total DHBV DNA-specific and cccDNA-specific primer/probe sets (Table 4-1) were run using serial dilutions of DHBV DNA.

#### 4.2.10 Fluorescence analysis

Cultures maintained on collagen-coated polystyrene dishes were imaged using a Zeiss Axiovert 100 microscope. GFP expression was imaged using a fluorescein isothiocyanate (FITC) filter.

#### 4.2.11 Statistical Analysis

Statistical significance of results was analysed using GraphPad Prism Version 4.0 for Windows (GraphPad Software, San Diego, CA). Student's *t*-test was used to compare differences between two groups. Results were considered significant when probability values were <0.10.

<b>Almost full-length DHBV genome primers</b>	FW 33	5'-CTACATTGCTGTTGTCGTGTGT-3'
	REV2932	5'-AGGAGGTTTGTGCCTGGAT-3'
<b>Total DHBV DNA-specific (rcDNA, dsDNA, cccDNA)</b>	FW1374	5'-GGCTAGATTGGTGGTGGATT-3'
	REV1520	5'-AAAGCCTGAGATAGGTCCAAAG-3'
	PROBE1426	5'[FAM]-CGCTTCCAAAGATACTGGAGCCCA-[TAMRA]3'
<b>DHBV cccDNA-specific</b>	FW125	5'-TCCTGATTGGACGGCTTT-3'
	REV272	5'-GTCACACACGACAACAGCAA-3'
	PROBE216	5'[FAM]-CCTTCGGAGCTGCTTGCCAAG-[TAMRA]3'
<b>GAPDH-specific</b>	FW2242	5'-TGGGATAGCCAGTGCTCTTA-3'
	REV2322	5'-ACAGGAGATGGGTTGGAAC-3'
	PROBE2267	5'[FAM]-TGAGCCATCATCATCTCCGCTG-[TAMRA]3'

**Table 4-1.** Primer/probe sets designed to amplify different DHBV DNA forms.

## 4.3 Results

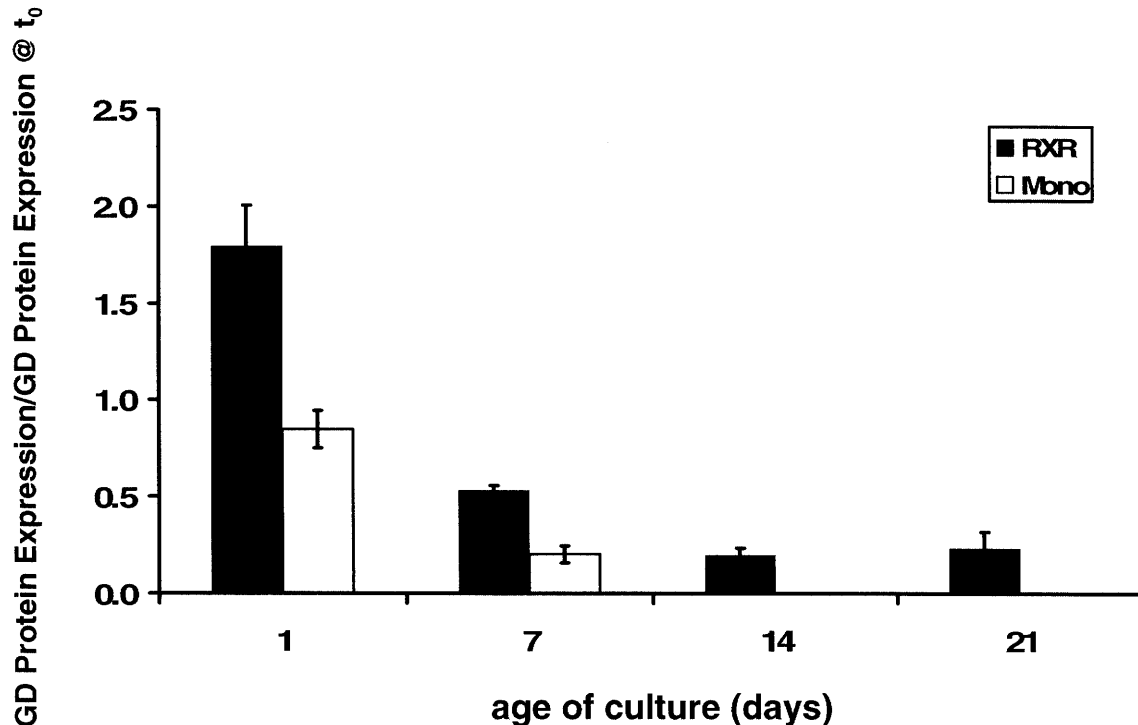
### 4.3.1 Maintenance of factors necessary for DHBV replication

It has been previously demonstrated that duck glycine decarboxylase (DGD) is a necessary protein that mediates a postbinding step in DHBV replication [146]. These previous studies revealed that diminished primary duck hepatocyte (PDH) susceptibility to DHBV infection correlates with declined DGD protein expression. Sprinzl et. al. [175] demonstrate that upon transfection with the DHBV genome immediately following plating, primary rat hepatocytes produce both cccDNA and infectious DHBV progeny. This evidence indicates that by circumventing the natural process the DHBV employs to penetrate the host cell, the rat homolog of proteins such as glycine decarboxylase are sufficient to establish productive replication.

Following rat liver perfusion, PRHs were cultured in both the collagen-coated microreactor and standard collagen-coated monolayer on polystyrene. At multiple timepoints during culture cell samples were lysed in RIPA buffer and analyzed for rat glycine decarboxylase (GD). Western blot analysis indicates GD is better maintained in microreactor culture than standard monolayer culture (Fig. 4-2). Using band intensity analysis the GD expression at multiple timepoints was compared to GD expression in PRHs immediately following the perfusion. In microreactor culture there is a ~2-fold increase in GD expression after 1 day in culture. By day 7 there is ~50% GD being expressed relative to that found in PRHs immediately following perfusion. Over the next 2 weeks the GD expression decreases such that there is ~25% retention of rGD after 21 days in microreactor culture. In contrast, PRHs in monolayer culture demonstrated ~90%

retention of GD expression following 1 day in culture. By day 7 GD expression is ~25%.

There was no GD expression seen by day 14 in monolayer culture.



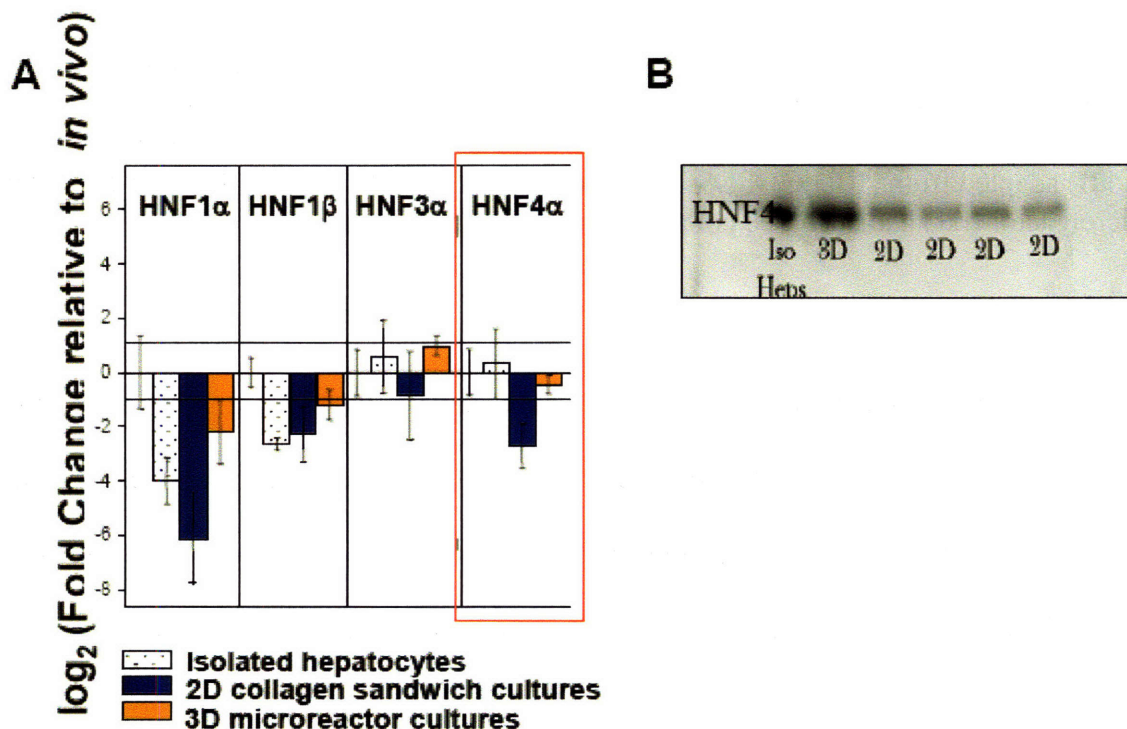
**Figure 4-2.** Glycine decarboxylase expression over 21 days in culture. At indicated timepoints cells were lysed and SDS-PAGE analysis was run using equal amounts of total protein for all timepoints. Bar graph data represents band pixel intensity at indicated timepoint relative to band pixel intensity measured in cells immediately following rat liver perfusion. Mean GD expression is significantly different between the monolayer and microreactor cultures (null hypothesis rejected for  $p < 0.10$ ).

Glycine decarboxylase belongs to a multienzyme complex known as the glycine cleavage complex that is the primary pathway for glycine catabolism. While this complex is located in the mitochondria, GD has been shown to be available on the cell surface in PDHs as well as in stably transfected 293 cells and transiently transfected LMH and Bosc cells [145].



Tang and McLachlan [148] have also indentified liver-enriched transcription factors that support DHBV replication in nonhepatic cells. Upon transfection of a replication-competent DHBV genome and various liver-enriched transcription factors it was shown that Hepatocyte Nuclear Factor 3 (HNF3) and HNF4 support replication of DHBV DNA intermediates. Previous studies in our group have demonstrated that the microreactor displays better maintenance of various liver enriched transcription factor mRNAs including HNF3 $\alpha$  and HNF4 $\alpha$  mRNA following 7 days in culture in comparison to standard 2D cultures (Fig 4-3a). Western blot analysis demonstrates that this better maintenance extends to the protein level (Fig 4-3b).

The representative blot in Figure 4-3c shows that the microreactor demonstrates better HNF4 $\alpha$  protein expression at 21 days in culture in comparison to standard monolayer culture.





**Figure 4-3.** Liver-enriched mRNA and protein expression over time in culture. A) Total mRNA isolated on day 7 of culture using TRIzol. Baseline in the plot represents mRNA detected in liver slices taken directly after rat sacrifice. B) SDS-PAGE analysis of HNF4 $\alpha$  expressed by day 7 in culture. IsoHeps: hepatocytes in suspension following rat perfusion, 3D: liver microreactor, 2D: collagen gel sandwich culture. A) and B) adapted from [10]. C) SDS-PAGE analysis of HNF4 $\alpha$  expression in microreactor (rxr) and adsorbed collagen monolayer (mono) culture.

#### 4.3.2 Early and late DCPD-transfection in monolayer culture

As discussed in the previous chapter DCPD expression via adenoviral transfection can be increased using increasing Ad MOI but this also results in greater cell death. Ad MOI =10 was used in the following experiments because it achieves a sufficient transfection efficiency (assessed visually under microscope) while causing only moderate cell death. Figure 4-4a shows representative images of 72h cultures of cells transfected

~6h after plating. These images confirm that there is some cell death but a decent percentage of these cells are transfected as evidenced by GFP expression. In the previous chapter total protein analysis revealed that this cell death was not significantly different than that observed in No Ad control cultures.

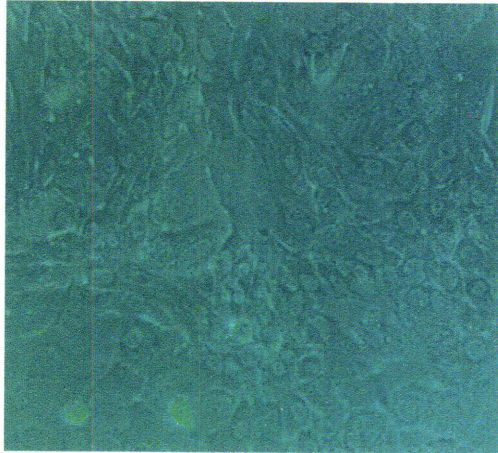
In Figure 4-4b cultures were maintained for 14 days prior to exposure to Ad MOI = 10. Total cell number present at these longer time points tend to be less than that originally seeded. In order to ensure that the Ad MOI = 10 at the later timepoint it was necessary to maintain parallel cultures. On the day that the adenovirus was added total DNA was extracted from the parallel cultures and real-time PCR using primers specific for GAPDH DNA was used to determine total cell number (Table 4-1). A standard curve was previously prepared using known cell concentrations taken directly from multiple rat perfusions.

Phase contrast images demonstrate significant morphological changes. The hepatocytes tend to clump into nodes while fibroblast-like cells appear in between the nodes. The fluorescent images demonstrate that fewer GFP-positive cells are present. This is either due to an overall loss in hepatocytes or a loss in factors necessary for the recombinant adenovirus to successfully deliver the GFP and DCPD transgenes. Previous studies have shown that the Coxsackie- and Adenovirus (CAR) receptor mRNA is down-regulated over time in collagen gel sandwich culture (Section 2.7.2, Fig. 2-10). Assuming similar behavior in the adsorbed collagen monolayer culture employed here the decrease in GFP-positive cells could be a result of decreased adenoviral uptake.

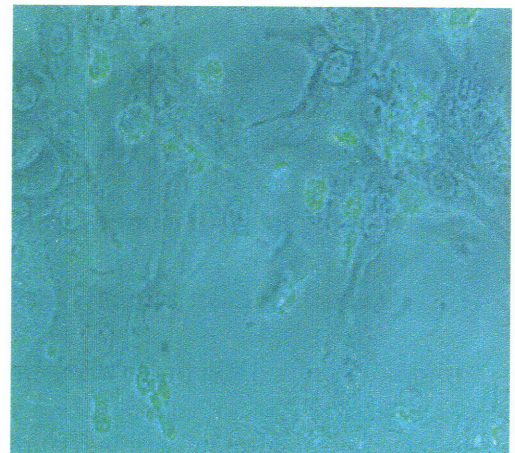


**A**

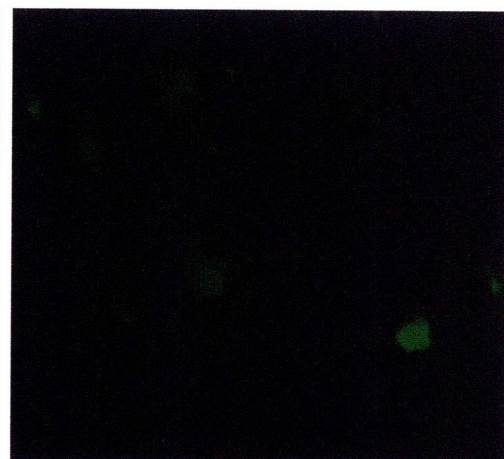
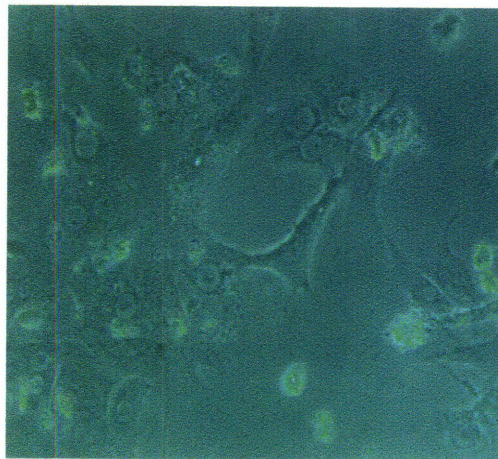
no Ad



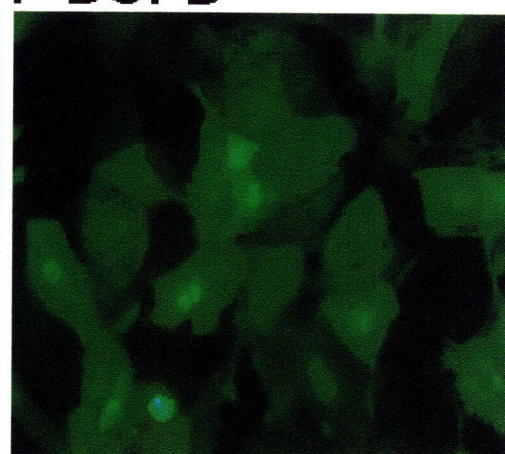
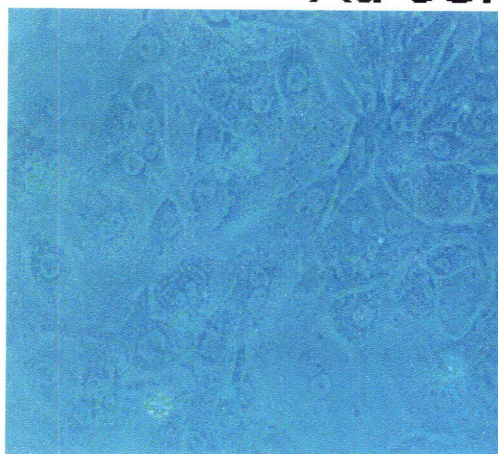
Ad-e



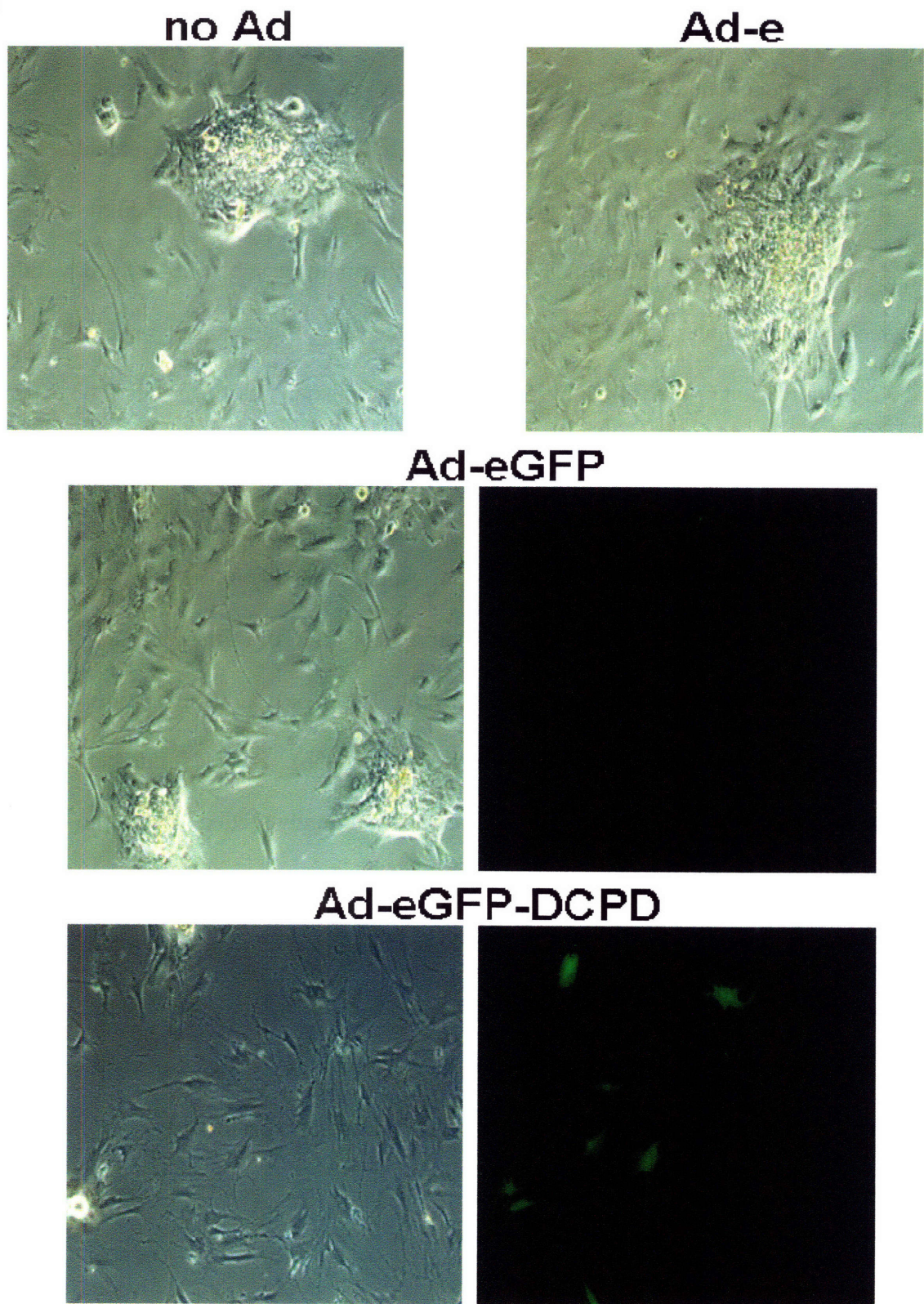
Ad-eGFP



Ad-eGFP-DCPD





**B**

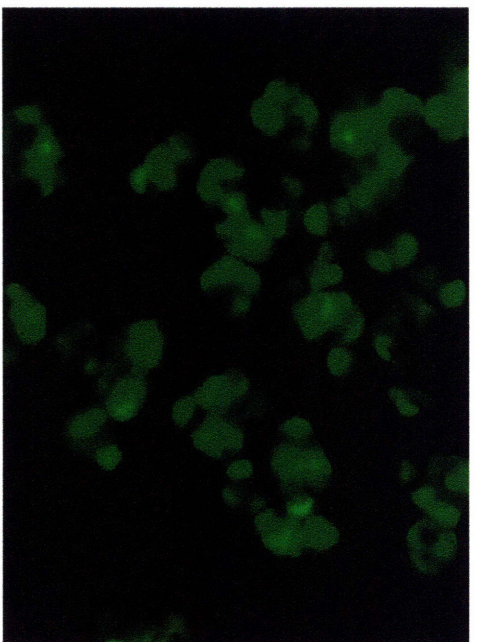
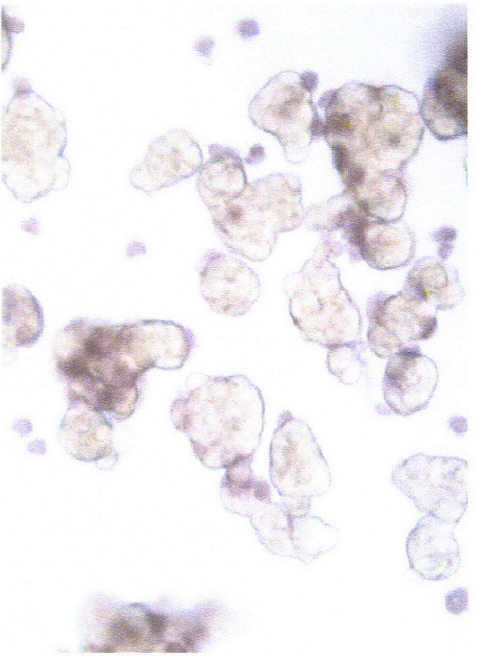
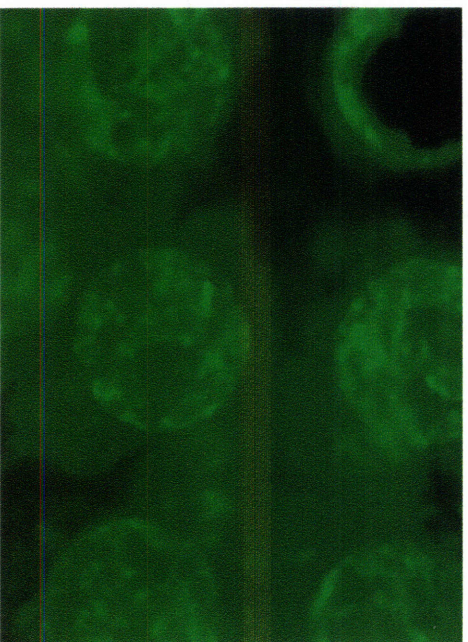
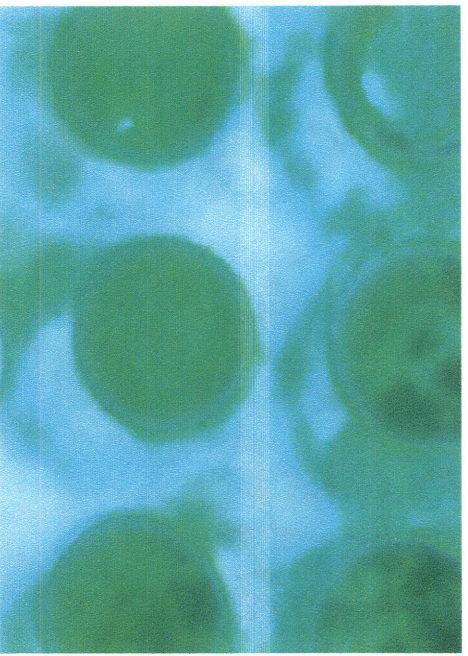
**Figure 4-4.** Early and late DCPD-transfection in monolayer culture. PRH cultures plated on collagen-coated polystyrene were exposed to adenovirus (Ad MOI=10) either A) ~6h following plating or B) after 2 weeks in culture.

### ***4.3.3 Early and late DCPD-transfection in microreactor culture***

Originally, microreactor culture incorporated seeding of spheroidal cell aggregates [164]. To maintain a similar timecourse of DHBV exposure it was necessary to add the adenovirus to the spinner flask as the PRHs were forming spheroids. Qualitatively the majority of the non-filtered spheroids appear GFP-positive after 24h in culture (Fig 4-5a). Trypan blue exclusion confirms good cell viability in these spheroids. One day following seeding into the microreactor demonstrates tissue-like structures present (Fig 4-5b). The GFP expression (~48h following Ad exposure) has also increased as would be expected based on monolayer studies.

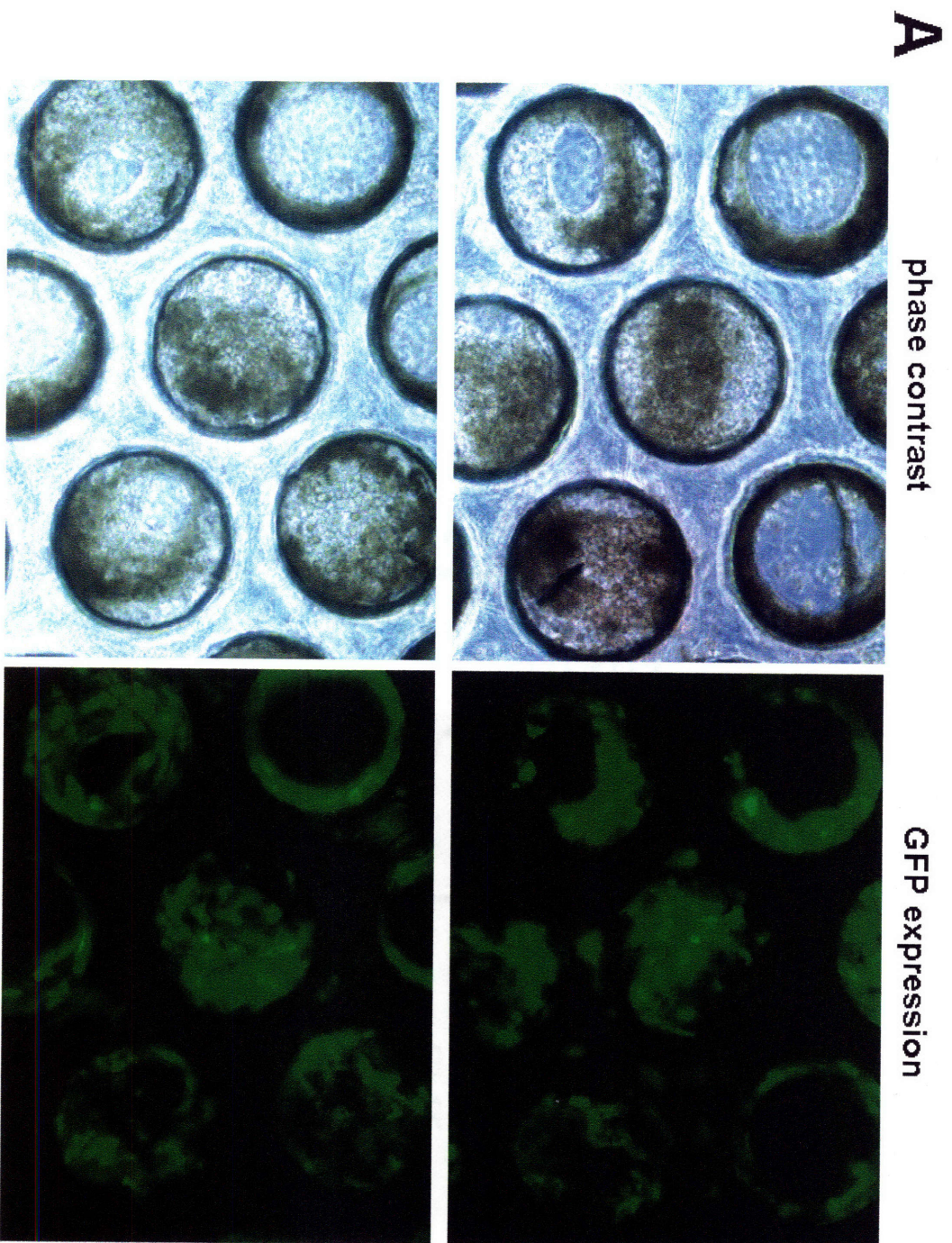
More recently our group has investigated seeding microreactor cultures with single cells taken immediately from the perfusion. Approximately 6h following microreactor seeding the adenovirus is added to the microreactor reservoir. Images taken 24h later indicate GFP-positive tissue structures forming (Fig. 4-6a). Cells maintained for longer time periods were also exposed to adenovirus (Fig. 4-6b). Total cell number present at these longer time points tend to be less than that originally seeded. Similar to the monolayer situation described in the previous section, parallel cultures were maintained. On the day that the adenovirus was added total DNA was extracted from the parallel cultures and real-time PCR using primers specific for GAPDH DNA was used to determine total cell number (Table 4-1). A standard curve was previously prepared using known cell concentrations taken directly from multiple rat perfusions.



**A****B**

**Figure 4-5.** DCPD transfection of spheroidal cell aggregates. A) Phase contrast image of spheroids formed after 24h in spinner flasks. Trypan blue was added to the spheroids in order to determine cell viability. GFP expression was used as a marker of transfection. B) Phase-contrast images taken 24h after spheroids seeded into the microreactor. GFP expression reveals high level of transfection. 20x objective.





**Figure 4-6.** DCPD transfection of microreactor seeded with single cells. A) Phase contrast of tissue structures formed after 24h in culture. Adenovirus was added to the cultures ~6h after cells seeded into microreactor. GFP expression is a marker of successful adenovirus transfection. 20x objective B) Cultures were maintained for up to 2 weeks. Adenovirus was added at either day 7 or day 14. Images were taken 24h following adenovirus exposure. 5x objective

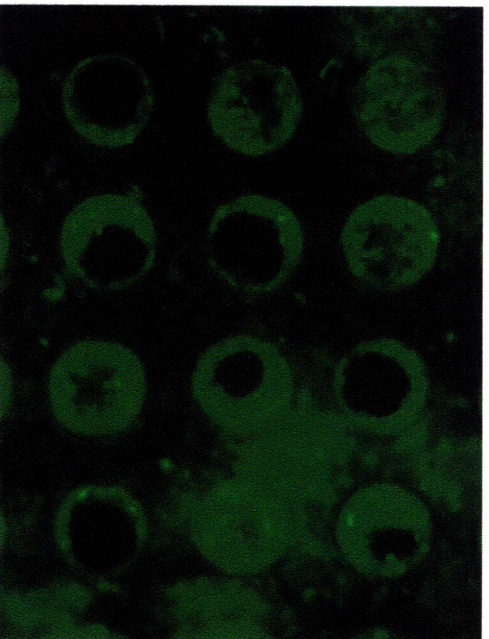
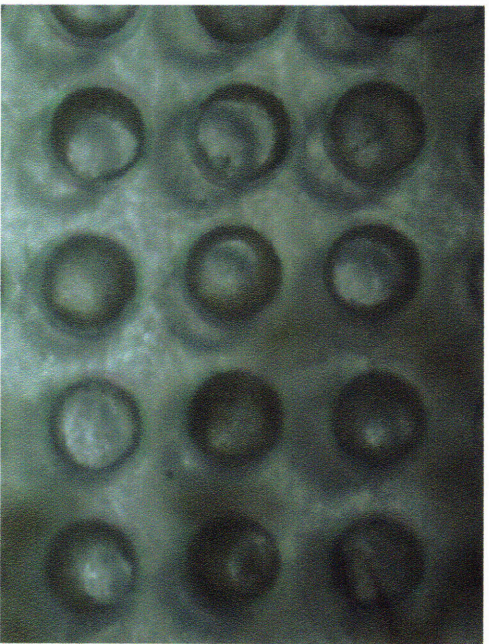


**B**

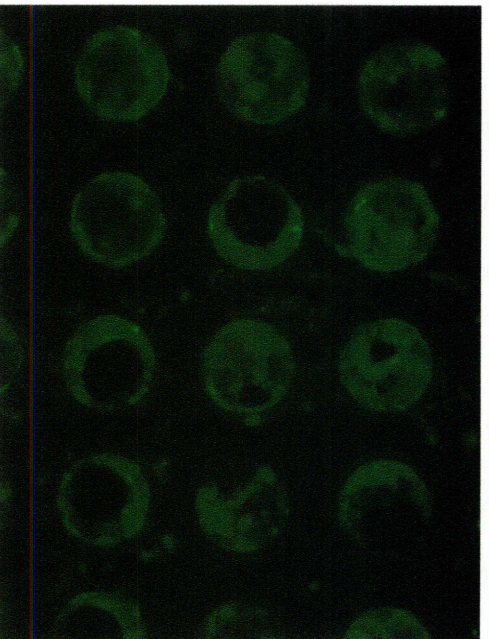
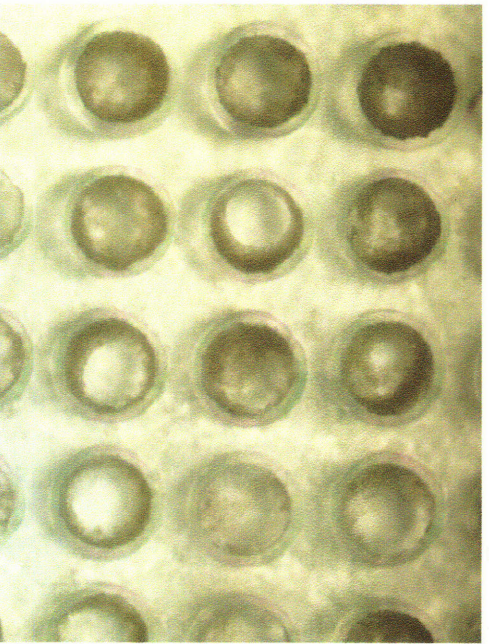
phase contrast

GFP expression

d7



d14



**Figure 4-6.** DCPD transfection of microreactor seeded with single cells. A) Phase contrast of tissue structures formed after 24h in culture. Adenovirus was added to the cultures ~6h after cells seeded into microreactor. GFP expression is a marker of successful adenovirus transfection. 20x objective B) Cultures were maintained for up to 2 weeks. Adenovirus was added at either day 7 or day 14. Images were taken 24h following adenovirus exposure. 5x objective

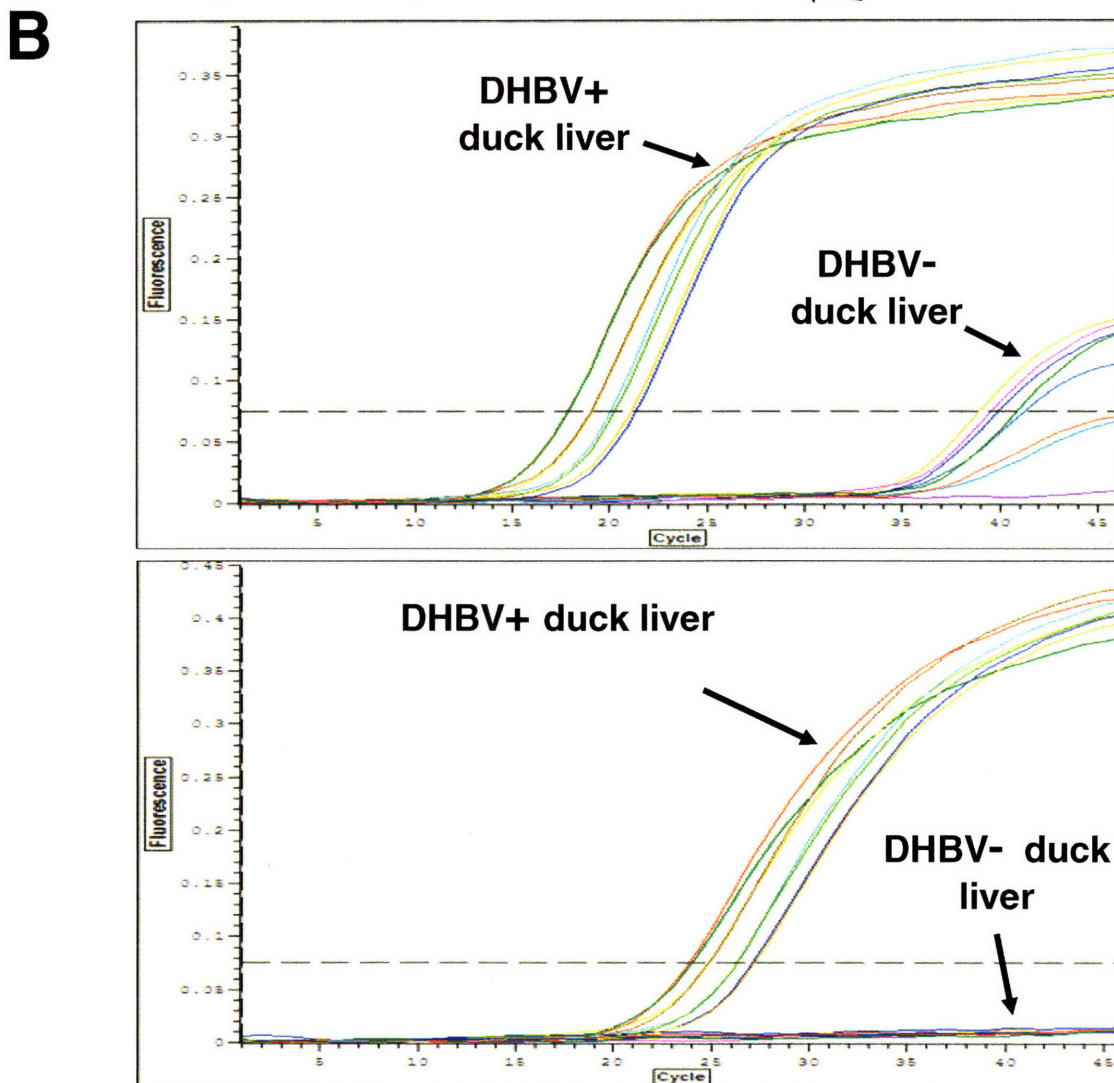
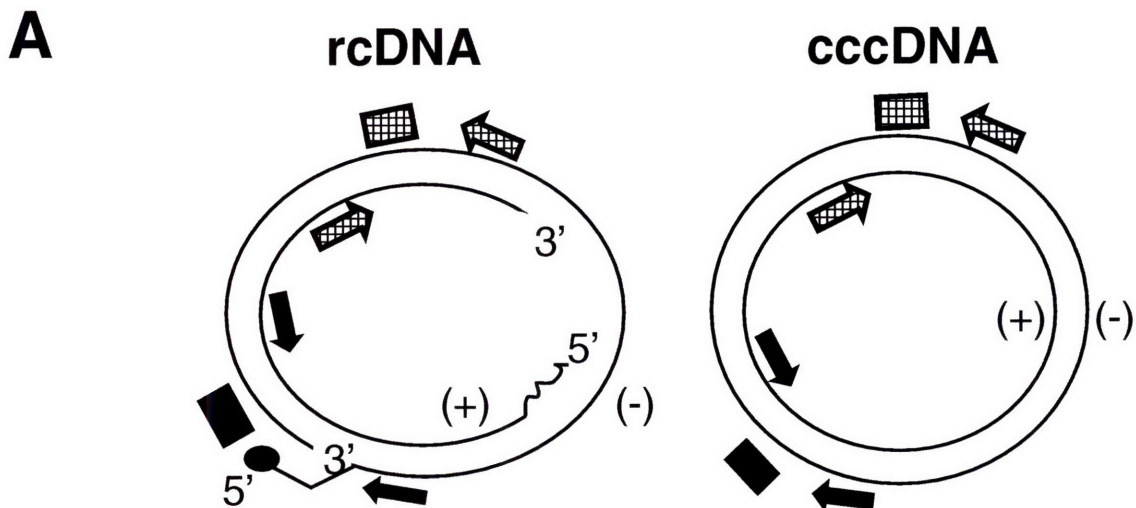
#### ***4.3.4 Development of real-time PCR assay to quantify total DHBV DNA and cccDNA***

A real-time PCR method was developed in order to quantitatively measure both total DHBV DNA and particularly the cccDNA form (Fig. 4-7a). Using a strategy adapted from Kock and Schlicht [198] primers and a probe were developed using Primer3 that targets a region of the DHBV genome that is common to all viral DNA forms (Table 4-1). For dsDNA, the region targeted by the totalDNA primer/probe set is unaffected by the linear nature of the viral DNA. It should be noted that the ssDNA includes the complete (-) strand and would be detected by the probe and the forward primer of the totalDNA primer set. However, since the (+) strand is absent, ssDNA would not be amplified during the PCR and therefore would not contribute significantly to the fluorescent signal. The second primer probe set (Table 4-1) is designed to converge upon the gap region in the (-) strand of the DHBV genome. This gap is present in rcDNA but not in cccDNA. Again, ssDNA would not contribute significantly to the signal for the reason mentioned earlier. dsDNA is also not detected by Primer/Probe Set B because the gap region is effectively infinite due to the linearity of the viral DNA form. Therefore cccDNA primer/probe set is selective for cccDNA. For DNA isolated from DHBV-infected duck livers the primer/probe sets amplify products above the threshold at separate cycles (Fig. 4-7b). For DNA isolated from uninfected duck livers the cccDNA primer/probe set amplifies nothing over 45 cycles. The totalDHBV probe set does seem to non-specifically amplify a product that reaches the threshold of detection at Ct ~40 (Fig. 4-7b). This late amplification is considered non-specific since these ducks were identified as being uninfected.

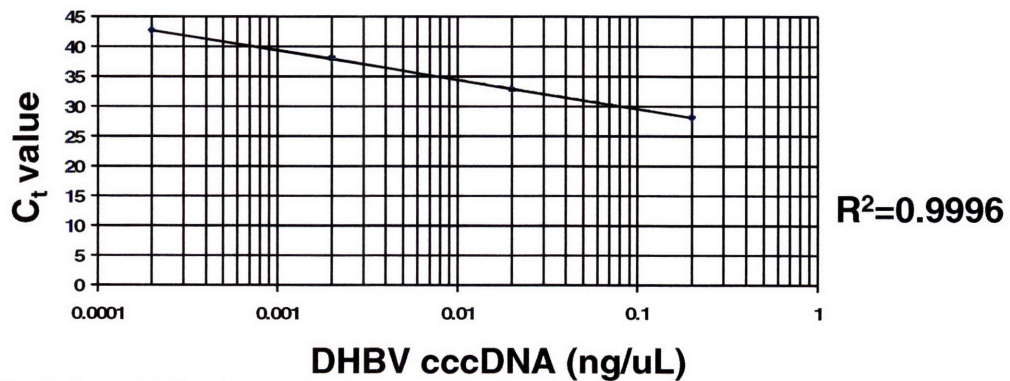
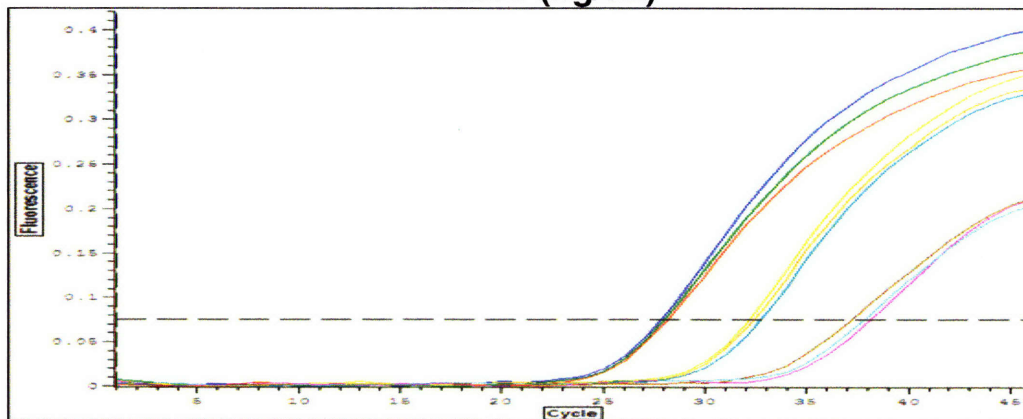
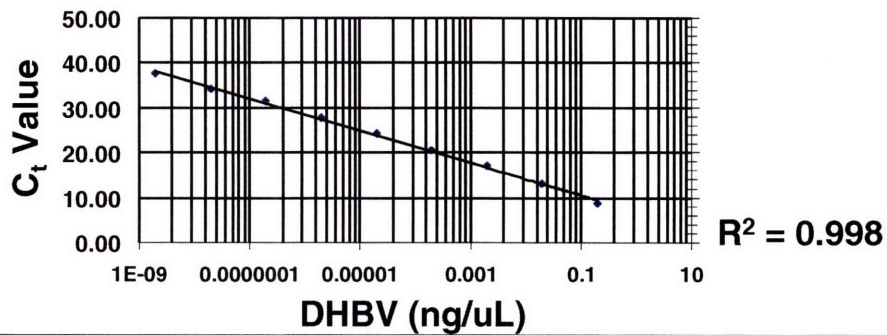
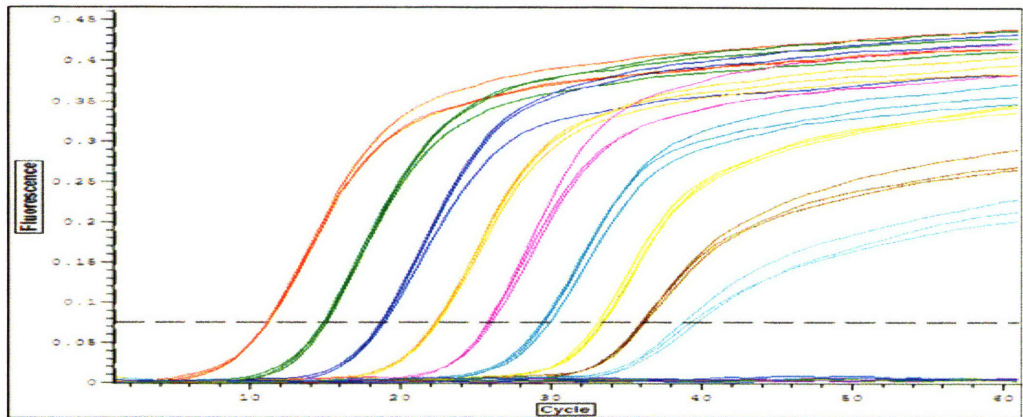
For total DHBV DNA the standard curve is linear over 9 orders of magnitude and for the cccDNA the standard curve is linear over three orders of magnitude (Fig. 4-8). The

lower limit of detection for this analysis is 0.67 viral genome equivalents (vge) for total DHBV DNA and  $1.3 \times 10^4$  vge for cccDNA. Using this real-time PCR assay the viral load of the DHBV+ duck serum was determined to be  $\sim 3.6 \times 10^9$  vge/mL which is consistent with the literature for congenitally-infected Pekin ducks.





**Figure 4-7.** Development of real-time PCR assay for DHBV DNA quantification. A) Illustration of DHBV rcDNA and cccDNA viral forms. Two primer/probe sets target different regions (one region that is common to both viral DNA forms and another region that is specific for cccDNA). B) Total DNA isolated from both DHBV+ and DHBV- duck liver and subject to real-time PCR analysis using both primer/probe sets.

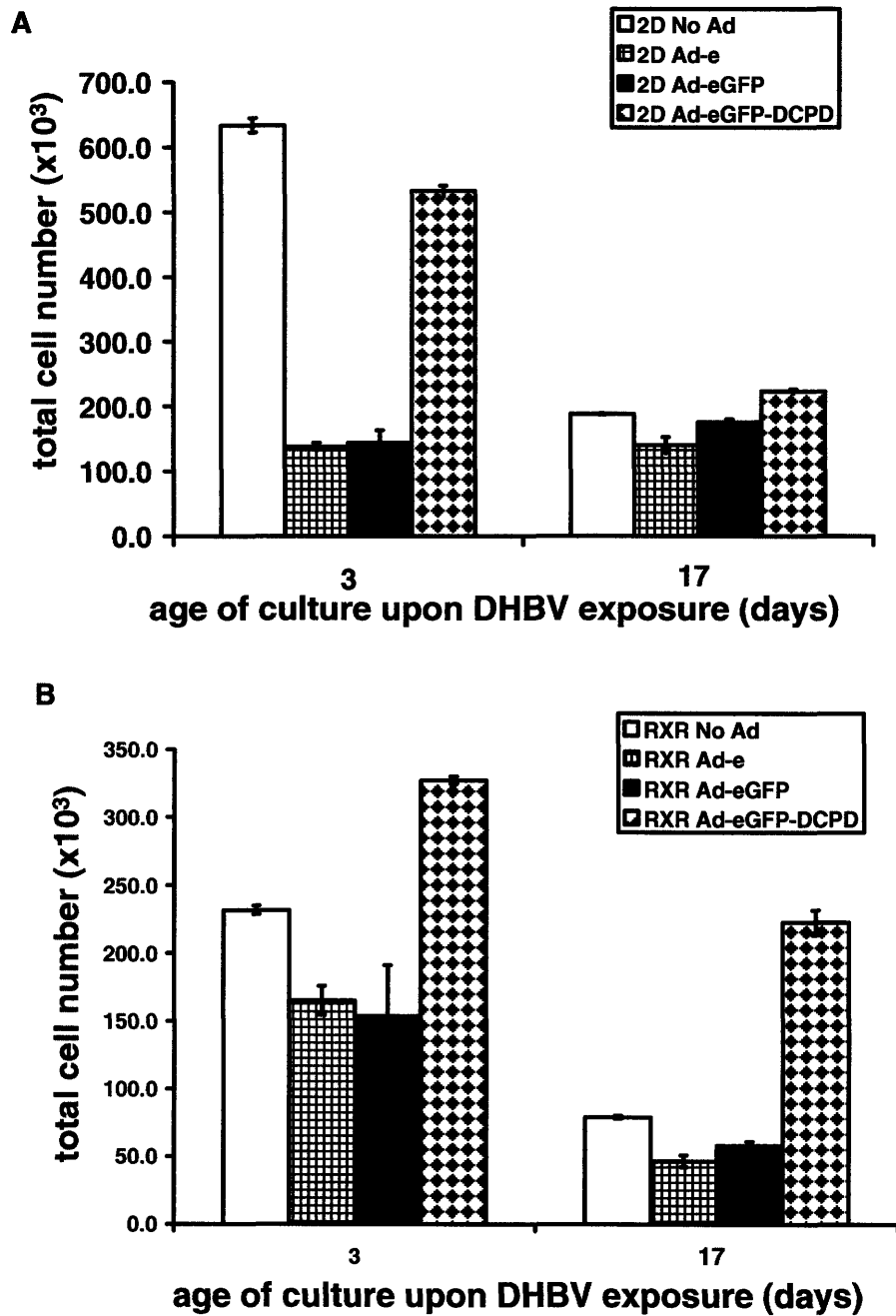


**Figure 4-8.** Real-time PCR primers/probe specific for either total DHBV DNA or DHBV cccDNA. Serial dilutions of purified DHBV DNA were analyzed with either the total DNA-specific primer/probe set or the cccDNA-specific primer/probe set. The total DHBV DNA standard curve is linear over 9 orders of magnitude. The DHBV cccDNA standard curve is linear over 3 orders of magnitude.



#### ***4.3.5 DCPD protects against Ad-mediated cytotoxicity in microreactor culture***

The Ad-mediated cytotoxicity that has been observed in freshly isolated PRH in standard monolayer culture is also seen in microreactor culture. Ad control vectors (Ad-e and Ad-eGFP) were incubated with either freshly isolated PRHs or PRHs that had been maintained in culture for 2 weeks. Using measurement of total protein as an indicator of cell number it is evident that increased cell loss occurs when freshly-isolated hepatocytes are exposed to the control Ad vectors (Figure 4-9a). In contrast, DCPD-transfected cultures demonstrate no significant cell loss compared to the control No Ad condition (Figure 4-9b). Ad-mediated cytotoxicity is not observed in PRHs that are maintained in culture for 2 weeks prior to being exposed to the adenovirus in monolayer culture. Decreased cytotoxicity is observed in microreactor cultures but DCPD still appears to have a protective effect in cultures maintained for 2 weeks prior to adenovirus exposure. As discussed in the previous chapter adenoviral uptake occurs through receptor-mediated endocytosis. The decreased cytotoxicity could be due to a loss of necessary factors for either Ad-specific uptake (e.g. Coxsackie- and Adenovirus Receptor) or hepatocyte-specific replication machinery. Previous characterization in the lab has shown that the in comparison to in vivo liver, CAR mRNA is down-regulated 7-fold in collagen gel sandwich but only 2-fold in microreactor culture [7].



**Figure 4-9.** Total cell number in monolayer and microreactor culture was determined by measurement of total GAPDH DNA using real-time PCR analysis. A) DCPD protects against Ad-mediated toxicity at early timepoints in monolayer culture. B) DCPD protects against Ad-mediated toxicity at both early and late timepoints in microreactor cultures. N=1 biological replicate.

#### **4.3.6 DHBV DNA evidence in DCPD-transfected PRHs**

In monolayer culture DCPD-transfected PRHs demonstrate a significant loss in intracellular DHBV DNA levels (75%) when transfected at late timepoints (Fig. 4-10a). The experimental timecourse is shown in Table 4.2. Real-time PCR analysis using cccDNA specific primers demonstrates that the majority of the DNA present is in cccDNA form (Fig. 4-10b). This loss of susceptibility to DHBV infection correlates with the loss of factors that are necessary for DHBV replication shown earlier (Fig. 4-2 and Fig. 4-3). Evidence of DHBV DNA in control Ad vectors is not significantly greater than the No Ad control condition.

DCPD-transfected microreactor cultures demonstrate increased DHBV DNA levels in comparison to monolayer culture (Figure 4-11a). Real-time PCR analysis using cccDNA-specific primers confirms that the majority of this DNA is in cccDNA form (Fig. 4-11b). The significant 3-fold increase in intracellular DNA in PRHs transfected after 2 weeks is surprising given that various factors necessary for DHBV infection (e.g. GD, HNF4 $\alpha$ ) are down-regulated by this timepoint. It should be noted that this data represents one biological replicate (2 technical replicates). Microreactor culture demonstrates well-to-well variability that is most likely user-related (data not shown). It is possible that the actual cell number used to determine the amount of adenovirus to add to the culture could have been greater than the actual cell number present in the wells for the given experimental condition. Further study is needed in order to determine whether this phenomenon is typical.

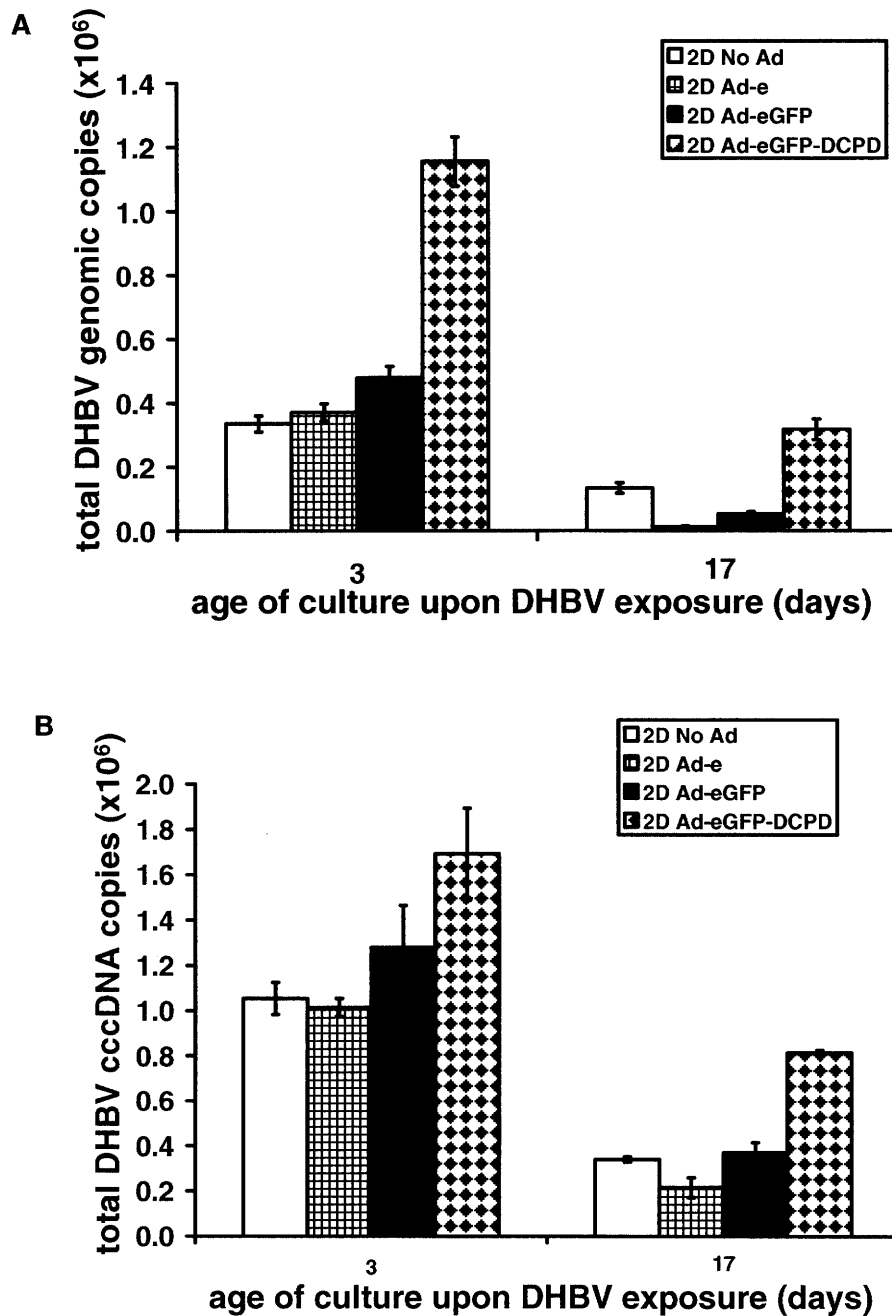
Ad control vectors demonstrate significantly higher DHBV DNA levels than the No Ad condition and the real-time PCR confirms that there is cccDNA present. As

discussed in previous chapter (Section 3.4) it appears that Ad vectors are capable of mediating some DHBV uptake although the precise mechanism is unknown.

It should be noted that the DCPD-transfected PRHs in microreactor cultures demonstrate ~10-80 DHBV cccDNA copies/cell while the monolayer cultures demonstrate ~0.1-10 DHBV cccDNA copies/cell. Persistent DHBV infection of the hepatocyte is characterized by the presence of cccDNA. In natural DHBV infection process rcDNA is delivered to the host cell nucleus where it is converted into episomal cccDNA. This viral DNA serves as the template for all viral mRNA s that are translated and assembled into viral progeny. Early during the infection cycle the DNA within nascent viral capsids is re-imported into the nucleus which results in amplification of cccDNA and increased viral replication. Late during infection the newly forming viral capsids are redirected to the secretory pathway by the large envelop protein. This eventually leads to the secretion of enveloped viral particles. Different groups report that infected primary duck hepatocytes express 10 – 100 copies of cccDNA [126]. The greater pool size of cccDNA measured in the DCPD-transfected microreactor cultures could translate into greater viral replication. Further studies are warranted in which infected cultures are assayed for markers of viral replication at multiple timepoints following DHBV exposure.

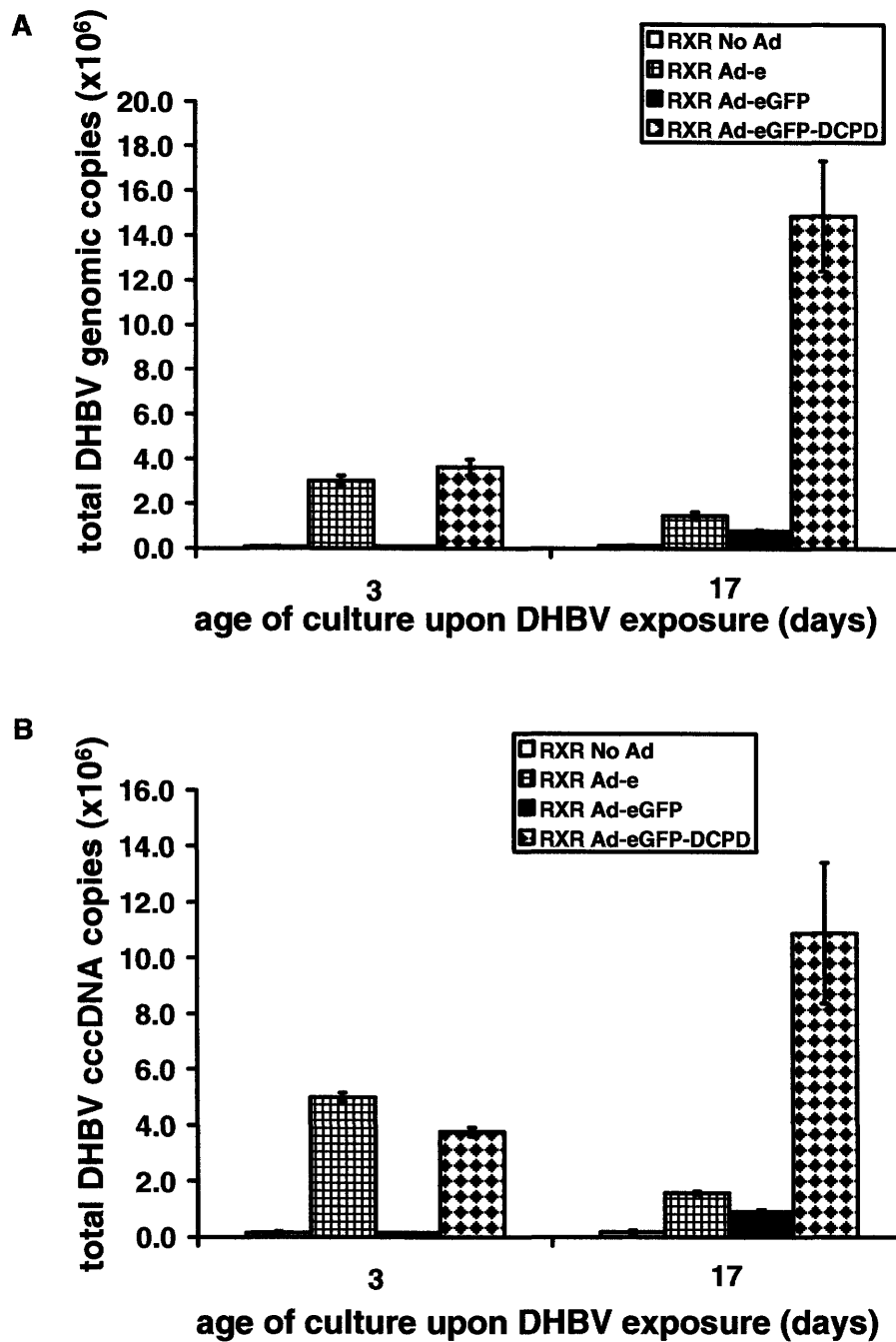
day	monolayer (early DCPD transfection)	monolayer (late DCPD transfection)	microreactor (early DCPD transfection)	microreactor (late DCPD transfection)
0	plate cells (50,000 cells/cm <sup>2</sup> ) add Ad (MOI=10)	plate cells (50,000 cells/cm <sup>2</sup> )	seed microreactors (8x10 <sup>5</sup> cells/rx)	seed microreactors (8x10 <sup>5</sup> cells/rx)
1	wash out Ad (PBS wash 3x)	change HGM	later add Ad (MOI=10) reverse crossflow	reverse crossflow
2	add DHBV (1/5 dilution)	change HGM	wash out Ad (HGM wash 2x) change HGM	change HGM
3	wash out DHBV (PBS wash 3x)	change HGM	add DHBV (1/5 dilution)	change HGM
4	collect cell & supernatant samples	change HGM	wash out DHBV (HGM wash 2x)	change HGM
5		change HGM	collect cell & supernatant samples	change HGM
6		change HGM		change HGM
7		change HGM		change HGM
8		change HGM		change HGM
9		change HGM		change HGM
10		change HGM		change HGM
11		change HGM		change HGM
12		change HGM		change HGM
13		change HGM		change HGM
14		add Ad (MOI=10)		add Ad (MOI=10)
15		wash out Ad (PBS wash 3x)		wash out Ad (HGM wash 2x)
16		add DHBV (1/5 dilution)		change HGM
17		wash out DHBV (PBS wash 3x)		add DHBV (1/5 dilution)
18		collect cell & supernatant samples		wash out DHBV (HGM wash 2x)
19				collect cell & supernatant samples

**Table 4-2.** Experimental timecourse for early and late DCPD transfection in both monolayer and microreactor cultures.



**Figure 4-10.** DCPD-transfected PRHs demonstrate decreasing susceptibility following extended culture (2weeks) in monolayer. A) Real-time PCR analysis using total DHBV DNA-specific probe/primers. B) Real-time PCR analysis using DHBV cccDNA specific probe/primers.





**Figure 4-11.** DCPD-transfected PRHs demonstrate increased susceptibility following extended culture (2 weeks) in microreactor. A) Real-time PCR analysis using total DHBV DNA-specific probe/primers. B) Real-time PCR analysis using DHBV cccDNA specific probe/primers.

#### 4.4 Discussion

Previous studies (Chapter 3) investigated the ability of PRHs to support DHBV infection when transfected with DCPD, the internalization receptor for DHBV, soon after plating. Replicative intermediates (i.e. ssDNA) indicated that DCPD-transfected cells are capable of productive DHBV infection. In this study we attempted to investigate the ability of DCPD-transfected PRHs maintained in a 3D perfused culture system to support DHBV infection at longer timepoints. Using various assays (e.g biochemical production, tissue morphology, mRNA transcriptional profile, and enzyme activity) the microreactor has been shown to maintain a more liver-like phenotype than conventional tissue culture systems (i.e. collagen-coated monolayer, collagen gel sandwich) [9, 10].

Western blot analysis demonstrated that PRHs cultured in the microreactor maintain more of the necessary factors for DHBV replication than PRHs cultured on collagen-coated polystyrene. These factors include GD which mediates a postbinding step during DHBV infection. The loss of DGD in primary duck hepatocyte cultures correlates with the loss of susceptibility to DHBV infection [146]. After 3 weeks in culture PRHs in the microreactor retain greater GD expression than monolayer cultures. Among the liver-enriched transcription factors HNF4 is known to support DHBV replication [148]. HNF4 $\alpha$  is considered to be a master transcription factor due to its ability to regulate the expression of a disproportionately large number of hepatic genes that include fatty acid, cholesterol and glucose metabolism, urea biosynthesis, apolipoprotein synthesis, liver development, and other transcription factors (e.g. HNF1 $\alpha$  and HNF6) [149-152]. Previous studies in our group have shown better maintenance HNF4 $\alpha$  maintenance at both the mRNA and protein

level after 7 days in culture [10]. In this study it was demonstrated that the microreactor maintains better HNF4 $\alpha$  protein expression at even long timepoints (21 days) in culture.

Monolayer cultures transfected with adenovirus at early timepoints following plating demonstrate significant transgene transduction (as confirmed via GFP expression). FACS analysis from the previous chapter revealed that for the given Ad-eGFP-DCPD MOI ~90% of GFP-expressing cells also express the DCPD transgene. PRHs maintained for 2 weeks in monolayer culture prior to adenovirus exposure demonstrate decreased transgene transduction evidenced by fewer GFP-positive cells. The decreased transduction could be due to a loss of necessary factors for either Ad-specific uptake (e.g. Coxsackie and Adenovirus Receptor) or hepatocyte-specific replication machinery. These cultures have lost hepatocyte morphology and appear to clump together into nodes. The appearance of fibroblast-like cells suggests the proliferation of another cell type in these cultures. Cultures are seeded with a hepatocyte-enriched-fraction (~95%). It is possible that a population of the non-parenchymal cell (NPC) percentage is proliferating in these cultures which are not susceptible to adenovirus uptake. The ratios of the different cell types in culture at early timepoints most likely differ from the ratios present at later timepoints. These NPCs do not appear GFP-positive.

DCPD was also shown to protect microreactor PRH cultures at early time points. As discussed in the previous chapter the mechanism likely involves NO production. The Ad-mediated toxicity was less evident in microreactor cultures maintained 2 weeks prior to Ad exposure. Down-regulation of factors necessary for adenovirus uptake (e.g. CAR receptor) could account for the decreased cytotoxicity.

Spheroidal cell aggregates were previously used to seed microreactor cultures. To maintain a similar timecourse of Ad exposure between monolayer and microreactor culture the adenovirus was added directly to the spinner flasks as the PRHs formed spheroids. The majority of the spheroids appear viable and GFP-positive following 24h spinner flask incubation. Tissue-like structures appear to be forming after 24h in the microreactor (a total of 48h after Ad exposure) and GFP has increased as expected. Use of spheroids is non-ideal for these studies. Adenovirus exposure in the spinner flasks likely resulted in equal access to all the PRHs due to the constant mixing. In order to study PRHs transfected with Ad at later timepoints the Ad would be added to the microreactor ~14 days following seeding. Unlike spinner flask incubation, mass transport considerations in the microreactor probably do not allow for equal access to PRHs throughout the tissue structures in each channel. Single cell seeding allows Ad vectors to be added to the early timepoint and late timepoint microreactors under similar conditions. GFP expression suggests that there is a decrease in transduction when PRHs are transfected at later timepoints. As suggested earlier this could be due to a loss of necessary factors for either Ad-specific uptake (e.g. Coxsackie and Adenovirus Receptor) or hepatocyte-specific replication machinery.

A quantitative real-time PCR assay was developed that incorporates 2 sets of primers, one of which converges upon the gap region in the (-) strand of the DHBV rcDNA genome. DHBV cccDNA does not contain this gap region so these primers will only amplify a signal in the presence of cccDNA.

Monolayer cultures demonstrate approximately 75% decrease in total DHBV genome copies when transfected with DCPD after 2 weeks in culture. The majority of this

DNA is in cccDNA form. Such a decrease correlates with the decrease of necessary factors such as GD and HNF4. In contrast, DCPD-transfected microreactor cultures demonstrate ~300% increase in total DHBV genome copies when transfected with DCPD after 2 weeks in culture. The well-to-well variability observed in microreactor culture could have over-estimated the actual cell number present which would have led to a cells being exposed to a higher Ad MOI. These data represent one biological replicate (2 technical replicates) and must be repeated to confirm this phenomenon.

One will also note that the microreactor cultures demonstrate total DHBV genome copies that are an order of magnitude higher than the monolayer cultures. This evidence implies that more effective replication is taking place in the microreactor. This observation could be skewed by proliferation of different cell types in monolayer and microreactor culture. Cell number was determined using GAPDH detection which is present in PRHs as well as NPCs.

Currently, there is a need for an in vitro model that mimics a more natural HBV infection process. This process begins with the viral particle binding to its host cell receptor(s) and is followed by internalization, uncoating, nuclear delivery, and genome repair. Previous work has demonstrated that later viral life cycle events are not rigidly host-restricted [175]. In this study we have attempted to demonstrate that by providing PRHs with the known DHBV internalization receptor that a 3D perfused culture could facilitate the study of some of the early viral life cycle events. This work could be extended to study HBV and potential human hepatocyte HBV receptors.

Ultimately, the goal is to learn more about human HBV and the in vitro system characterized in this thesis can be extended towards this purpose. There are various

putative receptors for HBV. This system could be extended to artificially deliver one of the putative HBV receptors to primary rat hepatocytes. Due to the strict host-specificity of these viruses this system represents a promising method to preferentially isolate putative HBV receptors in cells with a well-differentiated liver phenotype. Successful HBV replication would provide strong evidence for the involvement of the receptor in the HBV life cycle.



## Chapter 5.

### Conclusions and Recommendations

Chronic hepatitis B infection leads to a host of diseases that include cirrhosis and hepatocellular carcinoma. Currently available therapeutics demonstrate modest efficacy and/or promotion of resistant DHBV strains. These therapeutics are the products of research based on the current understanding of the molecular biology of HBV. Research is hampered due to the lack of in vitro systems in which the entire viral life cycle can be studied. More is known about the later events in the viral life cycle (i.e. transcription, encapsidation reverse transcription, virion assembly, export) due to studies in which the viral genome is transfected into established hepatoma cell lines (e.g. HepG2, Huh7). However, there is less understanding of the early stages that include virus attachment, internalization, uncoating, genome repair, and nuclear transport. These cell lines do not mimic natural infection which limits their usefulness. An in vitro system that will allow us to target other aspects of the viral life cycle is needed for the development of future therapeutics.

This thesis focused on developing an in vitro model of the early aspects of the DHBV life cycle using a microfabricated reactor system that mimics key facets of the in vivo liver microenvironment. Similar genome organization, virus structure, and replication characteristics among hepadnaviruses warrant the study of hepadnaviruses found in other species. Many of the principles of hepadnavirus life cycle were elucidated by studying duck hepatitis B virus (DHBV) as a model for HBV. These principles include the replication by reverse transcriptase [125], cccDNA formation [126], and host-range

determinants [127-129]. DHBV was employed in this thesis as a surrogate model for HBV.

Using length scales which foster cellular reorganization the microreactor was designed to maintain cells in tissue-like units that are uniformly perfused with culture medium. Previous characterization was done using a broad spectrum of gene expression, protein expression, and biochemical assays [9, 10]. These metrics indicate that the microreactor is capable of maintaining PRHs with a phenotype closer to that of native liver than PRHs kept in conventional in vitro culture systems.

Recombinant adenovirus vectors were used to transfect primary rat hepatocytes with DCPD in order to study the ability of a normally non-susceptible species to support DHBV replication. Earlier studies have shown that primary rat hepatocytes are capable of supporting DHBV replication upon adenoviral transfection of the viral genome, confirming that the later events of the viral life cycle are not rigidly host-restricted [175]. We generated recombinant vectors in which both DCPD and green fluorescent protein (GFP) are incorporated in the adenoviral genome. DHBV replication was initiated in primary rat hepatocytes when DCPD was transduced via adenoviral delivery, providing the first evidence that DCPD is sufficient to cross the species barrier and establish a DHBV infection in primary rat hepatocytes. Viral markers indicate a relatively inefficient process in monolayer cultures but similar inefficiency is seen during DHBV infection of in vitro cultures of PDHs. DCPD-transfected microreactor cultures demonstrate increased levels of DHBV replication at longer timepoints. It should be noted that all these studies were done in the absence of DMSO or hydrocortisone, known inducers of cellular differentiation, which are standard additives that are almost universally applied to primary

duck hepatocyte cultures. This culture system allows one to study isolated aspects of the viral life cycle without such additives that are not present during natural infection.

Ultimately, the goal is to learn more about human HBV and the in vitro system characterized in this thesis can be extended towards this purpose. There are various putative receptors for HBV. Using this system it is possible to artificially deliver one of the putative HBV receptors to primary rat hepatocytes. Due to the strict host-specificity of these viruses this system represents a promising method to preferentially isolate putative HBV receptors in cells with a well-differentiated liver phenotype. Successful HBV replication would provide strong evidence for the involvement of the receptor in the HBV life cycle.

Characterization of the multiple DCPD forms that appear in these DCPD-transfected cultures would help to illuminate the trafficking of this receptor in these cells. Unlike other studies that found only transient expression of DCPD at the cell surface these studies demonstrate that the majority of the transfected receptor is expressed at the cell surface. Further studies should be done to determine how the two proteins detected by the DCPD antibody differ. Measurement of DCPD in supernatant samples would also help clarify whether soluble DCPD is being produced via the DCPD transgene.

Further efforts to characterize the ratio of cell types present at both early and late timepoints in microreactor culture is warranted. Current studies use GAPDH DNA which is present in all cells. The differential proliferation of the various cell types present could alter the actual DCPD-expressing cell population and therefore, alter the ratio of DHBV copies per cell.

This thesis also provided evidence that recombinant adenoviral vectors (with no transgene or only eGFP transgene) can mediate an alternative mechanism by which DHBV can non-specifically penetrate primary rat hepatocytes. Initially it was assumed that given the appropriate MOI the recombinant replication-incompetent adenovirus would be a biologically inert device to effectively deliver the DCPD transgene. On the contrary, these studies demonstrate that the adenoviral vectors have significant effects on these primary rat hepatocytes. Measurement of adenoviral gene products would help to elucidate how the adenovirus allows the subsequently added DHBV to artificially penetrate the primary rat hepatocytes in the absence of DCPD.

## References

1. Rappaport AM, *The microcirculatory hepatic unit*. Microvasc Res, 1973. **6**(2): p. 212-28.
2. Malarkey DE, J.K., Ryan L, Boorman G, Maronpot RR, *New insights into functional aspects of liver morphology*. Toxicol Pathol, 2005. **33**(1): p. 27-34.
3. Beck J, N.M., *Hepatitis B virus replication*. World J Gastroenterol, 2007. **13**(1): p. 48-64.
4. Racanelli V, R.B., *The liver as an immunological organ*. Hepatology, 2006. **43**(2 Suppl 1): p. S54-62.
5. Inman SW, *Development of a high throughput 3D Perfused Liver Tissue Bioreactor*, in *Mechanical Engineering*. 2006, Massachusetts Institute of Technology: Cambridge. p. 178.
6. Sivaraman A, *A microfabricated 3D tissue engineered "liver on a chip": high information content assays for in vitro drug metabolism studies*, in *Chemical Engineering*. 2004, Massachusetts Institute of Technology: Cambridge. p. 228.
7. Tedford, N., *Quantitative Analysis of Non-viral Gene Therapy in Primary Liver Culture Systems*, in *Biological Engineering*. 2007, Massachusetts Institute of Technology: Cambridge. p. 255.
8. Mast EE, W.C., Fiore AE, Alter MJ, Bell BP, Finelli L, Rodewald LE, Douglas JM Jr, Janssen RS, Ward JW, *A comprehensive immunization strategy to eliminate transmission of hepatitis B virus infection in the United States: recommendations of the Advisory Committee on Immunization Practices (ACIP) Part II: immunization of adults*. MMWR Recomm Rep, 2006. **55**(RR-16): p. 1-33.
9. Powers MJ, J.D., Wack KE, Baker CS, Beer Stolz D, Griffith LG, *Functional behavior of primary rat liver cells in a three-dimensional perfused microarray bioreactor*. Tissue Eng, 2002. **8**(3): p. 499-513.
10. Sivaraman A, L.J., Townsend S, Iida T, Hogan BJ, Stolz DB, Fry R, Samson LD, Tannenbaum SR, Griffith LG, *A microscale in vitro physiological model of the liver: predictive screens for drug metabolism and enzyme induction*. Curr Drug Metab, 2005. **6**(6): p. 569-91.
11. Schultz U, G.E., Nassal M, *Duck hepatitis B virus: an invaluable model system for HBV infection*. Adv Virus Res, 2004. **63**: p. 1-70.
12. Perz JF, A.G., Farrington LA, Hutin YJ, Bell BP, *The contributions of hepatitis B virus and hepatitis C virus infections to cirrhosis and primary liver cancer worldwide*. J Hepatol, 2006. **45**(4): p. 529-38.
13. Lavanchy D, *Hepatitis B virus epidemiology, disease burden, treatment, and current and emerging prevention and control measures*. J Viral Hepat, 2004. **11**(2): p. 97-107.
14. Gust ID, *Epidemiology of hepatitis B infection in the Western Pacific and South East Asia*. Gut, 1996. **38** Suppl 2: p. S18-23.
15. Mohamed R, D.P., Suh DJ, Amarapurkar D, Gane E, Guangbi Y, Hou JL, Jafri W, Lai CL, Lee CH, Lee SD, Lim SG, Guan R, Phiet PH, Piratvisuth T, Sollano J, Wu JC, *Practical difficulties in the management of hepatitis B in the Asia-Pacific region*. J Gastroenterol Hepatol, 2004. **19**(9): p. 958-69.

16. Brooks EA, L.L., Payne SL, Miller DW, *Economic evaluation of lamivudine compared with interferon-alpha in the treatment of chronic hepatitis B in the United States.* Am J Manag Care, 2001. **7**(7): p. 677-82.
17. Yang BM, P.S., Hahn OS, Yi DH, Choi MS, Payne S, *Economic evaluation of the societal costs of hepatitis B in South Korea.* J Gastroenterol Hepatol, 2001. **16**(3): p. 301-8.
18. Hoofnagle JH, P.M., Mullen KD, Jones DB, Rustgi V, Di Bisceglie A, Hallahan C, Park Y, Meschievitz C, Jones EA, *Randomized, controlled trial of recombinant human alpha-interferon in patients with chronic hepatitis B.* Gastroenterology, 1988. **95**: p. 1318-25.
19. Di Bisceglie AM, F.T., Fried MW, Swain MG, Baker B, Korenman J, Bergasa NV, Waggoner JG, Park Y, Hoofnagle JH, *A randomized, controlled trial of recombinant alpha-interferon therapy for chronic hepatitis B.* Am J Gastroenterol, 1993. **88**: p. 1887-92.
20. Fattovich G, G.G., Brollo L, Guido M, Pontisso P, Noventa F, Alberti A, *Therapy for chronic hepatitis B with lymphoblastoid interferon-alpha and levamisole.* Hepatology, 1992. **16**(5): p. 1115-9.
21. Craxi A, C.W., *Pegylated interferons for chronic hepatitis B.* Antiviral Res, 2003. **60**(2): p. 87-9.
22. Cooksley WG, P.T., Lee SD, Mahachai V, Chao YC, Tanwandee T, Chutaputti A, Chang WY, Zahm FE, Pluck N, *Peginterferon alpha-2a (40 kDa): an advance in the treatment of hepatitis B e antigen-positive chronic hepatitis B.* J Viral Hepat, 2003. **10**(4): p. 298-305.
23. Papatheodoridis GV, D.E., Papadimitropoulos V, *Nucleoside analogues for chronic hepatitis B: antiviral efficacy and viral resistance.* Am J Gastroenterol, 2002. **97**(7): p. 1618-28.
24. Santantonio T, M.M., Iacovazzi T, Miglietta A, Guastadisegni A, Pastore G, *Long-term follow-up of patients with anti-HBe/HBV DNA-positive chronic hepatitis B treated for 12 months with lamivudine.* J Hepatol, 2000. **32**(2): p. 300-6.
25. Perrillo R, S.E., Yoshida E, Statler A, Hirsch K, Wright T, Gutfreund K, Lamy P, Murray A, *Perrillo R, Schiff E, Yoshida E, Statler A, Hirsch K, Wright T, Gutfreund K, Lamy P, Murray A.* Hepatology, 2000. **32**(1): p. 129-34.
26. Perrillo R, H.H., Mutimer D, Willems B, Leung N, Lee WM, Moorat A, Gardner S, Woessner M, Bourne E, Brosgart CL, Schiff E, *Adefovir dipivoxil added to ongoing lamivudine in chronic hepatitis B with YMDD mutant hepatitis B virus.* Gastroenterology, 2004. **126**(1): p. 81-90.
27. Sims KA, W.A., *Entecavir: a new nucleoside analog for the treatment of chronic hepatitis B infection.* Pharmacotherapy, 2006. **26**(12): p. 1745-57.
28. Fung SK, F.R., *Management of drug-resistant chronic hepatitis B.* Clin Liver Dis, 2006. **10**(2): p. 275-302.
29. Colombatto P, C.L., Bizzarri R, Oliveri F, Choudhury S, Gieschke R, Bonino F, Brunetto MR, *A multiphase model of the dynamics of HBV infection in HBeAg-negative patients during pegylated interferon-alpha2a, lamivudine and combination therapy.* Antivir Ther, 2006. **11**(2): p. 197-212.
30. van Zonneveld M, Z.P., Cakaloglu Y, Simon C, Akarca US, So TM, Flink HJ, de Man RA, Schalm SW, Janssen HL, *Peg-interferon improves liver histology in*



- patients with HBeAg-positive chronic hepatitis B: no additional benefit of combination with lamivudine.* Liver Int, 2006. **26**(4): p. 399-405.
31. Kiernan F, *The anatomy and physiology of the liver.* Philos Trans R Soc Lond (Biol), 1833. **123**: p. 711-770.
  32. Rappaport AM, B.A., Lougheed WM, Lotto WN, *Subdivision of hexagonal liver lobules into a structural and functional unit.* Anat Rec, 1954. **119**: p. 11-33.
  33. Moorman AF, D.B.P., Geerts WJ, Van den Zande L, Lambers WH, Charles R, *Complimentary distribution of carbamoylphosphate synthetase (ammonia) and glutamine synthetase in rat liver acinus is regulated at a pretranslational level.* J Histochem Cytochem, 1988. **36**: p. 751-55.
  34. Jungermann K, *Metabolic zonation of liver parenchyma.* Semin Liver Dis, 1988. **8**: p. 329-41.
  35. Thurman RG, K.F., *Sublobular compartmentation of pharmacological events (SCOPE): metabolic fluxes in periportal and pericentral regions of the liver lobule.* Hepatology, 1985. **5**: p. 144-51.
  36. Nathanson MH, B.J., *Mechanisms and regulation of bile secretion.* Hepatology, 1991. **14**: p. 551-566.
  37. Matsumoto T, K.M., *The unit-concept of hepatic parenchyma--a re-examination based on angioarchitectural studies.* Acta Pathol Jpn, 1982. **32 Suppl 2**: p. 285-314.
  38. Bhunchet E, W.K., *The portal lobule in rat liver fibrosis: A re-evaluation of the liver unit.* Hepatology, 1998. **27**(2): p. 481 - 487.
  39. Lamers WH, H.A., Furt E, Smith J, Jonges GN, van Noorden CJ, Janzen JW, Charles R, Moorman AF, *Hepatic enzymic zonation: a reevaluation of the concept of the liver acinus.* Hepatology, 1989. **10**(1): p. 72-6.
  40. MacSween RNM, D.V., Roskams T, Scothorne RJ, *Developmental anatomy and normal structure,* in *Pathology of the Liver*, B.A. MacSween RNM, Portmann BC, Ishak KG, Scheuer PJ, Anthony PP, Editor. 2002, Churchill Livingstone: New York. p. 1-66.
  41. Weibel ER, S.W., Gnagi HR, Hess FA, *Correlated morphometric and biochemical studies on the liver cell. I. Morphometric model, stereologic methods, and normal morphometric data for rat liver.* J Cell Biol, 1969. **42**(1): p. 68-91.
  42. Wisse E, D.Z.R., Charels K, Van Der Smissen P, McCuskey RS, *The liver sieve: Considerations concerning the structure and function of endothelial fenestrae, the sinusoidal wall and the space of Disse.* Hepatology, 1985. **5**: p. 683-92.
  43. Oda M, N.M., Watanabe N, Ohya Y, Sekuzuka E, Tsukada N, Yonei Y, Komatsu H, Nagata H, Tsuchiya M, *Some dynamic aspects of the hepatic microcirculation – demonstration of sinusoidal endothelial fenestrae as a possible regulatory factor,* in *Intravital Observation of Organ Microcirculation*, W.H. Tsuchiya M, Oda M, Okazaki I, Editor. 1983, Excerpta Medica: Amsterdam. p. 105-38.
  44. Oda M, T.N., Watanabe N, Tsuchiya M, *Heterogeneity of hepatic lobule – some ultrastructural aspects of hepatic microcirculation system.* J Clin Electron Microscopy, 1983. **16**: p. 5-6.
  45. Frenzel H, K.B., Hucker H, *The liver sinusoids under various pathological conditions. A TEM and SEM study of rat liver after respiratory hypoxia, telecobalt-*

- irradiation and endotoxin application.*, in *Kupffer and other liver sinusoidal cells*, K.D. Wisse E, Editor. 1977, Elsevier: Amsterdam. p. 213-22.
46. Dobbs BR, R.G., Xing HY, Fraser R, *Endotoxin-induced defenestration of the hepatic sinusoidal endothelium: a factor in the pathogenesis of cirrhosis?* Liver, 1994. **14**: p. 230-33.
  47. Steffan AM, P.C., Bingen A, Valle M, Martin JP, Koehren F, Royer C, Gendrault JL, Kirn A, *Mouse hepatitis virus type 3 infection provokes a decrease in the number of sinusoidal endothelial fenestrae both in vivo and in vitro.* Hepatology, 1995. **22**: p. 395-401.
  48. Mori T, O.T., Sawa Y, Hori N, Ohta M, Kagawa K, *Defenestration of the sinusoidal endothelial cell in a rat model of cirrhosis.* Hepatology, 1993. **17**: p. 891-897.
  49. Fraser R, B.L., Wisse E, *Agents related to fibrosis, such as alcohol and carbon tetrachloride, acutely effect endothelial fenestrae which cause fatty liver.*, in *Connective Tissue of the Normal and Fibrotic Human Liver*, P.J. Gerlach V, Rauterberg J, Vob B, Editor. 1982, Thieme G verlag: Stuttgart. p. 159-60.
  50. Vidal-Vanaclocha F, A.-V.A., Ayala R, Barberá-Guillem E., *Functional variations in liver tissue during the implantation process of metastatic tumour cells.* Virchows Archiv A Pathol Anat. Histopathol, 1990. **416**: p. 189-95.
  51. McCuskey RS, *The hepatic microvascular system*, in *The liver: Biology and Pathobiology*, B.J. Arias IM, Fausto N, Jakoby WB, Schachter DA, and Shafritz DA, Editor. 1994, Raven Press, Ltd: New York. p. 1089-1106.
  52. Bilzer M, R.F., Gerbes AL, *Role of Kupffer cells in host defense and liver disease.* Liver Int, 2006. **26**(10): p. 1175-86.
  53. Sleyster EC, K.D., *Relation between localization and function of rat liver Kupffer cells.* Lab Invest, 1982. **47**(5): p. 484-90.
  54. van Furth R, *Production and migration of monocytes and kinetics of macrophages*, in *Mononuclear Phagocytes. Biology of Monocytes and Macrophages*, van Furth R, Editor. 1992, Kluwer: Dordrecht. p. 3-12.
  55. Li D, F.S., *Liver fibrogenesis and the role of hepatic stellate cells: new insights and prospects for therapy.* J Gastroenterol Hepatol, 1999. **14**(7): p. 618-33.
  56. Geerts A, *History, heterogeneity, developmental biology, and functions of quiescent hepatic stellate cells.* Semin Liver Dis, 2001. **21**(3): p. 311-35.
  57. Kawada N, *Human hepatic stellate cells are resistant to apoptosis: implications for human fibrogenic liver disease.* Gut, 2006. **55**(8): p. 1073-4.
  58. Zou Z, E.W., Wake K, *Zonal and regional differences identified from precision mapping of vitamin A-storing lipid droplets of the hepatic stellate cells in pig liver: a novel concept of addressing the intralobular area of heterogeneity.* Hepatology, 1998. **27**(4): p. 1098-108.
  59. Ramadori G, S.B., *Inflammation, damage repair, immune cells, and liver fibrosis: specific or nonspecific, this is the question.* Gastroenterology, 2004. **127**(3): p. 997-1000.
  60. Rockey DC, *Hepatic fibrosis, stellate cells, and portal hypertension.* Clin Liver Dis, 2006. **10**(3): p. 459-79, vii-viii.

61. Issa R, W.E., Trim N, Kendall T, Arthur MJ, Reichen J, Benyon RC, Iredale JP, *Apoptosis of hepatic stellate cells: involvement in resolution of biliary fibrosis and regulation by soluble growth factors*. Gut, 2001. **48**(4): p. 548-57.
62. Iredale JP, B.R., Pickering J, McCullen M, Northrop M, Pawley S, Hovell C, Arthur MJ, *Mechanisms of spontaneous resolution of rat liver fibrosis. Hepatic stellate cell apoptosis and reduced hepatic expression of metalloproteinase inhibitors*. J Clin Invest, 1998. **102**(3): p. 538-49.
63. Nakatani K, K.K., Seki S, Nakajima Y *Pit cells as liver-associated natural killer cells: morphology and function*. Med Electron Microsc, 2004. **37**(1): p. 29-36.
64. Bouwens L, W.E., *Pit cells in the liver*. Liver, 1992. **12**(1): p. 3-9.
65. Wisse E, L.D., Vermijlen D, Kanellopoulou C, De Zanger R, Braet F, *On the function of pit cells, the liver-specific natural killer cells*. Semin Liver Dis, 1997. **17**(4): p. 265-86.
66. Alpini G, P.J., LaRusso NF, *The Biology of Biliary Epithelia*, in *The Liver: Biology and Pathobiology*, B.J. Arias IM, Fausto N, Jakoby WB, Schachter DA, and Shafritz DA, Editor. 1994, Raven Press, Ltd.: New York.
67. Marzioni M, G.S., Francis H, Phinizy JL, LeSage G, Alpini G, *Functional heterogeneity of cholangiocytes*. Semin Liver Dis, 2002. **22**(3): p. 227-40.
68. Alpini G, R.S., Kuntz SM, Ueno Y, Gubba S, Podila PV, LeSage G, LaRusso NF, *Morphological, molecular, and functional heterogeneity of cholangiocytes from normal rat liver*. Gastroenterology, 1996. **110**(5): p. 1636-43.
69. Mathis GA, W.S., D'Amico P, Gengo TF, Sirica AE, *Enzyme profile of rat bile ductular epithelial cells in reference to the resistance phenotype in hepatocarcinogenesis*. Hepatology, 1989. **9**(3): p. 477-85.
70. Alpini G, G.S., Robertson W, Rodgers RE, Phinizy JL, Lasater J, LeSage GD, *Large but not small intrahepatic bile ducts are involved in secretin-regulated ductal bile secretion*. Am J Physiol, 1997. **272**(5 Pt 1): p. G1064-74.
71. LeSage GD, G.S., Marucci L, Benedetti A, Phinizy JL, Rodgers R, Caligiuri A, Papa E, Tretjak Z, Jezequel AM, Holcomb LA, Alpini G, *Acute carbon tetrachloride feeding induces damage of large but not small cholangiocytes from BDL rat liver*. Am J Physiol, 1999. **276**(5 Pt 1): p. G1289-301.
72. Lesage G, G.S., Gubba S, Robertson WE, Phinizy JL, Lasater J, Rodgers RE, Alpini G, *Regrowth of the rat biliary tree after 70% partial hepatectomy is coupled to increased secretin-induced ductal secretion*. Gastroenterology, 1996. **111**(6): p. 1633-44.
73. Alpini G, U.Y., Glaser SS, Marzioni M, Phinizy JL, Francis H, Lesage G, *Bile acid feeding increased proliferative activity and apical bile acid transporter expression in both small and large rat cholangiocytes*. Hepatology, 2001. **34**(5): p. 868-76.
74. Stamatoglou SC, H.R., *Cell adhesion molecules in liver function and pattern formation*. FASEB J, 1994. **8**(6): p. 420-7.
75. Ben-Ze'ev A, R.G., Bucher NL, Farmer SR, *Cell-cell and cell-matrix interactions differentially regulate the expression of hepatic and cytoskeletal genes in primary cultures of rat hepatocytes*. Proc Natl Acad Sci USA, 1988. **85**(7): p. 2161-5.
76. Schuetz EG, L.D., Omiecinski CJ, Muller-Eberhard U, Kleinman HK, Elswick B, Guzelian PS, *Regulation of gene expression in adult rat hepatocytes cultured on a basement membrane matrix*. J Cell Physiol, 1988. **134**(3): p. 309-23.

77. Kocarek TA, S.E., Guzelian PS, *Expression of multiple forms of cytochrome P450 mRNAs in primary cultures of rat hepatocytes maintained on matrigel*. Mol Pharmacol, 1993. **43**(3): p. 328-34.
78. Svegliati-Baroni G, R.F., Di Sario A, Casini A, Marucci L, Gaggiotti G, Orlandoni P, Macarri G, Perego L, Benedetti A, Folli F, *Insulin and insulin-like growth factor-1 stimulate proliferation and type I collagen accumulation by human hepatic stellate cells: differential effects on signal transduction pathways*. Hepatology, 1999. **29**(6): p. 1743-51.
79. Bridle KR, L.L., O'Neill R, Britton RS, Bacon BR, *Coordinate activation of intracellular signaling pathways by insulin-like growth factor-1 and platelet-derived growth factor in rat hepatic stellate cells*. J Lab Clin Med, 2006. **147**(5): p. 234-41.
80. Ferre N, C.J., *New insights into the regulation of liver inflammation and oxidative stress*. Mini Rev Med Chem, 2006. **6**(12): p. 1321-30.
81. Hossain MA, W.H., Izuishi K, Okano K, Yachida S, Maeta H, *The role of prostaglandins in liver ischemia-reperfusion injury*. Curr Pharm Des, 2006. **12**(23): p. 2935-51.
82. Farzaneh-Far R, M.K., *Cysteinyl-leukotrienes and the liver*. Prostaglandins Other Lipid Mediat, 2003. **72**(1-2): p. 35-50.
83. Tejima K, A.M., Ikeda H, Tomiya T, Yanase M, Inoue Y, Nagashima K, Nishikawa T, Watanabe N, Omata M, Fujiwara K, *Ischemic preconditioning protects hepatocytes via reactive oxygen species derived from Kupffer cells in rats*. Gastroenterology, 2004. **127**(5): p. 1488-96.
84. Rodgarkia-Dara C, V.S., Erlach N, Losert A, Bursch W, Berger W, Schulte-Hermann R, Grusch M, *The activin axis in liver biology and disease*. Mutant Res, 2006. **613**(2-3): p. 123-37.
85. Fausto N, C.J., Riehle KJ, *Liver regeneration*. Hepatology, 2006. **43**(2 Suppl 1): p. S45-53.
86. Hwa AJ, *Microvessel structure formation in a 3D perfused co-culture of rat hepatocytes and liver endothelial cells*, in *Biological Engineering*. 2006, Massachusetts Institute of Technology. p. 145.
87. Vinken M, P.P., Snykers S, De Rop E, Henkens T, Chipman JK, Rogiers V, Vanhaecke T, *Involvement of cell junctions in hepatocyte culture functionality*. Crit Rev Toxicol, 2006. **36**(4): p. 299-318.
88. Hou DX, A.M., Fukuda M, Oka T, Fujii M, *Expression of cell adhesion molecule and albumin genes in primary culture of rat hepatocytes*. Cell Biol Int, 2001. **25**(3): p. 239-44.
89. Yang J, I.A., Tsuchiya T, *A novel function of connexin 32: marked enhancement of liver function in a hepatoma cell line*. Biochem Biophys Res Commun, 2003. **307**(1): p. 80-5.
90. Yuasa C, T.Y., Shono M, Ishimura K, Ichihara A, *Importance of cell aggregation for expression of liver functions and regeneration demonstrated with primary cultured hepatocytes*. J Cell Physiol, 1993. **156**(3): p. 522-30.
91. Stumpel F, O.T., Willecke K, Jungermann K, *Connexin 32 gap junctions enhance stimulation of glucose output by glucagon and noradrenaline in mouse liver*. Hepatology, 1998. **28**(6): p. 1616-20.

92. Kojima T, Y.T., Murata M, Chiba H, Kokai Y, Sawada N, *Regulation of the blood-biliary barrier: interaction between gap and tight junctions in hepatocytes*. Med Electron Microsc, 2003. **36**(3): p. 157-64.
93. Abu-Absi SF, F.J., Hansen LK, Hu WS, *Structural polarity and functional bile canaliculi in rat hepatocyte spheroids*. Exp Cell Res, 2002. **274**(1): p. 56-67.
94. Bode HP, W.L., Cassio D, Leite MF, St-Pierre MV, Hirata K, Okazaki K, Sears ML, Meda P, Nathanson MH, Dufour JF, *Expression and regulation of gap junctions in rat cholangiocytes*. Hepatology, 2002. **36**(3): p. 631-40.
95. Nathanson MH, R.-V.L., Burgstahler AD, Mennone A, *Communication via gap junctions modulates bile secretion in the isolated perfused rat liver*. Gastroenterology, 1999. **116**(5): p. 1176-83.
96. Hamilton GA, J.S., Gilbert D, Coon DJ, Barros S, LeCluyse EL, *Regulation of cell morphology and cytochrome P450 expression in human hepatocytes by extracellular matrix and cell-cell interactions*. Cell Tissue Res, 2001. **306**(1): p. 85-99.
97. Shoda T, M.K., Onodera H, Toyoda K, Uneyama C, Imazawa T, Hirose M, *The relationship between decrease in Cx32 and induction of P450 isozymes in the early phase of clofibrate hepatocarcinogenesis in the rat*. Arch Toxicol, 1999. **73**(7): p. 373-80.
98. Jungermann K, K.N., *Functional specialization of different hepatocyte populations*. Physiol Rev, 1989. **69**(3): p. 708-64.
99. Corlu A, I.G., Cariou S, Lamy I, Loyer P, Guguen-Guillouzo C, *The coculture: a system for studying the regulation of liver differentiation/proliferation activity and its control*. Cell Biol Toxicol, 1997. **13**(4-5): p. 235-42.
100. Heermann KH, K.F., Seifer M, Gerlich WH, *Immunogenicity of the gene S and Pre-S domains in hepatitis B virions and HBsAg filaments*. Intervirology, 1987. **28**(1): p. 14-25.
101. Heermann KH, G.U., Schwartz W, Seyffarth T, Baumgarten H, Gerlich WH, *Large surface proteins of hepatitis B virus containing the pre-s sequence*. J Virol, 1984. **52**(2): p. 396-402.
102. Tan WS, D.M., Murray K, *Two distinct segments of the hepatitis B virus surface antigen contribute synergistically to its association with the viral core particles*. J Mol Biol, 1999. **286**(3): p. 797-808.
103. Bruss V, *Envelopment of the hepatitis B virus nucleocapsid*. Virus Res, 2004. **106**(2): p. 199-209.
104. Prange R, S.R., *Novel transmembrane topology of the hepatitis B virus envelope proteins*. EMBO J, 1995. **14**(2): p. 247-56.
105. Bruss V, L.X., Thomssen R, Gerlich WH, *Post-translational alterations in transmembrane topology of the hepatitis B virus large envelope protein*. EMBO J, 1994. **13**(10): p. 2273-9.
106. Lambert C, P.R., *Chaperone action in the posttranslational topological reorientation of the hepatitis B virus large envelope protein: Implications for translocational regulation*. Proc Natl Acad Sci USA, 2003. **100**(9): p. 5199-204.
107. Gripon P, L.S.J., Rumin S, Guguen-Guillouzo C, *Myristylation of the hepatitis B virus large surface protein is essential for viral infectivity*. Virology, 1995. **213**(2): p. 292-9.

108. Bruss V, H.J., Gerhardt E, Galle PR, *Myristylation of the large surface protein is required for hepatitis B virus in vitro infectivity*. *Virology*, 1996. **218**(2): p. 396-409.
109. Persing DH, V.H., Ganem D, *The preS1 protein of hepatitis B virus is acylated at its amino terminus with myristic acid*. *J Virol*, 1987. **61**(5): p. 1672-7.
110. Zlotnick A, C.N., Stahl SJ, Conway JF, Steven AC, Wingfield PT, *Localization of the C terminus of the assembly domain of hepatitis B virus capsid protein: implications for morphogenesis and organization of encapsidated RNA*. *Proc Natl Acad Sci USA*, 1997. **94**(18): p. 9556-61.
111. Seeger C, M.W., *Hepatitis B virus biology*. *Microbiol Mol Biol Rev*, 2000. **64**(1): p. 51-68.
112. Sheldon J, R.B., Zoulim F, Bartholomeusz A, Soriano V, *Mutations affecting the replication capacity of the hepatitis B virus*. *J Viral Hepat*, 2006. **13**(7): p. 427-34.
113. Locarnini S, *Molecular virology of hepatitis B virus*. *Semin Liver Dis*, 2004. **24**(Suppl 1): p. 3-10.
114. Bouchard MJ, S.R., *The enigmatic X gene of hepatitis B virus*. *J Virol*, 2004. **78**(23): p. 12725-34.
115. Blum HE, Z.Z., Galun E, von Weizsacker F, Garner B, Liang TJ, Wands JR, *Hepatitis B virus X protein is not central to the viral life cycle in vitro*. *J Virol*, 1992. **66**(2): p. 1223-7.
116. Tang H, O.N., Kaneko S, Murakami S, *Molecular functions and biological roles of hepatitis B virus x protein*. *Cancer Sci*, 2006. **97**(10): p. 977-83.
117. Dandri M, V.T., Lutgehetmann M, Petersen J, *Animal models for the study of HBV replication and its variants*. *J Clin Virol*, 2005. **34**(Suppl 1): p. S54-62.
118. Walter E, K.R., Niederost B, Pult I, Blum HE, *Hepatitis B virus infection of tupaia hepatocytes in vitro and in vivo*. *Hepatology*, 1996. **24**(1): p. 1-5.
119. Baumert TF, Y.C., Schurmann P, Kock J, Ziegler C, Grulich C, Nassal M, Liang TJ, Blum HE, von Weizsacker F, *Hepatitis B virus mutations associated with fulminant hepatitis induce apoptosis in primary Tupaia hepatocytes*. *Hepatology*, 2005. **41**(2): p. 247-56.
120. Mabit H, V.C., Dubanchet S, Capel F, Franco D, Petit MA, *Primary cultured normal human hepatocytes for hepatitis B virus receptor studies*. *J Hepatol*, 1996. **24**(4): p. 403-12.
121. Sells MA, C.M., Acs G, *Production of hepatitis B virus particles in Hep G2 cells transfected with cloned hepatitis B virus DNA*. *Proc Natl Acad Sci USA*, 1987. **84**(4): p. 1005-9.
122. Gripon P, R.S., Urban S, Le Seyec J, Glaise D, Cannie I, Guyomard C, Lucas J, Trepo C, Guguen-Guillouzo C, *Infection of a human hepatoma cell line by hepatitis B virus*. *Proc Natl Acad Sci USA*, 2002. **99**(24): p. 15655-60.
123. Tennant BC, T.I., Peek SF, Jacob JR, Menne S, Hornbuckle WE, Schinazi RD, Korba BE, Cote PJ, Gerin JL, *Hepatocellular carcinoma in the woodchuck model of hepatitis B virus infection*. *Gastroenterology*, 2004. **127**(5 Suppl 1): p. S283-93.
124. Menne S, C.P., *The woodchuck as an animal model for pathogenesis and therapy of chronic hepatitis B virus infection*. *World J Gastroenterol*, 2007. **13**(1): p. 104-24.



125. Summers J, M.W., *Replication of the genome of a hepatitis B--like virus by reverse transcription of an RNA intermediate*. Cell 1982. **29**(2): p. 403-15.
126. Tuttleman JS, P.C., Summers J, *Formation of the pool of covalently closed circular viral DNA in hepadnavirus-infected cells*. Cell, 1986. **47**(3): p. 451-60.
127. Tong S, L.J., Wands JR, *Interaction between duck hepatitis B virus and a 170-kilodalton cellular protein is mediated through a neutralizing epitope of the pre-S region and occurs during viral infection*. J Virol, 1995. **69**(11): p. 7106-12.
128. Kuroki K, E.F., Ishikawa T, Turck C, Harada F, Ganem D, *gp180, a host cell glycoprotein that binds duck hepatitis B virus particles, is encoded by a member of the carboxypeptidase gene family*. J Biol Chem, 1995. **270**(25): p. 15022-8.
129. Ishikawa T, G.D., *The pre-S domain of the large viral envelope protein determines host range in avian hepatitis B viruses*. Proc Natl Acad Sci USA, 1995. **92**(14): p. 6259-63.
130. Pugh JC, S.J., *Infection and uptake of duck hepatitis B virus by duck hepatocytes maintained in the presence of dimethyl sulfoxide*. Virology, 1989. **172**(2): p. 564-72.
131. Galle PR, S.H., Kuhn C, Schaller H, *Replication of duck hepatitis B virus in primary duck hepatocytes and its dependence on the state of differentiation of the host cell*. Hepatology, 1989. **10**(4): p. 459-65.
132. Jilbert AR, M.D., Scougall CA, Turnbull H, Burrell CJ, *Kinetics of duck hepatitis B virus infection following low dose virus inoculation: one virus DNA genome is infectious in neonatal ducks*. Virology, 1996. **226**(2): p. 338-45.
133. Pugh JC, S.H., *Duck hepatitis B virus infection of Muscovy duck hepatocytes and nature of virus resistance in vivo*. J Virol, 1994. **68**(4): p. 2487-94.
134. Pugh JC, D.Q., Mason WS, Simmons H, *Susceptibility to duck hepatitis B virus infection is associated with the presence of cell surface receptor sites that efficiently bind viral particles*. J Virol, 1995. **69**(8): p. 4814-22.
135. Fernholz D, W.G., Will H, *Minor envelope proteins of duck hepatitis B virus are initiated at internal pre-S AUG codons but are not essential for infectivity*. Virology, 1993. **197**(1): p. 64-73.
136. Kuroki K, C.R., Marion PL, Ganem D, *A cell surface protein that binds avian hepatitis B virus particles*. J Virol, 1994. **68**(4): p. 2091-6.
137. Urban S, K.C., Multhaup G, *A soluble form of the avian hepatitis B virus receptor. Biochemical characterization and functional analysis of the receptor ligand complex*. J Biol Chem, 1999. **274**(9): p. 5707-15.
138. Eng FJ, N.E., Kuroki K, Ganem D, Fricker LD, *gp180, a protein that binds duck hepatitis B virus particles, has metallo-carboxypeptidase D-like enzymatic activity*. J Biol Chem, 1998. **273**(14): p. 8382-8.
139. Wang CY, G.J., Smith BF, *Development of viral disinfectant assays for duck hepatitis B virus using cell culture/PCR*. J Virol Methods, 2002. **106**(1): p. 39-50.
140. Urban S, S.C., Marx UC, Zentgraf H, Schaller H, Multhaup G, *Receptor recognition by a hepatitis B virus reveals a novel mode of high affinity virus-receptor interaction*. EMBO J, 2000. **19**(6): p. 1217-27.
141. Breiner KM, U.S., Schaller H, *Carboxypeptidase D (gp180), a Golgi-resident protein, functions in the attachment and entry of avian hepatitis B viruses*. J Virol, 1998. **72**(10): p. 8098-104.

142. Eng FJ, V.O., Fricker LD, *Sequences within the cytoplasmic domain of gp180/carboxypeptidase D mediate localization to the trans-Golgi network.* Mol Biol Cell, 1999. **10**(1): p. 35-46.
143. Breiner KM, U.S., Glass B, Schaller H, *Envelope protein-mediated down-regulation of hepatitis B virus receptor in infected hepatocytes.* J Virol, 2001. **75**(1): p. 143-50.
144. Li JS, T.S., Wands JR, *Characterization of a 120-Kilodalton pre-S-binding protein as a candidate duck hepatitis B virus receptor.* J Virol, 1996. **70**(9): p. 6029-35.
145. Li J, T.S., Wands JR, *Identification and expression of glycine decarboxylase (p120) as a duck hepatitis B virus pre-S envelope-binding protein.* J Biol Chem, 1999. **274**(39): p. 27658-65.
146. Li J, T.S., Lee HB, Perdigoto AL, Spangenberg HC, Wands JR, *Glycine decarboxylase mediates a postbinding step in duck hepatitis B virus infection.* J Virol, 2004. **78**(4): p. 1873-81.
147. Glebe D, U.S., *Viral and cellular determinants involved in hepadnaviral entry.* World J Gastroenterol, 2007. **13**(1): p. 22-38.
148. Tang H, M.A., *Avian and Mammalian hepadnaviruses have distinct transcription factor requirements for viral replication.* J Virol, 2002. **76**(15): p. 7468-72.
149. Wiwi CA, W.D., *Role of hepatocyte nuclear factors in transcriptional regulation of male-specific CYP2A2.* J Biol Chem, 2005. **280**(5): p. 3259-68.
150. Watt AJ, G.W., Duncan SA, *HNF4: a central regulator of hepatocyte differentiation and function.* Hepatology, 2003. **37**(6): p. 1249-53.
151. Cereghini S, *Liver-enriched transcription factors and hepatocyte differentiation.* FASEB J, 1996. **10**(2): p. 267-82.
152. Duncan SA, N.M., Dufort D, Rossant J, Stoffel M, *Regulation of a transcription factor network required for differentiation and metabolism.* Science, 1998. **281**(5377): p. 692-5.
153. Kaestner KH, *The hepatocyte nuclear factor 3 (HNF3 or FOXA) family in metabolism.* Trends Endocrinol Metab, 2000. **11**(7): p. 281-5.
154. Gebhardt R, H.J., Muller D, Glockner R, Buenning P, Laube B, Schmelzer E, Ullrich M, Utesch D, Hewitt N, Ringel M, Hilz BR, Bader A, Langsch A, Koose T, Burger HJ, Maas J, Oesch F, *New hepatocyte in vitro systems for drug metabolism: metabolic capacity and recommendations for application in basic research and drug development, standard operation procedures.* Drug Metab Rev, 2003. **35**(2-3): p. 145-213.
155. Ringel M, v.M.M., Santos R, Feilen PJ, Brulport M, Hermes M, Bauer AW, Schormann W, Tanner B, Schon MR, Oesch F, Hengstler JG, *Hepatocytes cultured in alginate microspheres: an optimized technique to study enzyme induction.* Toxicology, 2005. **206**(1): p. 153-67.
156. Nussler AK, W.A., Neuhaus P, Fischer J, Yuan J, Liu L, Zeilinger K, Gerlach J, Arnold PJ, Albrecht W, *The suitability of hepatocyte culture models to study various aspects of drug metabolism.* ALTEX, 2001. **18**(2): p. 91-101.
157. Zeilinger K, S.I., Pless G, Strobel C, Rudzitis J, Wang A, Nussler AK, Grebe A, Mao L, Auth SH, Unger J, Neuhaus P, Gerlach JC, *Three-dimensional co-culture of primary human liver cells in bioreactors for in vitro drug studies: effects of the*

- initial cell quality on the long-term maintenance of hepatocyte-specific functions.* Altern Lab Anim, 2002. **30**(5): p. 525-38.
158. Michalopoulos GK, B.W., Mule K, Luo J, *HGF-, EGF-, and dexamethasone-induced gene expression patterns during formation of tissue in hepatic organoid cultures.* Gene Expr, 2003. **11**(2): p. 55-75.
  159. Steinberg MS, *Reconstruction of tissues by dissociated cells. Some morphogenetic tissue movements and the sorting out of embryonic cells may have a common explanation.* Science, 1963. **141**: p. 401-8.
  160. Ryan PL, F.R., Kohn J, Steinberg MS, *Tissue spreading on implantable substrates is a competitive outcome of cell-cell vs. cell-substratum adhesivity.* Proc Natl Acad Sci USA, 2001. **98**(8): p. 4323-7.
  161. Powers MJ, G.L., *Adhesion-guided in vitro morphogenesis in pure and mixed cell cultures.* Microsc Res Tech, 1998. **43**(5): p. 379-84.
  162. Steinberg MS, *On the mechanism of tissue reconstruction by dissociated cells. I. Population kinetics, differential adhesiveness. and the absence of directed migration.* Proc Natl Acad Sci USA, 1962. **48**: p. 1577-82.
  163. Lauffenburger DA, G.L., *Who's got pull around here? Cell organization in development and tissue engineering.* Proc Natl Acad Sci USA, 2001. **98**(8): p. 4282-4.
  164. Powers MJ, D.K., Kaazempur-Mofrad MR, Kalezi A, Capitano A, Upadhyaya A, Kurzawski P, Wack KE, Stolz DB, Kamm R, Griffith LG, *A microfabricated array bioreactor for perfused 3D liver culture.* Biotechnol Bioeng, 2002. **78**(3): p. 257-69.
  165. Seglen PO, *Preparation of isolated rat liver cells.* Methods Cell Biol, 1976. **13**: p. 29-83.
  166. Block GD, L.J., Bowen WC, Petersen BE, Katyal S, Strom SC, Riley T, Howard TA, Michalopoulos GK, *Population expansion, clonal growth, and specific differentiation patterns in primary cultures of hepatocytes induced by HGF/SF, EGF and TGF alpha in a chemically defined (HGM) medium.* J Cell Biol, 1996. **132**(6): p. 1133-49.
  167. Schwerer B, B.M., Bernheimer H, *ELISA for determination of albumin in the nanogram range: assay in cerebrospinal fluid and comparison with radial immunodiffusion.* Clin Chim Acta, 1987. **163**(3): p. 237-44.
  168. Akiyama TE, G.F., *Regulation of P450 genes by liver-enriched transcription factors and nuclear receptors.* Biochim Biophys Acta, 2003. **1619**(3): p. 223-34.
  169. Cheung C, A.T., Kudo G, Gonzalez FJ, *Hepatic expression of cytochrome P450s in hepatocyte nuclear factor 1-alpha (HNF1alpha)-deficient mice.* Biochem Pharmacol, 2003. **66**(10): p. 2011-20.
  170. Domansky K, I.W., Serdy J, Griffith L. *Perfused microreactors for liver tissue engineering.* in Conf Proc IEEE Eng Med Biol Soc. 2005.
  171. Inman SW, *Development of a High Throughput 3D Perfused Liver Tissue Bioreactor,* in Mechanical Engineering. 2006, Massachusetts Institute of Technology: Cambridge. p. 178.
  172. Ren S, N.M., *Hepatitis B virus (HBV) virion and covalently closed circular DNA formation in primary tupaia hepatocytes and human hepatoma cell lines upon HBV*

- genome transduction with replication-defective adenovirus vectors.* J Virol, 2001. **75**(3): p. 1104-16.
173. Klingmuller U, S.H., *Hepadnavirus infection requires interaction between the viral pre-S domain and a specific hepatocellular receptor.* J Virol, 1993. **67**(12): p. 7414-22.
  174. Tong S, L.J., Wands JR, *Carboxypeptidase D is an avian hepatitis B virus receptor.* J Virol, 1999. **73**(10): p. 8696-702.
  175. Sprinzl MF, O.H., Schaller H, Protzer U, *Transfer of hepatitis B virus genome by adenovirus vectors into cultured cells and mice: crossing the species barrier.* J Virol, 2001. **75**(11): p. 5108-18.
  176. Song L, F.L., *Tissue distribution and characterization of soluble and membrane-bound forms of metalcarboxypeptidase D.* J Biol Chem, 1996. **271**(46): p. 28884-9.
  177. Varlamov O, F.L., *Intracellular trafficking of metalcarboxypeptidase D in AtT-20 cells: localization to the trans-Golgi network and recycling from the cell surface.* J Cell Sci, 1998. **111**(Pt 7): p. 877-85.
  178. Varlamov O, E.F., Novikova EG, Fricker LD, *Localization of metalcarboxypeptidase D in AtT-20 cells. Potential role in prohormone processing.* J Biol Chem, 1999. **274**(21): p. 14759-67.
  179. Kalinina E, V.O., Fricker LD, *Analysis of the carboxypeptidase D cytoplasmic domain: Implications in intracellular trafficking.* J Cell Biochem, 2002. **85**(1): p. 101-11.
  180. Miller-Jensen K, J.K., Wong YL, Griffith LG, Lauffenburger DA, *Adenoviral vector saturates Akt pro-survival signaling and blocks insulin-mediated rescue of tumor necrosis-factor-induced apoptosis.* J Cell Sci, 2006. **119**(Pt 18): p. 3788-98.
  181. Tauber B, D.T., *Molecular regulation and biological function of adenovirus early genes: the E4 ORFs.* Gene, 2001. **278**(1-2): p. 1-23.
  182. Qiao M, S.C., Duszynski A, Burrell CJ, *Kinetics of early molecular events in duck hepatitis B virus replication in primary duck hepatocytes.* J Gen Virol, 1999. **80**(Pt 8): p. 2127-35.
  183. Funk A, M.M., Lin L, Will H, Sirma H, *Itinerary of hepatitis B viruses: delineation of restriction points critical for infectious entry.* J Virol, 2004. **78**(15): p. 8289-300.
  184. Yao E, T.J., *Kinetics of synthesis and turnover of the duck hepatitis B virus reverse transcriptase.* J Biol Chem, 2003. **278**(2): p. 1201-5.
  185. Yoshimura K, R.M., Seth P, Crystal RG, *Adenovirus-mediated augmentation of cell transfection with unmodified plasmid vectors.* J Biol Chem, 1993. **268**(4): p. 2300-3.
  186. Seth P, R.M., Higginbotham J, Crystal RG, *Mechanism of enhancement of DNA expression consequent to cointernalization of a replication-deficient adenovirus and unmodified plasmid DNA.* J Virol, 1994. **68**(2): p. 933-40.
  187. Meier O, B.K., Hammer SV, Keller S, Stidwill RP, Hemmi S, Greber UF, *Adenovirus triggers macropinocytosis and endosomal leakage together with its clathrin-mediated uptake.* J Cell Biol, 2002. **158**(6): p. 1119-31.
  188. Varlamov O, K.E., Che FY, Fricker LD, *Protein phosphatase 2A binds to the cytoplasmic tail of carboxypeptidase D and regulates post-trans-Golgi network trafficking.* J Cell Sci, 2001. **114**(Pt 2): p. 311-22.

189. Thomas CE, E.A., Kay MA, *Progress and problems with the use of viral vectors for gene therapy*. Nat Rev Genet, 2003. 4(5): p. 346-58.
190. Shtrichman R, S.R., Kleinberger T, *Adenovirus E4orf4 protein interacts with both Balpha and B' subunits of protein phosphatase 2A, but E4orf4-induced apoptosis is mediated only by the interaction with Balpha*. Oncogene, 2000. 19(33): p. 3757-65.
191. Novikova EG, E.F., Yan L, Qian Y, Fricker LD, *Characterization of the enzymatic properties of the first and second domains of metallo-carboxypeptidase D*. J Biol Chem, 1999. 274(41): p. 28887-92.
192. Song L, F.L., *Purification and characterization of carboxypeptidase D, a novel carboxypeptidase E-like enzyme, from bovine pituitary*. J Biol Chem, 1995. 270(42): p. 25007-13.
193. Hadkar V, S.S., Vogel SM, Brovkovich V, Skidgel RA, *Carboxypeptidase-mediated enhancement of nitric oxide production in rat lungs and microvascular endothelial cells*. Am J Physiol Lung Cell Mol Physiol, 2004. 287(1): p. L35-45.
194. Chen T, Z.R., Zuckerbraun B, Billiar TR, *Role of nitric oxide in liver injury*. Curr Mol Med, 2003. 3(6): p. 519-26.
195. Mitrenga D, A.W., Muller O, Mayersbach HV, *The fate of injected human IgG in the mouse liver: Uptake, immunological inactivation, and lysosomal reactions*. Cell Tissue Res, 1975. 156(3): p. 359-76.
196. Seignerès B, M.P., Werle B, Schorr O, Jamard C, Rimsky L, Trepo C, Zoulim F, *Effects of pyrimidine and purine analog combinations in the duck hepatitis B virus infection model*. Antimicrob Agents Chemother, 2003. 47(6): p. 1842-52.
197. Zoulim F, B.P., Guerhier FL, Seignerès B, Germon S, Pichoud C, Cheng YC, Trepo C, *Animal models for the study of HBV infection and the evaluation of new anti-HBV strategies*. J Gastroenterol Hepatol, 2002. 17 Suppl: p. S460-3.
198. Kock J, S.H., *Analysis of the earliest steps of hepadnavirus replication: genome repair after infectious entry into hepatocytes does not depend on viral polymerase activity*. J Virol, 1993. 67(8): p. 4867-74.
199. Le Mire MF, M.D., Foster WK, Burrell CJ, Jilbert AR, *Covalently closed circular DNA is the predominant form of duck hepatitis B virus DNA that persists following transient infection*. J Virol, 2005. 79(19): p. 12242-52.

# Appendix 1

## MilliF Microreactor Assembly Protocol

### Preparation prior to Day of Assembly.

**NB: Never autoclave the polycarbonate reactor body parts.**

**NB: It is not necessary to autoclave the black cover plate or clamps.**

For each bioreactor, the following reactor parts should be autoclaved prior to assembly:

#### **Autoclave bag 1:**

- 1) Four port connectors.
- 2) Five screws (4mm).
- 3) One retaining ring with o-ring attached.

#### **Autoclave bag 2:**

- 4) One custom cut Durapore filter (5 $\mu$ m pore size).
- 5) One thick gasket.
- 6) One thin gasket (pre-clean by rubbing with EtOH (70%) on a Kim-wipe)

#### **Autoclave bag 3:**

- 7) Two silicon scaffolds.

**NB: Pick up using PLASTIC forceps to avoid scratching the silicon.**

#### **Autoclave bag 4:**

- 8) Two blue autoclave sheets.

#### **Autoclave bags 5, 6, 7, 8, 9 and 10:**

- 9) Screwdriver.
- 10) Hexagonal connector driver.
- 11) Two syringe pistons.
- 12) Metal tweezers.
- 13) Plastic tweezers.
- 14) Metal flat-end tweezers.

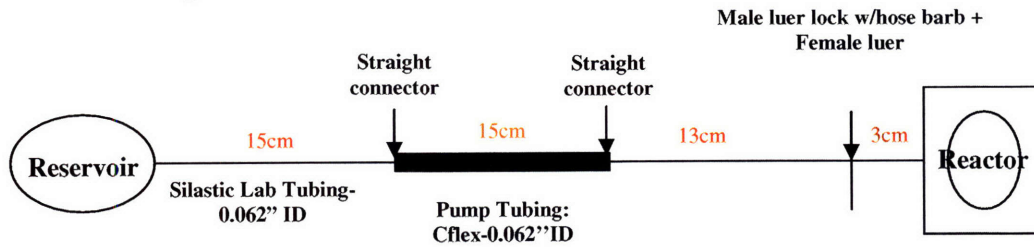
#### **Autoclave bag 11:**

One polypropylene reservoir with custom cut tubing pieces attached (Figure 1).

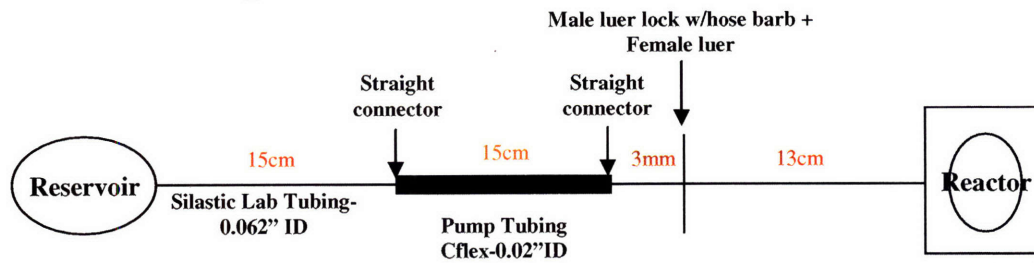
**Figure 1: Tubing Lengths (for 2-pump experiments).**



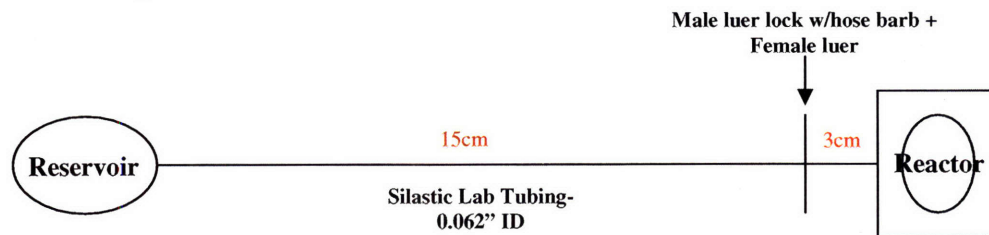
**Axial Inlet Tubing:**



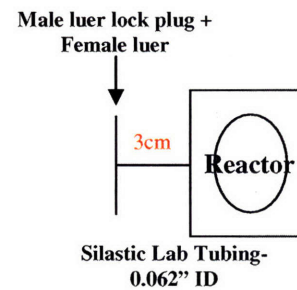
**Cross-flow Inlet Tubing:**



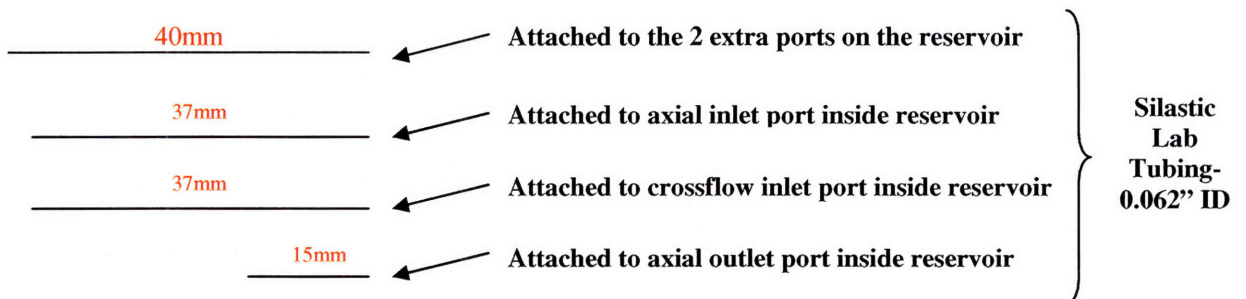
**Outlet Tubing:**

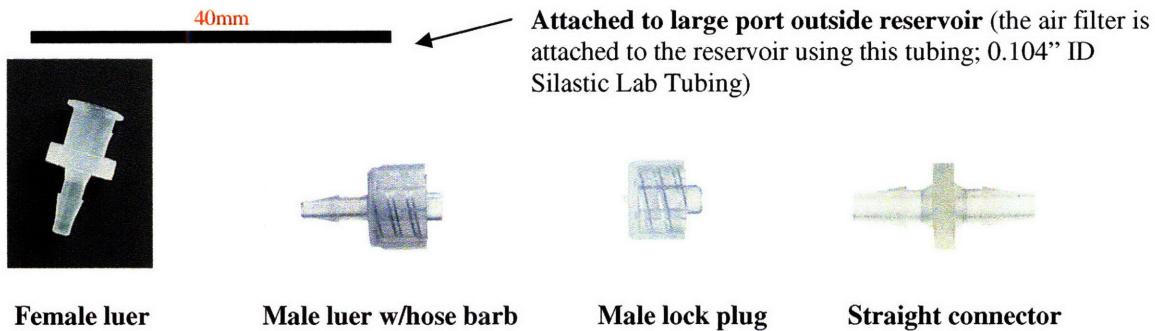


**Extra Port:**



**Reservoir Connector Tubing:**





### Preparation on Day of Assembly.

- 1) Incubate polycarbonate reactor body parts in 70% EtOH (30min) in a petri-dish.
- 2) Incubate black cover plate and clamps in 70% EtOH (30min).
- 3) Incubate Durapore filter in 10ml 1% BSA (in PBS) solution in a small petri-dish (30min).
- 4) Incubate one silicon scaffold in 25ml collagen solution in a petri-dish (30min).

**NB: Remove air bubbles from within the scaffold by shaking the petri-dish.**

### Assembly.

- 1) Place autoclaved blue sheets on the working surface inside a tissue-culture hood.
- 2) Transfer polycarbonate reactor body parts into a petri-dish containing 25ml PBS.

**NB: Ensure the reactor body parts are completely immersed in PBS and that ethanol is rinsed out of the parts. The significant surface tension between PBS and ethanol means that the reactor parts move around on a film of ethanol when initially placed in PBS. If the reactor is well rinsed and forcefully immersed into PBS, it will sink to the bottom.**

- 3) Place polycarbonate reactor parts on the blue paper, using the plastic tweezers.
- 4) Remove excess PBS from the reactor parts using a vacuum manifold and pipette.

**NB: Hold the pipette horizontal to the reactor to prevent scratching of the optical window.**

**NB: Leave some PBS in the reactor trough to provide the surface tension necessary to hold the gasket in place.**

- 5) Place thin gasket into the reactor trough, using plastic tweezers.
- 6) Push thin gasket into the trough, using the rubber portion of the syringe piston.
- 7) Rinse collagen-coated silicon scaffold in PBS.

**NB: This helps to minimize the attachment of cells to the top of the silicon chip.**

- 8) Place collagen-coated silicon chip into the trough, using metal flat-head tweezers.
- 9) Push silicon chip into the trough, using the rubber portion of the syringe piston.
- 10) Place filter into the trough, using metal flat-head tweezers.
- 11) Push filter into the trough, using the rubber portion of the syringe piston.

**NB: Ensure there are no bubbles remaining between the filter and scaffold.**

- 12) Place non-collagen coated silicon chip into the trough, using metal flat-head tweezers.
- 13) Push silicon chip into the trough, using the rubber portion of the syringe piston.
- 14) Place thick gasket into the trough, using plastic tweezers.
- 15) Push thick gasket into the trough, using the rubber portion of the syringe piston.
- 16) Place retaining ring with O-ring attached into the trough, using plastic tweezers.
- 17) Push retaining ring into the trough, using the rubber portion of the syringe piston.

**NB: With repeated use, the O-ring wears down ⇒ Replace after each experiment.**

- 18) Add PBS (1-2 drops, using a 1ml syringe) to the reactor trough.

**NB: This maintains the surface tension, required to hold the filter to the chip.**

- 19) Place the bottom polycarbonate reactor part on top of the trough.

**NB: It is reasonable to use gloved hands at this point.**

- 20) Use three 4mm screws to attach the bottom and top polycarbonate reactor bodies.

**NB: Tighten screws evenly to ensure an even distribution of stress on the O-ring.**

- 21) Turn the reactor upside down so the optical window faces upwards.
- 22) Use two 4mm screws to attach the black cover plate to the reactor.

**NB: Make sure that the holes in the reactor line up with the holes in the black cover plate so that the reactor is flush against the edge of the black cover plate.**

23) Screw the 4 connectors into their respective ports, using the hexagonal driver.


24) Add HGM (15ml) to the reservoir.

25) Attach a 0.2 $\mu$ m filter to the gas exchange tubing on top of the reservoir.

26) Connect exterior tubing to the reactor and reservoir as shown (Figure 2).

**NB: The reservoir interior has 2 x 37mm pieces of tubing attached to the inlet port and cross-flow port and 1 x 15mm piece of tubing attached to the outlet port. There is also a 40mm piece of tubing attached to the extra ports as shown in Figure 2. There is also a 0.104" piece of tubing attached to the large port on the outside of the reservoir.**

27) Prime reactor and tubing by running the system at the desired flow rates (1hr).

**Axial Pump Setting (Top):** (0.5ml/min) reactor  reservoir

**Cross-flow Pump Setting (Bottom):** (40 $\mu$ l/min) reactor  reservoir

28) Remove any air bubbles by flicking the lines with fingers.

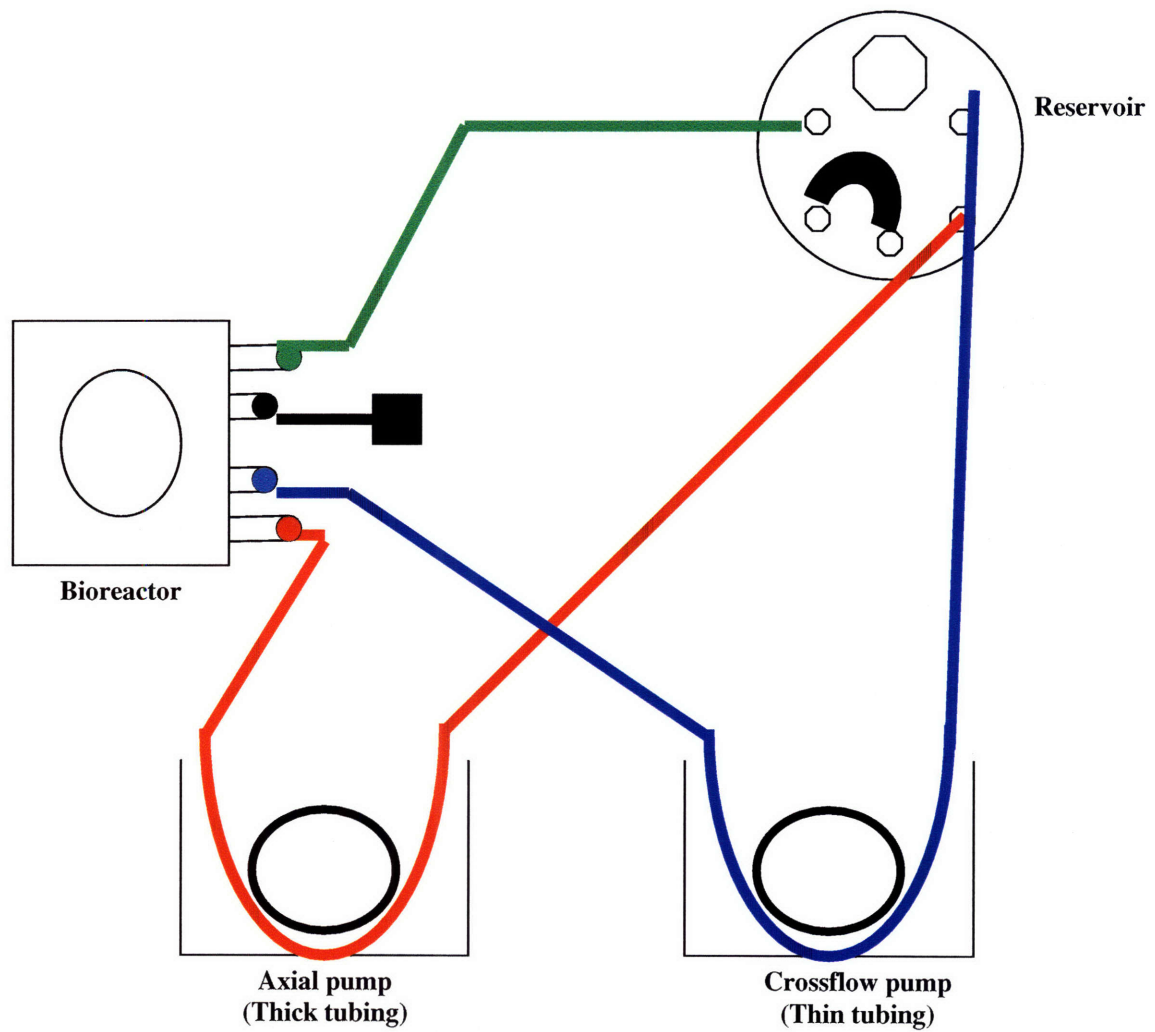
**NB: Keep reservoir elevated relative to the reactor; bubbles move upwards to the reservoir.**

### Precautions.

- Never touch the silicon scaffold, filter, retaining ring or gaskets with fingers.
- Clean the reactor tools with ethanol after each use.
- If the reactor leaks during priming, the O-ring probably needs replacing. Place the reactor back into the sterile hood, disassemble and change the O-ring.

**Figure 2: Tubing Attachments.**

**NB:** After adding cells to the bioreactor, turn on the cross-flow pump first for a few seconds before turning on the axial pump. This should ensure that the cells are pulled down into the channel.

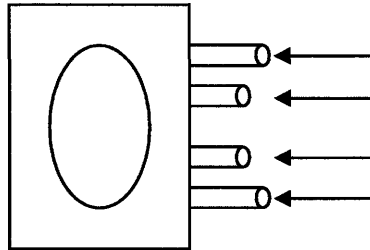


## Appendix 2

### MilliF Bioreactor Seeding & Maintenance Protocol

The system should have been primed for at least one hour prior to seeding.

#### Top View of MilliF:



#### Day 1.

- 1) Remove any bubbles from the axial inlet and crossflow line by flicking the line with fingers.
- 2) Clamp off the crossflow line; allow any bubbles to exit.
- 3) Remove crossflow tubing from the pump.
- 4) Disconnect female luer from the male luer lock w/ barbed hose on the outlet line.
- 5) Attach 1ml syringe to the short outlet tubing of the outlet line.
- 6) Turn on axial pump to fill the syringe.

**NB: Keep unconnected tubes on the sterile autoclave paper.**

- 7) Draw up 1ml of spheroids (100-300 $\mu$ m diameter) in another 1ml syringe.

**NB: Remove any bubbles in the syringe by inverting and gently tapping it.**

- 8) Disconnect female luer from the male luer lock w/ barbed hose on the inlet line.
- 9) Pinch the short tubing on the inlet line and attach the syringe containing spheroids.

**NB: Ensure that there is a liquid-liquid contact between the female luer and the syringe.**

- 10) Hold spheroid syringe vertical and remove clamp on the crossflow line.
- 11) Hold both syringes vertical and slowly inject the spheroids into the reactor.

**NB: Rotate the syringe to maintain the spheroids in suspension.**

12) When the piston on the syringe attached to the outlet line begins to move, the receptor channels are full. If the piston does not move, repeat steps 7-11.

13) Re-clamp crossflow line.

14) Remove bubbles from axial inlet line using the syringe attached to the outlet line.

15) Remove syringe attached to the inlet line and reattach connectors.

**NB: Ensure that there is a liquid-liquid contact between the connectors.**

16) Remove syringe attached to the outlet line and reattach connectors.

**NB: Ensure that there is a liquid-liquid contact between the connectors.**

17) Unclamp crossflow line.

18) Turn on axial pump at 0.5ml/min.

19) Turn on crossflow pump in the forward direction (**Rxr** → **Res**) at 40-80µl/min.

20) Incubate bioreactors (37°C, 8.5% CO<sub>2</sub>).

**Day 2 (24 hours post-seeding).**

1) Turn off axial flow pump and crossflow pump.

2) Clamp axial inlet and outlet tubing.

3) Unhook male luer/female luer on the crossflow inlet line.

4) Add a new 0.8/0.2µm filter between the male and female luer.

5) Reverse crossflow (**Res** → **Rxr**) and prime new filter using a high flow rate.

6) Turn off crossflow pump.

7) Re-hook male luer/filter/female luer to the crossflow inlet tubing.

8) Take off male lock plug on the extra port.

9) Turn on crossflow pump using a low flow rate; allow bubbles in reactor to escape.

10) Turn off crossflow pump.

11) Re-attach male lock plug to the extra port.



12) Unclamp axial inlet tubing and outlet tubing.

13) Turn on axial pump and crossflow pump (still running in the reverse direction).

14) Replace media after 1 hour since some nutrients will be stuck on the new filter.

**NB: Check for bubbles twice a day; Change in-line filter once every three days.**

## **Appendix 3**

### **Giant Microreactor Assembly, Seeding, & Maintenance Protocol**

#### **Materials List:**

- 1 Top window
- 1 Middle body
- 1 Bottom piece
- 6 small screws
- 6 large screws
- 2 port screws w/ O-rings
- 1 Middle-sized silicon O-ring
- 1 Large-sized silicon O-ring
- 4 screw end-barbed end connectors w/ silicon O-ring on screw end
- 2 oblong silicon gaskets w/ pin holes
- 2 polycarbonate scaffolds w/ pin holes
- 1 Oblong Millipore filter w/ pin holes
- 1 Metal retaining ring (oblong shape)
- 6 barbed end-barbed end connectors
- 6 female luer-barbed end connectors
- 2 female luer-sealed end connector
- 4 male luer-barbed end connectors
- 2 0.093" ID silicon peristaltic tubes (paralyne coated)
- 5 6" silastic tubes (Teflon tubing, 3/8" ID)
- 6 3" silastic tubes (Teflon tubing, 3/8" ID)
- 2 4" silastic tube (Teflon tubing, 3/8" ID)
- 2 reservoirs w/ two inner silastic tubes, two outer openings sealed with tubes, 1 outer tube for air filter
- 1 5 um inline filter
- 1 1.2 um inline filter
- 1 0.8/0.2 um inline filter
- 2 0.2 um inline filter
- 3 150 X 75 Pyrex dish
- 1 complete peristaltic pump (w/ 2 instech pumps)
- 2 13.5/35 VDC power supply (CAUTION: ALWAYS SET AT 13.5 VDC)
- Autoclaved blue paper (at least 3 squares)
- Tools: screwdrivers, tweezers, flat-head tongs, hex wrench
- 30 ug/mL type I rat tail collagen in 1X PBS
- 1% w/v BSA in 1X PBS
- 1X PBS

#### **Assembly protocol**

1. Autoclave screws, connectors (place lower connectors, except 1 male lower and 1 sealed end, in separate bag), reservoir, silastic tubing (Teflon tubing), O-rings, tools (except screwdrivers), gaskets, Millipore filter, retaining ring, 2 Pyrex dishes and blue paper.
2. Scrub polycarbonate Giant RXR body parts w/alconox, rinse with milliQ water, place parts in previously autoclaved Pyrex dish, cover parts with milliQ water.
3. Replace water with 70% EtOH and let stand at least ten minutes before putting in hood. Make sure all RXR bodies are completely submerged. CAUTION: POLYCARBONATE SHOULD NOT BE EXPOSED TO ETOH FOR MORE THAN 30 MINS.
4. Place polycarbonate scaffolds in Petri dish, cover withalconox water, shake gently, removealconox, cover with milliQ water to rinse, shake gently, rinse repeatedly.
5. Place polycarbonate scaffolds w/ body parts in Pyrex dish w/ milliQ water, put in sonicator for 2 mins.
6. Remove milliQ water, cover parts with 70% EtOH, sonicate for 2 mins. Leave parts in EtOH. CAUTION: POLYCARBONATE SHOULD NOT BE EXPOSED TO ETOH FOR MORE THAN 30 MINS.
7. Place body parts in Pyrex dish in sterile hood, along with: autoclaved Pyrex dish, tools (including EtOH sprayed-down screwdrivers), connectors (except lower connectors, include 1 male lower and 1 sealed end), screws, reservoir, tubing, O-rings, gaskets, Millipore filters, retaining ring, and blue paper. Spray all autoclave packets thoroughly with EtOH before putting them in the hood and keep them away from the blue paper surface that the reservoir is on.
8. Cover surface of working area in sterile cabinet with autoclaved blue paper.
9. Fill one autoclaved Pyrex dish  $\frac{3}{4}$  full with 1X PBS, this will be used to rinse all parts. Fill a 10 cm Petri dish with 1X PBS to rinse scaffolds separately from other parts.
10. Fill the other autoclaved Pyrex dish  $\frac{3}{4}$  full with 70% EtOH, and use the flat tongs to place the two peristaltic tubings in the ethanol, swirling the tubes around the dish to get the inner tubing surfaces exposed as well. Make sure all tube ends are submerged in the ethanol.
11. Place collagen solution (at least 10-15 mL) in a 10 cm Petri dish. Do same for 1% BSA solution.
12. Rinse both scaffolds in 1X PBS. Put the top scaffold into the collagen solution, shaking gently until no air bubbles are seen. The corresponding bottom scaffold can stay in the pBS or be put in another Petri dish with PBS if you are keeping track of many RXRs. For polycarbonate scaffolds, keep in collagen solution for 2 hours, and then dry for 2 hours by balancing the scaffold on a 60 mm dish inside a 10 cm dish in side the hood. For silicon scaffolds only 30 min in the collagen solution is required.
13. Rinse filter in PBS and then place in the BSA solution for at least 30 minutes.
14. Use tongs and tweezers to take out middle body part (sides may be touched by gloved hands, but should be avoided) from EtOH, rinse in 1X PBS, and place on blue paper top-side up.
15. Using tweezers, rinse middle-sized silicon O-ring in 1X PBS (this helps parts interact with each other more smoothly), place O-ring in its channel in top of

- middle part. Use tweezers to hold down O-ring while flathead of tongs is used to smoothly place the O-ring into channel to avoid tearing the O-ring.
16. Rinse top window in 1X PBS, place on top of middle body part.
  17. Use the 6 small screws to secure window on middle part (PBS rinsed). Tighten screws (lightly at first) in a crisscross pattern, eventually tightening without cracking polycarbonate parts (don't overly tighten). Make sure O-ring in compressed uniformly.
  18. Screw in port screws slowly and loosely to middle body part, make sure there are no burrs on that screw threads catching that can damage the threading on the reactor body
  19. Tighten port screws, stop at a little resistance. Otherwise you can break the flow channel inlet and outlet, compression of the O-ring is all that is needed to seal the injection port.
  20. Keep middle/top window assembly open chamber face down on the sterile blue paper. Use the hex wrench to lightly-tighten 2 screw end-barbed end connectors to middle body part.
  21. Flip the RXR body around so that the open pocket is facing up. Be very careful not to wave hands or arms over the reactor now.
  22. Using tools, rinse 1 silicon gasket in PBS, place gasket in middle body part, using pins/pin holes as a guide. Use flathead of tongs to lay gasket down flat and make sure no air bubbles are stuck under the gasket.
  23. Place dried top scaffold in middle body atop the gasket, use pin/pin holes as guide. Make sure scaffold is flat on gasket and that the letter or number symbol is facing you at the top pin to ensure alignment with the bottom support scaffold.
  24. Place filter in middle body atop scaffold using pin/pin holes as guide. Flatten with tongs onto scaffold. Be especially careful not to tear the filter, as this will affect control over cross-flow.
  25. Using tools, rinse support scaffold in PBS if not already in PBS, place scaffold in middle body atop Millipore filter using pin/pin holes as guide. Make sure scaffold is flat and that the letter or number is at the top pin and facing you to ensure the best alignment.
  26. Using tools, rinse second silicon gasket in PBS, place gasket in middle body atop scaffold using pin/pin holes as guide. Flatten with tongs onto scaffold. The pins should only extend about halfway up into the holes on this gasket.
  27. Using tools, rinse retaining ring in PBS, place ring in middle body atop gasket with channel for O-ring facing upward.
  28. Using tweezers, rinse large-sized silicon O-ring in 1X PBS, place O-ring in its channel between retaining ring and middle part. Use tweezers to hold down O-ring while flathead of tongs is used to smoothly place the O-ring into channel.
  29. Rinse bottom piece of RXR in PBS. Place on middle body part, and use the large screws to secure. As with the top window, tighten screws (lightly at first) in a crisscross pattern, eventually tightening without cracking polycarbonate parts (don't overly tighten). Make sure O-ring in compressed uniformly.
  30. Use hex wrench to lightly-tighten 2 screw end-barbed end connectors to bottom piece. Flip RXR top-side up with bottom connectors towards assembler.

31. Place one 6" silastic tube (or Teflon tube) into right side connector and one into bottom-right connector. Place one PBS rinsed 3" silastic tube (or Teflon tube) into bottom-left connector and one into left side connector.
32. **Put male luer**-barbed end connector into each 3" silastic tube (Teflon tube) at the bottom left port. Attach a female luer-barbed end connector onto connector coming out of right side of top chamber. Attach a female luer-sealed end connector onto connector coming out of bottom right chamber. Note: It's easiest to add these connectors onto the tubing before they are wrapped up in blue paper with the reservoir and other tubing and autoclaved.
33. Attach a 4" silastic tube (Teflon tube) between connector coming out of the right side of the top chamber and the reservoir (no inner silastic tube in reservoir).
34. Put complete peristaltic pump in safety cabinet connected to power supplies.
35. Rinse peristaltic tubes in PBS, evenly distribute a light coat of pump grease on tube length between pump locks.
36. Turn pump on to a slow speed and guide peristaltic tube into each Instech pump. Keep pump going on for a short period to allow all PBS to clear out.
37. Put 1 barb-barb end connector onto each end of each peristaltic tube. With the Instech pumps facing assembler, connect one 6" silastic (Teflon) tube onto left end of left peristaltic tube, connect this to reservoir (to an inner silastic tube in reservoir).
38. Connect right end of left peristaltic tube to silastic (Teflon) tube out of left side connector on RXR body.
39. Connect one 6" silastic (Teflon) tube onto left end of right peristaltic tube, connect this to reservoir (to an inner silastic tube in reservoir). Connect right end of right peristaltic tube to silastic (Teflon) tube out of bottom-left connector on RXR body.
40. Put 0.2 um inline filter in tube for air filter in reservoir. Fill reservoir with 30 mL of HGM (w/ or w/o BSA, depending on necessities of experiment).
41. Turn on left Instech pump at 3 mL/min, counterclockwise (calibration should be done before run). Allow top chamber of RXR to fill with HGM.
42. Turn on right Instech pump at 1 mL/min, counterclockwise. Flip RXR, bottom-side up, put reactor at a 45° angle so that bottom chamber fills up from bottom up (inflow tube on bottom). If bottom chamber starts to have a lot of air bubbles or foam starts to develop, open locked luer connector slightly to relieve pressure and get rid of bubbles/foam. Once all foam/bubbles are cleared out, lock connector again.
43. Let system prime for ~1 hour.

### **Seeding protocol**

All seeding is done inside sterile cabinets unless otherwise noted. Spheroids should be filtered (50 µm and 300 µm mesh), spun down at 50 g for 3 mins, resuspended in cold fresh medium, and put on ice before beginning this protocol.

1. Turn off pumps and unscrew top window, remove it, and place it on sterile autoclave paper.

2. Turn on pumps, reverse flow on crossflow line so that flow is going from top chamber to bottom chamber. Increase crossflow rate to 2.5 mL/min. Leave main flow on at 3 mL/min.
3. Seed reactor by pipetting ~1 mL of spheroid suspension evenly on seeding scaffold. Pipette gently, making sure spheroids are evenly distributed. Spheroids may be pipetted back up if doing so will not shear the spheroid.
4. Turn off main flow and rock reactor body back and forth to get even seeding of scaffold. Observe channels as well as possible. If all channels are not seeded properly, a smaller volume of spheroid suspension may be added to the required area of the scaffold. Make sure top chamber liquid level is always above scaffold by turning on main flow if it is too low. This prevents cells from drying.
5. Turn off all flow. Replace top window and screw back on in a similar fashion as done during assembly to ensure uniform compression of O-ring. Turn main flow on at 3 mL/min, and crossflow at 2.5 mL/min. Put reactor in 37°C incubator.
6. Change medium 1-2 hours after seeding. Put in 30 mL of fresh medium in reservoir.

### **Inserting Filters and Reversing Crossflow**

This protocol should be followed such that crossflow is reversed 24 hrs after seeding. Priming of filters requires an extra reservoir. However, all filters necessary can be primed from the same pump assembly.

1. Soak one peristaltic tube in 70% EtOH for <15 mins. Rinse in 1X PBS and place around pump head by turning pump on to a low setting. Grease tube before placing on head.
2. Insert one barbed end-barbed end connector to each end of peristaltic tube.
3. With pump heads facing user, attach one 6" peristaltic tube (Teflon tube) to left end of peristaltic tube. Attach other end to reservoir (inner silastic tube).
4. Attach one 3" peristaltic tube (Teflon tube) to right end of peristaltic tube, insert male lower-barbed end connector into free end and attach a 5  $\mu\text{m}$  inline filter to this connector. Attach a female lower-barbed end connector to free end of filter. Repeat this step for 1.2  $\mu\text{m}$  inline filter and 0.8/0.2  $\mu\text{m}$  inline filter, placing a 3" silastic tube (Teflon tube) between each filter.
5. Connect 0.8/0.2  $\mu\text{m}$  inline filter to reservoir (inner silastic tube) with a 4" silastic tube (Teflon tube). If more than one reactor requires inline filters, repeat step 4 for those filters before attaching this final tube to the reservoir.
6. Place one 3" silastic tube to open connector on reservoir (no inner silastic tube), insert a female lower-barbed end connector into free end and seal with a male lower-sealed end connector. Insert 0.2  $\mu\text{m}$  inline filter into air intake tube.
7. Put 30 mL of fresh medium into reservoir. Turn on pump in a counterclockwise direction at full speed.
8. Hold filters up such that they will be filled from the bottom up so that most air is removed from the filter. After filters have been filled with medium, shake them and tap them gently against pump or sterile cabinet to shake out any air bubbles that may have been trapped inside them.

9. Once all air bubbles are cleared, allow filters to prime for ~1 hour.
10. Take reactor out of incubator and place in sterile cabinet. Turn off pumps.
11. Open lower locked connectors in outflow line. Turn on main flow just so liquid level gets to end of male lower connector and then turn off.
12. Remove 5  $\mu\text{m}$  inline filter from lower lock and lock with the outflow line of the reactor assembly. Detach female lower lock connector from 0.8/0.2  $\mu\text{m}$  inline filter outlet and attach this filter to female lower-barbed end connector left open on reactor assembly.
13. Reverse crossflow on reactor so that it flows from bottom chamber to top chamber, and set at 1 mL/min. Hold reactor at a 45° degree angle such that the inlet of the bottom chamber is lower than the sealed end. Open the sealed end slightly to allow air bubbles to escape through this opening. Once all air bubbles are removed, close seal. Turn on main flow at 3 mL/min.
14. Change medium with 30 mL of fresh, 37°C-warmed medium. Medium may be changed every 24, 48 or 72 hours beyond this point depending on the needs of each experiment. Inline filters should be changed every 72 hours by repeating this protocol.



## Appendix 4

### Multi-well Microreactor Assembly, Seeding, & Maintenance Protocol (taken from “Multi-well Bioreactor Manual for use with Generation E Systems”)

Chapter 1: Prior to Use

#### **The following steps can all be done outside of the hood.**

1.1 Cleaning and Washing Components

1.1.1 Cleaning Fluidic and Pneumatic Plates

**Components you will need:**

- Fluidic Plate (1)
- Pneumatic Plate (1)

1. Place fluidic and pneumatic plates in a tub filled with a 1-3% 7x soap solution.
2. Wash plates thoroughly. Look for any debris blocking the small channels and holes in both the fluidic and pneumatic plates. In particular, pay attention to the angled channels in the fluidic plate. Use compressed air to clean the debris. If compressed air cannot dislodge debris, ask for assistance.
3. After washing, rinse plates in distilled
4. Dry off all components thoroughly.

1.1.2 Cleaning Reactor Well Components

**Components you will need:**

- Scaffolds (12)
- Gaskets (12)
- Retaining Rings (24)
- Filter Supports (12)

NOTE: Experience shows that it helps to prepare 1 to 2 extra of each component before experiment.

**Tools you will need:**

- Glass Dish (1)
- Petri Dish (1)

**Prior to use of the reactor, these components must be cleaned as follows:**

1. Place scaffolds in Petri dish filled with a 1-3% 7X soap solution. Place retaining rings, filter supports, gaskets in a glass dish filled with an 1-3% 7X soap solution.
2. Sonicate these components for 10 to 15 minutes.
3. After sonicating, rinse all components in XX water until soap is rinsed off.
4. Fill dishes with XX water and sonicate these components for 10 to 15 minutes.

5. Fill dishes with 70% ethanol and sonicate all components except fluidic and pneumatic plates for 5 to 10 minutes.

6. Dry off all components.

## 1.2 Autoclaving Components

### Components you will need:

- Fluidic Plate (1)
- Scaffolds (12)
- 24 Pack - Filters (1)
- 12 Pack - Filters (1)
- Gaskets (12)
- Retaining Rings (24)
- Filter Supports (12)

### Tools you will need:

- Tweezers (1)
- Tamping Tool (1)

### Autoclave Instructions

1. Place all the remaining tools into one autoclave bag and seal.

2. Place each set of components into a separate autoclave bag and seal.

3. All components except the membrane should be put in a standard autoclave on a dry cycle with 45

minutes of sterilization and 15 minutes of drying.

**DO NOT AUTOCLAVE PNEUMATIC PLATE!** The pneumatic plate does not need to be autoclaved, and the material will melt if placed in autoclave.

## 1.3 EtO Chamber

Make sure that you have been officially trained to use EtO Chamber.

### Components you will need:

- Polyurethane Membrane (wrapped in blue paper) (1)

### Tools you will need:

- EtO Chamber

### EtO Chamber Instructions

1. Label the autoclave bag for each membrane with the date of sterilization.

2. The membrane should be sterilized in an EtO autoclave and outgassed for a minimum of 3 days.

NOTE: To be efficient, you can sterilize more than one membrane at a time.

## 1.4 Preparing Pneumatic Plate

**Components you will need:**

- Pneumatic Plate (1)

**Tools you will need:**

- Tape (1)
- X-Acto Knife (1)

**Preparing Pneumatic Plate**

1. Spray pneumatic plate 70% ethanol and dry very well. (The device will not work well if there is any liquid in the pneumatic channels.)
2. Wipe the bottom of the plate with 100% isopropanol and let dry.
3. Cover the bottom of the plate with tape making sure all channels are covered and there are no air bubbles in the tape.
4. Press tape firmly to plate to ensure adhesion along channels.
5. Carefully cut holes for screws with X-Acto knife. Make sure to not peel up tape near pneumatic channels, and be sure to fully remove tape that has been cut away.

Chapter 2: Prior to Start of Experiment

**The following steps should all be done in sterile environment.**

2.1 Coating scaffolds with collagen

**Components you will need:**

- Scaffolds (12)

**Tools you will need:**

- Petri Dish (2)

**Solutions you will need:**

- 10 mL Collagen Solution of Type 1 rat tail collagen (30  $\mu\text{g}$  / mL)
- PBS
- 70% ethanol

**To coat the scaffolds with collagen:**

**If you are using SILICON scaffolds:**

1. Fill petri dish with 70% ethanol.
2. Place scaffolds in ethanol solution to remove all air bubbles.
3. To remove air bubbles, check under microscope or wash with PBS.
4. Fill 2nd petri dish with collagen solution.
5. Soak the scaffolds in the collagen solution for 30 to 45 minutes. Pipette the collagen solution onto the scaffolds.
6. Rinse scaffolds in dish with PBS to remove excess collagen.

If you are using POLYMER scaffolds:

1. Fill petri dish with 70% ethanol.
2. Place scaffolds in ethanol solution to remove all air bubbles.
3. To remove air bubbles, check under microscope or wash with PBS.
4. Fill 2nd petri dish with collagen solution.
5. Soak the scaffolds in the collagen solution for 2 hours.
6. Dry the scaffolds by allowing them to stand along the edge of the Petri dish. Excess collagen will drop to the base of the scaffold.
7. Aspirate off excess collagen.
8. Rinse scaffolds in dish with PBS prior to placing them into reactor.

## 2.2 Preparing other components

Components you will need:

- 24 Pack Filters (1)

Tools you will need:

- Petri Dish (1)

Solutions you will need:

- PBS with 1% BSA(Sterile)

Component Preparation:

1. Fill petri dish with PBS with 1% BSA and soak filters in this solution for at least 30 minutes.

## Chapter 3: Reactor Assembly

The following steps should be done under the hood.

Components you will need:

- Lid (A 96 Well Plate Lid works fine) (1)
- Polyurethane Membrane (1)
- Fluidic Plate (1)
- Pneumatic Plate (1)
- Hex Screws (14)

Tools you will need:

- Hexdriver (1)
- Sterile Blue Paper (2)

Reactor Assembly:

1. Spread out 2 sheets of blue paper in the hood to provide a sterile surface.

2. Spray base of pneumatic plate with ethanol being careful not to get it in the fluidic channels. Do not spray top of pneumatic plate with any fluid because fluid in channels will prevent pumping. Dry pneumatic plate.
3. Place polyurethane membrane on top of the pneumatic plate using the alignment pins as guides. Center the holes in the membrane around the screw holes. Make sure to eliminate folds that would prevent the membrane from laying flat between the plates. When handling the membrane, try to only touch the corners and keep the membrane as sterile as possible.
4. Place fluidic plate over the pneumatic plate and membrane.
5. Flip the assembly over and make sure that the membrane covers all the fluidic channels.
6. Tighten screws starting from the middle and working outward. Do not tighten all the way first. Screw in all screws, and then go back and tighten until the membrane becomes clear between the fluidic and pneumatic plates. This is a sign that you have a good seal.
7. Once you have a good seal, cover the fluidic plate with the lid; you are ready to prime the reactor.

#### Chapter 4: Priming the Reactor

The following steps should be done under the hood.

##### Components you will need:

- Reactor Assembly (1)
- Reactor Controller (1)

##### Solutions you will need:

- 50 mL warm HGM

##### Priming the Reactor:

1. Fill each reservoir well with roughly 1.5 mL of HGM.
2. Connect the pump controller to the vacuum and pressure sources. Both gauges should read  $30 \pm 5$  kPa when flowing.
3. Connect the tubing from the controller to the reactor assembly.
4. Turn on the controller to UPWARD setting.
5. Begin flowing in the UPWARD setting.
6. Look to see if fluid is pumping into the reactor well.
7. Once you have verified that your system is functioning, fill reactor wells and make sure fluid connects across the surface channel.

**YOU SHOULD SET UP YOUR REACTOR THE DAY BEFORE AND ALLOW TO RUN OVERNIGHT IN INCUBATOR AND REFRESH MEDIA BEFORE SEEDING CELLS.**

#### Chapter 5: Setting up the Wells

The following steps should be done under the hood.

##### Components you will need:

- Assembled Reactor (1)
- 24 Pack Filters (1)
- Gaskets (12)
- Filter Supports (12)

**Tools you will need:**

- Glass Dish (1)
- Tweezers (1)
- Tamping Tool (1)

**Solutions you will need:**

- PBS

**Setting Up Reactor Wells:**

1. Place all filter supports in 50 mL Falcon Tube.
2. Fill Falcon Tube with PBS and tap the bottom of the tube to remove trapped bubbles from filter supports.
3. Place all gaskets in dish of PBS.
4. Place gaskets in all of the reactor wells. Push down with tamping tool.
5. Pour filter supports into glass dish or 90 mm petri dish.
6. Place filter support in all reactor wells with concentric rings facing up.
7. Push down with tamping tool.
8. Rinse filter gently in PBS and then place one filter in all wells.
9. Rinse scaffolds gently, and gently place one in each reactor well.
10. Put one retaining ring in each well. Push them down gently as too much pressure can cause the silicon scaffolds to break. However, still make sure that the ring is tight and pushed down all the way to ensure the path of the fluid is through the filter and scaffold and not around it.

Chapter 6: Seeding Cells

**Components you will need:**

- Reactor Assembly (1)
- Reactor Controller (1)

**Tools you will need:**

- P1000 Pipette + Wide Orifice Tips

**Solutions you will need:**

- HGM
- Isolate Cell Suspension

6.1 Refreshing the Media

1. If your reactor has been priming overnight, aspirate as much media as possible from both the reactor and reservoir making sure to leave a thin layer of media above the scaffold

in the reactor well and the filter in the reservoir well as to not introduce air bubbles beneath the filter.

2. Add back cold, fresh medium to the reactor well only. Do not create a fluidic connection between the reactor well and reservoir well.

## 6.2 Seeding the Single Cells

1. Make sure that the reactor is set for downward flow through the scaffold.

2. Check to make sure the retaining rings are pushed all the way down.

**For 800 channel scaffolds:**

3. Use a P1000 pipette.

4. Pause flow.

5. Ensure that the reactor well and reservoir well are not fluidically connected.

6. Hold pipette straight up and slowly pipette the desired amount of your cell suspension in a pattern over the entire scaffold.

7. Check seeding under microscope. See appendix for tips if poorly distributed.

8. Once you are comfortable with seeding distribution, resume downward flow and immediately begin fill reservoir to fill line with media (approximately 2.5 mL - 2.7 mL).

Make sure that you have no dry spots

across the fluidic channel as this will disrupt oxygen transport.

## 6.3 Setting the Flowrate and Reversal Time

1. Set the controller for reverse flow and select a flowrate.

2. Set a reversal time of 8 hours.

## Chapter 7: Experiment Maintenance

### 7.1 4 Hours After Experiment Start

The following steps can be done outside of the hood except where noted.

**Components you will need:**

- Reactor Assembly (1)
- Reactor Controller (1)

**Tools you will need:**

- 10 ml pipette
- Aspirator

**Solutions you will need:**

- 50 mL HGM – Warm

1. Remove your reactor from the incubator and walk with it carefully to the hood trying not to shake the reactor as media may spill out of the channel.

2. Under the hood, remove the lid from your reactor and aspirate off any media from the lid and on the surface of the reactor plate.



3. Aspirate media from the reservoir wells by taking your aspirator tip and bringing it to the top of the retaining ring and aspirating off the media. Be careful to not aspirate off media to the point of creating air bubbles under the filter as this interrupts the flow through the reactor.
4. Aspirate media from reactor wells by taking your aspirator tip near the wall of the reactor well. Be sure not to aspirate media directly from above the cells. Be sure to leave approximately 1 - 2 mm of media above the cells as to not disrupt them significantly.
5. Add 2.5 - 2.7 mL to each reservoir well filling only to the fill line. Be careful and keep your pipette clear of bubbles. Make sure that you have no dry spots across the fluidic channel as this will disrupt oxygen transport.
6. Cover your reactor and return your reactor to the incubator.
7. Make sure the pressure and vacuum gauges are bouncing between  $30 \pm 5$ .

## 7.2 24 Hours After Experiment Start

The following steps can be done outside of the hood except where noted.

### Components you will need:

- Reactor Assembly (1)
- Reactor Controller (1)
- 12 Pack Filters (1)

### Tools you will need:

- 10 ml pipette
- Aspirator
- Tweezers (1)
- Tamping Tool (1)
- Petri Dish (2)

### Solutions you will need:

- 50 mL HGM – Warm
- 1% BSA Solution
- PBS

### 7.2.1 Replenishing Media

1. Begin soaking 12 new filters in petri dish filled with 1% BSA Solution.
2. Remove your reactor from the incubator and walk with it carefully to the hood trying not to shake the reactor as media may spill out of the channel.
3. Under the hood, remove the lid from your reactor and aspirate off any media from the lid and on the surface of the reactor plate.
4. Aspirate media from the reservoirs by taking your aspirator tip and bringing it to the top of the retaining ring and aspirating off the media. Be careful to not aspirate off media to the point of creating air bubbles under the filter as this interrupts the flow through the reactor.
5. Aspirate media from reactor wells by taking your aspirator tip near the wall of the reactor well. Be sure not to aspirate media directly from above the cells. Be sure to leave approximately 1 - 2 mm of media above the cells as to not disrupt them significantly.

6. Remove retaining ring from reservoir side, and place aside in petri dish filled with PBS.
7. Remove filters from reservoir and discard.
8. Gently place new BSA-soaked filters in reservoir. Tamp in place.
9. Put one retaining ring in each well, and push down firmly with tamping tool to ensure tight fluidic seal.
10. Put ~2mL of new warm media in each reservoir well being careful to keep your pipette clear of bubbles.  
Make sure that you have no dry spots across the fluidic channel as this will disrupt oxygen transport.
11. Cover your reactor and return your reactor to the incubator.
12. Make sure the pressure and vacuum gauges are bouncing between  $30 \pm 5$ .

### 7.3 More than 24 Hours After Experiment Start

1. Remove your reactor from the incubator and walk with it carefully to the hood trying not to shake the reactor as media may spill out of the channel.
2. Under the hood, remove the lid from your reactor and aspirate off any media from the lid and on the surface of the reactor plate.
3. Aspirate media from the reservoirs by taking your aspirator tip and bringing it to the top of the retaining ring and aspirating off the media. Be careful to not aspirate off media to the point of creating air bubbles under the filter as this interrupts the flow through the reactor.
4. Aspirate media from reactor wells by taking your aspirator tip near the wall of the reactor well. Be sure not to aspirate media directly from above the cells. Be sure to leave approximately 1 - 2 mm of media above the cells as to not disrupt them significantly.
5. Put ~2mL of new warm media in each reservoir well being careful to keep your pipette clear of bubbles.  
Make sure that you have no dry spots across the fluidic channel as this will disrupt oxygen transport.
6. Cover your reactor and return your reactor to the incubator.
7. Make sure the pressure and vacuum gauges are bouncing between  $30 \pm 5$ .